

This work is protected by copyright and other intellectual property rights and duplication or sale of all or part is not permitted, except that material may be duplicated by you for research, private study, criticism/review or educational purposes. Electronic or print copies are for your own personal, non-commercial use and shall not be passed to any other individual. No quotation may be published without proper acknowledgement. For any other use, or to quote extensively from the work, permission must be obtained from the copyright holder/s.



**Keele**

UNIVERSITY



# Statistical significance of three-dimensional stochastic fluvial reservoir modelling

**Chester Huw Christopher Davies**

Supervisors:

Dr. Stuart M. Clarke

Dr. Andrew J. Mitten

This thesis is submitted in accordance with the requirements of Keele University for the degree of Master of Philosophy

June 2024



## Foreword

The bulk of the analysis of the data was carried out using the StReAMS (Davies and Mitten, 2023) Python package which is planned to be further worked on and made available after this thesis is submitted. StReAMS uses the novel methodology described in Chapter 3 for the determination of a search area by utilising standard deviation and periodicity analysis. This is useful for the determination of a statistically significant suite of three-dimensional stochastic fluvial reservoir models. The StReAMS beta can be found at: <https://github.com/chesterdavies/StReAMS-Beta>.

## Acknowledgements

After what has been an incredibly long, stressful, and ultimately, an extremely rewarding year (and a bit), it would be remiss of me to not acknowledge the incredible amounts of support that happens behind the scenes. For this, I would first like to thank both Mum and Dad for their continued support and all the late-night phone calls with me trying to answer the never-ending question of 'okay, well how do I do this?', whilst a lot of the time I was speaking complete drivel, it really helped to talk the problem through, and for that, I will always cherish those memories. I would also like to thank my grandparents for enduring many a deluded rant about something related to computers that probably went straight over your heads!

It is difficult to pinpoint the amount of support my friends have also given throughout this project, from helping me to take my mind off things, talking through problems and other general support, first to the Hills group, second to the Kings Lynn boys and finally to the CoD crew – thank you all.

Many thanks also to both of my supervisors, Stu and Andy, whom throughout this incredibly challenging project had both incredible amounts of belief, patience and support throughout. Thanks too to Rich, whom I could not have completed all the Petrel runs without his technical support.

Thanks should also go to the other inhabitants of the lab (Dave, Mark, Victor and Muraine) for your continued support, and for putting up with me over this seemingly endless process! Finally, many thanks (and apologies) to the rest of the BDRG, who have endured several rather disjointed presentations throughout this project, and for all their help and encouragement this past year. A special thanks too to Bernard for the encouragement and enthusiasm shown throughout.

## Abstract

Fluvial systems, characterized by complex structures at multiple scales, often serve as excellent reservoirs for both hydrocarbons and carbon storage. Locating such reservoirs, and assessing their quality is challenging due to their sub-seismic nature. Reservoir modelling plays a crucial role in the prediction of distribution, and the consequent assessment of the reservoir's viability. This study will focus on stochastic, geocellular reservoir models due to their industry usage and uncertainty associated with stochastic processes.

Whilst current research employs ten to twenty realizations for developing stochastic three-dimensional fluvial reservoir models, this is derived from two-dimensional experiments, and so the applicability is questionable given the extra complexity associated with a third dimension. Little research has been done surrounding how these two-dimensional results can be applied to three-dimensions.

This novel methodology determines the optimal number of realizations by creating a sample reservoir model population. It compares the distribution of properties within this smaller population to the entire dataset, using two boundary conditions: the lower bound set by the number of realizations required to model the maximum standard deviation of the whole population, and the upper bound determined by the number of realizations required for reservoir property repetition. This search window identifies the size of the sample population that best matches the whole population, providing the total number of realizations for a statistically significant dataset.

This methodology uses three different reservoir modelling algorithms with a wide range of input parameters to generate suites of synthetic reservoir models to develop and test the proposed methodology, which is then applied to a previously established example (Tuscher Canyon). Three output parameters are retrieved from the Schlumberger™ Petrel v.2020 software representing the properties of the modelled reservoir: target fraction, average geobody thickness, and standard deviation of geobody thickness. The average of all the synthetic reservoir model suites

indicated that an average of 32 realizations is required to sufficiently reduce the uncertainty of the models, independent of algorithm or model input parameters, but showed significant variability. When Tuscher Canyon is considered, the number of realizations for a statistically significant dataset is markedly different from that suggested by the synthetic dataset, meaning that there is no standardized number of realizations. The standard deviation of geobody thickness is important when reservoir modelling as it gives insight into the variation of how connected individual geobodies are and is highly variable between realizations, making it the most suitable reservoir property to be used for determining the number of realizations to use. This methodology will help to reduce uncertainty of fluvial reservoir models, resulting in better characterization, de-risking, and better assessment of economic viability.

## Table of Contents

Foreword .....	ii
Acknowledgements .....	iii
Abstract .....	iv
Table of Contents .....	vi
List of Figures.....	ix
List of Tables .....	xiv
List of Equations .....	xv
1 Introduction.....	1
1.1 Research aims and objectives.....	5
1.2 Thesis signposting.....	6
1.2.1 Chapter 2 – Literature Review .....	6
1.2.2 Chapter 3 – Methodology.....	7
1.2.3 Chapter 4 – Analysis and Interpretation.....	7
1.2.4 Chapter 5 – Application: Tuscher Canyon.....	7
1.2.5 Chapter 6 – Discussion.....	8
1.2.6 Chapter 7 – Conclusion .....	8
2 Literature Review .....	9
2.1 Types of reservoir models .....	10
2.2 Rock model algorithms.....	11
2.2.1 Neural Network Based Methods: GAN’s .....	11
2.2.2 Pixel Based Methods: The Sequential Indicator Simulation .....	13
2.2.3 Object-based Methods: Object Based Modelling.....	19
2.2.4 Pixel Based Methods: Multiple-Point Statistics .....	22
2.3 Rock model analysis.....	26
2.4 Fluvial reservoir models.....	28
2.5 Model realisations – answers and problems.....	30
2.6 Summary and Discussion .....	34
3 Methodology.....	36
3.1 Data Collection .....	36
3.1.1 Reservoir Models .....	36
3.2 Statistical Modelling .....	43
3.2.1 Histograms .....	48
3.2.2 Periodogram.....	49
3.2.3 Goovaerts Plot .....	51
3.3 Analytical Statistical Modelling.....	52
3.3.1 Comparison Plot .....	53

3.3.2	Similarity Plot .....	54
3.3.3	Previously Used Realisations .....	54
3.3.4	Realisations Required .....	55
3.4	Summary .....	60
4	Analysis and Interpretation .....	61
4.1	Number of realisations .....	61
4.1.1	Mean geobody thickness .....	62
4.1.2	Standard deviation of geobody thickness – StDev Thickness .....	64
4.1.3	Target Fraction .....	65
4.1.4	PERG, GOO and RR Values .....	67
4.2	Percentage Similarity .....	90
4.3	Summary .....	92
5	Application: Tuscher Canyon .....	93
5.1	Geological Background .....	96
5.1.1	Lower Castlegate Sandstone, Tuscher Canyon, Utah .....	96
5.1.2	Jamuna River, northern India .....	96
5.2	Results .....	97
5.2.1	Mean geobody thickness .....	97
5.2.2	Standard Deviation of Geobody Thickness – StDev Thickness .....	100
5.2.3	Target Fraction .....	102
5.3	Tuscher Canyon Similarity .....	104
5.4	Summary .....	114
6	Discussion .....	116
6.1	Application to other environments .....	116
6.2	Methodology uncertainties and potential mitigation .....	116
6.3	Number of Realisations .....	117
6.3.1	Test Suite of Models .....	117
6.3.2	Tuscher Canyon Model .....	119
6.4	Limitations .....	123
7	Conclusion .....	125
7.1	Research aims and objectives .....	125
7.2	Further Work .....	126
7.2.1	Probabilistic Reservoir Models .....	126
7.2.2	Model Size .....	126
7.2.3	Static Connectivity .....	126
7.2.4	Nugget Effect .....	127
7.2.5	Input Parameters .....	127

8 References ..... 128

## List of Figures

Figure 2.1: Flowchart of the GAN workflow, showing the generator create realistic data from an input vector (a set of elements with a uniform or normal distribution) which is then compared to the training dataset by the discriminator. The loss function is then used to train the neural networks until the discriminator is unable to distinguish between training data and the generated data (Sun, Demyanov and Arnold, 2023a) .....	12
Figure 2.2: Synthetic variogram showing range, nugget, and sill. A variogram is a graphical depiction of the spatial variance of a variable. Variograms like this function as the basis for developing reservoir models using the sequential indicator simulation (SIS) algorithm after Ringrose and Bentley, 2015. ....	13
Figure 2.3: Graphical depiction of the indicator approach to the random nature of the selection of a cell for the SIS algorithm, with the random order of cells being visited, starting at $X_1$ (circled). Once the cell has been visited, and its facies decided, in this case sand or shale, a backtransformation is applied to the conditional cumulative distribution function (CCDF). The next cell would then be randomly selected ( $X_2$ ), with this process repeating until all cells in the model have been visited. ....	15
Figure 2.4: A generic flowchart for the SIS algorithm (adapted from Juang, Chen and Lee, 2004), detailing the workflow for the determination of the facies of each cell, backtransformation, and subsequently the creation of the reservoir model. ....	16
Figure 2.5: Comparison of equivalent synthetic reservoir models developed with the A) SIS, B) OBM, and C) MPS algorithm. The SIS model (A) was created using input parameters of 250 width, 2000m length, 10 vertical thickness, a nugget value of 0.0001, and target fraction of 50:50. The OBM model (B) was created using the input parameters of 250 amplitude, 500 wavelength, 250 width, 10 vertical thickness and target fraction of 50:50. The MPS model (C), was created using the OBM model (B) as a training image, and so effectively has the same input parameters. Models generated with the different modelling algorithms show distinct differences in both the representation, and style of the modelled geometries. The pixel-based algorithms (SIS – A and MPS – C) appear less clean than the object-based algorithm (OBM – B), with the individual cells being more prominently displayed. The SIS method appears far less realistic than the models generated with the other algorithms, and lacks any proper curvilinear, or naturality. The OBM algorithm produces almost idealised geobodies, and represents nature, and curvilinear features better than the SIS algorithm. The models produced using the MPS algorithm are far more realistic, and enable both curvilinearity, and the randomness and chaos of nature to be captured within the model, producing by far the best, most realistic models. ....	17
Figure 2.6: Aerial and cross-sectional view of the parameters used to define the channel structure within the object based modelling (OBM) algorithm. A) presents the aerial view, relating to channel direction and the central line of the channel, along with the width, whereas B) presents the cross-sectional view of the channel being presented in geocellular form, with relation to width, thickness, and position of the maximum thickness (dependent on the channel curvature) after Deutsch and Tran, 2002. ....	21
Figure 2.7: A) shows a variety of filters used on the local scale within the Multiple-Point Statistics (MPS) algorithm in order to transfer the general trends of the training image (TI) into the reservoir model. B) shows a worked example using the first filter presented in A) to provide a probability value to the cell, after Zhang, Switzer and Journel, 2006 .....	24
Figure 2.8: Pixel and Bunch Based approaches to the simulation process of Object Based Modelling (OBM). The top depicts the original grid, with the left showing a 3x3 grid of cells being simulated at the same time (bunch processing), and the right showing a singular cell being simulated. This can improve the computational time required for the MPS algorithm to develop models, after Rezaee et al., 2013.....	26

Figure 2.9: A) shows the two-dimensional representation of the connectivity-net to gross relationship, with the cascade zone appearing between 50% and 80%, whereas B) shows the same connectivity-net to gross relationship, with results being significantly shifted towards the left in the three-dimensional model. The drastic shift of the cascade zone of the connectivity of a three-dimensional model in comparison to a two-dimensional model suggests that two- and three-dimensional reservoir models should be treated as separate entities, with different characteristics (from Larue and Hovadik, 2006). ..... 28

Figure 2.10: the effect of sinuosity on two channels of the same width. Channel A has far lower sinuosity than Channel B, and as such has a smaller effective channel width. Effective channel width in this case is the total width that the channel occupies. A higher effective channel width results in higher probability of channel stacking, and consequently a higher channel connectivity. .... 30

Figure 2.11: The minipermeater data being used to create porosity permeability models, and the standard deviation of these models being plotted against number of realisations (lag), to produce variograms. The standard deviation values plateau at approximately 20 realisations, suggesting diminishing returns, when it comes to total variation of the models past this number of realisations (after Goovaerts, 1999). ..... 31

Figure 2.12: Flowchart showing the processes used to develop reservoir models from outcrop behind outcrop (OBO) models (after Falivene et al., 2006) ..... 33

Figure 2.13: Examples of the different two-dimensional panels achieved from the workflow in Figure 2.12, displaying the variation of different algorithms using similar input parameters. This hints at discrepancies in model representation being present (Falivene et al., 2006). ..... 34

Figure 3.1: Example synthetic fluvial reservoir models generated using the SIS modelling algorithm, using the same input parameters for the major direction (3000) and the nugget value (0.0001), with the width (minor direction) and the vertical thickness being altered (125 and 500, and 5 and 20 respectively), showing the differences between the models generated using the edge cases of some of the input values. .... 39

Figure 3.2: Example synthetic fluvial reservoir models generated using the OBM modelling algorithm, using the same input parameters for the channel width (125) and the wavelength (250), with the amplitude (minor direction) and the vertical thickness being altered (125 and 500, and 5 and 20 respectively), showing the differences between the models generated using the edge cases of some of the input values. .... 41

Figure 3.3: Example synthetic fluvial reservoir models generated using the MPS modelling algorithm, using the same input parameters for the channel width (125) and the wavelength (250), with the amplitude (minor direction) and the vertical thickness being altered (125 and 500, and 5 and 20 respectively), showing the differences between the models generated using the edge cases of some of the input values. .... 43

Figure 3.4: Example Petrel Output File showing all of the possible characteristics to analyse within the study, whilst also showing the output format. .... 44

Figure 3.5: Generalised workflow of the methodologies for this study, starting with the creation of histograms a) to highlight dataset distributions. This is followed by the creation of a periodogram b) and Goovaerts plot c) in order to find the PERG and GOO values to be used when comparing restricted model suite distributions to the initial model suite of 100 realisations d) overlain distribution histogram of all three, e) initial model suite of 100 realisations compared to 20 realisations, and f) similarity plot between the initial model suite of 100 realisations and GOO (top) and the initial model suite of 100 realisations and the PERG (bottom)). Finally, finding the optimal realisations and comparing this restricted model suite to the initial model suite of 100 realisations (g). .... 47

Figure 3.6: synthetic histogram showing the dataset distribution of target fraction values. .... 49

Figure 3.7: synthetic Lomb-Scargle periodogram showing one predominant peak (showing short-term periodicity), with a few smaller peaks which show longer term cyclicity within the dataset.	50
Figure 3.8: synthetic Goovaerts plot showing the creation of a sill when the standard deviations of an ever-increasing dataset (lag) is plotted, showing negligible changes to the distribution of the dataset.	52
Figure 3.9: synthetic comparison plot of the initial model suite of 100 realisations with the restricted ones created when using the PERG (periodic ergodicity) and GOO (point at which the standard deviation of an increasing dataset forms a plateau) values.	53
Figure 3.10: synthetic similarity plot using a restricted model suite (in this case, the first 35 realisations) to be compared to the initial model suite of 100 realisations (100 realisations), with the intersectional percentage being calculated. This is a numerical representation of how well a restricted model suite represents the variety of reservoir models present within a larger suite of models.	54
Figure 3.11: synthetic similarity plot comparing the initial model suite of 100 realisations (100 realisations) to the restricted model suite of the previously used number of realisations used (the first 20 realisations), with the intersection percentage being plotted. This is a numerical representation of how well a restricted model suite represents the variety of reservoir models present within a larger suite of models.	55
Figure 3.12: generalised workflow for finding the PERG (a and c) and GOO (b) values, and then these being used to compare restricted model suites with the initial model suite of 100 realisations (d) to then find the intersection percentages of increasing realisations numbers (e), until the optimal value is found (f) which is the largest intersectional percentage, giving the best representation of variety of reservoir models.	56
Figure 3.13: synthetic version of the similarity plot comparing the distributions of the restricted model suite to the first 18 realisations as given by the GOO value (top) and the first 38 realisations as given by the PERG value (bottom) to the initial model suite of 100 realisations, and then finding the intersection percentage of both to the initial model suite of 100 realisations.	58
Figure 3.14: synthetic similarity plot of the initial model suite of 100 realisations compared to the recommended number of realisations (35), showing the highest intersection percentage of all of the values for realisations between the GOO and the PERG. This produces the largest variety of reservoir models from the initial model suite of 100 realisations.	59
Figure 3.15: synthetic similarity plot comparing the initial model suite of 100 realisations to the restricted model suite of the previously used number of realisations used (the first 20 realisations), with the intersection percentage being plotted, giving a numerical value to the representation of the variety of reservoir models within the initial model suite of 100 realisations.	60
Figure 4.1: Comparison of the PERG, GOO and RR values for the mean geobody thickness values (bold lines), with the outlier values (residuals) removed (faint lines), across the (a) SIS, (b) OBM, and (c) MPS modelling algorithms, with values shown for all input target fractions.	63
Figure 4.2: Comparison of the PERG, GOO and RR values for the standard deviation of geobody thickness values (bold lines), with the outlier values (residuals) removed (faint lines), across the (a) SIS, (b) OBM, and (c) MPS modelling algorithms, with values shown for all input target fractions.	65
Figure 4.3: Comparison of the PERG, GOO and RR values for the output target fraction values (bold lines), with the outlier values (residuals) removed (faint lines), across the (a) SIS, (b) OBM, and (c) MPS modelling algorithms, with values shown for all input target fractions.	67
Figure 4.4: Comparison of the (a) PERG, (c) GOO and (e) RR values for the mean geobody thickness values, for each of the SIS, OBM, and MPS modelling algorithms, with values shown for all input	

target fractions. The standard deviations of these average results (detailing how spread out the values are) is given for the (b) PERG, (d) GOO, and (f) RR values. ....	69
Figure 4.5: Comparison of the (a) PERG, (c) GOO and (e) RR values for the standard deviation of geobody thickness values, for each of the SIS, OBM, and MPS modelling algorithms, with values shown for all input target fractions. The standard deviations of these average results (detailing how spread out the values are) is given for the (b) PERG, (d) GOO, and (f) RR values. ....	70
Figure 4.6: Comparison of the (a) PERG, (c) GOO and (e) RR values for the outputted target fraction values, for each of the SIS, OBM, and MPS modelling algorithms, with values shown for all input target fractions. The standard deviations of these average results (detailing how spread out the values are) is given for the (b) PERG, (d) GOO, and (f) RR values. ....	71
Figure 4.7: Distribution of the PERG values for the (a) mean geobody thickness, (b) standard deviation of geobody thickness, and (c) output target fraction, for the SIS algorithm. ....	73
Figure 4.8: Distribution of the PERG values for the (a) mean geobody thickness, (b) standard deviation of geobody thickness, and (c) output target fraction, for the OBM algorithm. ....	74
Figure 4.9: Distribution of the PERG values for the (a) mean geobody thickness, (b) standard deviation of geobody thickness, and (c) output target fraction, for the MPS algorithm. ....	76
Figure 4.10: Cumulative distribution function (CDF) of the PERG values for the mean geobody thickness, standard deviation of geobody thickness, and outputted target fraction, for each the SIS, OBM and MPS modelling algorithms, with the previously used 20 realisations marked on the graph. ....	77
Figure 4.11: Distribution of the GOO values for the (a) mean geobody thickness, (b) standard deviation of geobody thickness, and (c) output target fraction, for the SIS algorithm. ....	78
Figure 4.12: Distribution of the GOO values for the (a) mean geobody thickness, (b) standard deviation of geobody thickness, and (c) output target fraction, for the OBM algorithm. ....	80
Figure 4.13: Distribution of the GOO values for the (a) mean geobody thickness, (b) standard deviation of geobody thickness, and (c) output target fraction, for the MPS algorithm. ....	81
Figure 4.14: Cumulative distribution function (CDF) of the GOO values for the mean geobody thickness, standard deviation of geobody thickness, and outputted target fraction, for each the SIS, OBM and MPS modelling algorithms, with the previously used 20 realisations marked on the graph. ....	82
Figure 4.15: Distribution of the RR values for the (a) mean geobody thickness, (b) standard deviation of geobody thickness, and (c) output target fraction, for the SIS algorithm. ....	84
Figure 4.16: Distribution of the RR values for the (a) mean geobody thickness, (b) standard deviation of geobody thickness, and (c) output target fraction, for the OBM algorithm. ....	85
Figure 4.17: Distribution of the RR values for the (a) mean geobody thickness, (b) standard deviation of geobody thickness, and (c) output target fraction, for the MPS algorithm. ....	87
Figure 4.18: Cumulative distribution function (CDF) of the RR values for the mean geobody thickness, standard deviation of geobody thickness, and outputted target fraction, for each the SIS, OBM and MPS modelling algorithms, with the previously used 20 realisations marked on the graph. ....	88
Figure 4.19: Comparison of cumulative distribution function (CDF) of the RR values for the mean geobody thickness, standard deviation of geobody thickness, and outputted target fraction, for each the (a) SIS, (b) OBM and (c) MPS modelling algorithms. ....	89
Figure 4.20: Comparison of the total similarity (intersectional percentages) of the first 20 realisations compared to the RR value across all input target fractions, for each the (a) SIS, (b) OBM, and (c) MPS modelling algorithm. ....	91
Figure 5.1: variogram input data for the downstream accretion, lateral accretion, thalweg beform and channel element geobodies for the Tuscher Canyon SIS reservoir model (using data from the	

modern analogue of Jamuna River for the major and minor direction values) (from Mitten et al., 2020). .....	94
Figure 5.2: Comparison of the PERG, GOO and RR values for the mean geobody thickness values (bold lines), with the outlier values (residuals) removed (faint lines) for all values modelled in the developed suite of reservoir models, across the (a) SIS, (b) OBM, and (c) MPS modelling algorithms, with values shown for all input target fractions. The plots have then been overlaid with the actual PERG, GOO and RR values from the Tuscher Canyon model at each of the input target fractions for the specific architectural element (downstream accretion, lateral accretion, channel element, and thalweg bedform). .....	99
Figure 5.3: Comparison of the PERG, GOO and RR values for the standard deviation of geobody thickness values (bold lines), with the outlier values (residuals) removed (faint lines) for all values modelled in the developed suite of reservoir models, across the (a) SIS, (b) OBM, and (c) MPS modelling algorithms, with values shown for all input target fractions. The plots have then been overlaid with the actual PERG, GOO and RR values from the Tuscher Canyon model at each of the input target fractions for the specific architectural element (downstream accretion, lateral accretion, channel element, and thalweg bedform). .....	101
Figure 5.4: Comparison of the PERG, GOO and RR values for the outputted target fraction values (bold lines), with the outlier values (residuals) removed (faint lines) for all values modelled in the developed suite of reservoir models, across the (a) SIS, (b) OBM, and (c) MPS modelling algorithms, with values shown for all input target fractions. The plots have then been overlaid with the actual PERG, GOO and RR values from the Tuscher Canyon model at each of the input target fractions for the specific architectural element (downstream accretion, lateral accretion, channel element, and thalweg bedform). .....	103
Figure 5.5: Comparison of the total similarity (intersectional percentages) of the first 20 realisations compared to the RR value across the input target fractions of the downstream accretion, lateral accretion, channel element and thalweg bedform geobodies, for the mean geobody thickness, standard deviation of geobody thickness and outputted target fraction, for each the (a) SIS, (b) OBM, and (c) MPS modelling algorithm. ....	105
Figure 5.6: Comparison of the total similarity (intersectional percentages) of the first 20, 32 (RR for the suite of generated models), specific RR value for the Tuscher Canyon models, against 100 realisations. This is shown for the (a, d and g) mean geobody thickness, (b, e and h) standard deviation of geobody thickness, and (c, f and i) outputted target fraction, for each the (a, b and c) SIS, (d, e and f) OBM, and (g, h and i) MPS modelling algorithms. ....	108
Figure 5.7: Comparison of the total similarity (intersectional percentages) of the first 20, 32 (RR for the standard deviation of geobody thickness of the channel element for the suite of generated models), specific RR value for the Tuscher Canyon models, against 100 realisations. This is shown for the (a, d and g) mean geobody thickness, (b, e and h) standard deviation of geobody thickness, and (c, f and i) outputted target fraction, for each the (a, b and c) SIS, (d, e and f) OBM, and (g, h and i) MPS modelling algorithms. ....	112
Figure 6.1: Comparison of the (a) PERG, (c) GOO and (e) RR values for the mean geobody thickness values, for each of the SIS, OBM, and MPS modelling algorithms, with values shown for all input target fractions. The standard deviations of these average results (detailing how spread out the values are) is given for the (b) PERG, (d) GOO, and (f) RR values. ....	119
Figure 6.2: Comparison of the total similarity (intersectional percentages) of the first 20, 32 (RR for the standard deviation of geobody thickness of the channel element for the suite of generated models), specific RR value for the Tuscher Canyon models, against 100 realisations. This is shown for the (a, d and g) mean geobody thickness, (b, e and h) standard deviation of geobody thickness, and (c, f and i) outputted target fraction, for each the (a, b and c) SIS, (d, e and f) OBM, and (g, h and i) MPS modelling algorithms. ....	122

## List of Tables

Table 3.1: SIS input values showing major direction, minor direction, vertical height, and nugget values used to create the suite of fluvial reservoir models. ....	38
Table 3.2: OBM input values showing channel width, wavelength, amplitude, and vertical height values used to create the suite of fluvial reservoir models. ....	40
Table 3.3: MPS input values showing channel width, wavelength, amplitude, and vertical height values used to create the suite of fluvial reservoir models. ....	42
Table 5.1: input values for the downstream accretion, lateral accretion, thalweg bedform and channel element geobodies for the Tuscher Canyon OBM model (also acting as the training image conditioning data for the MPS algorithm), using data from Tuscher Canyon, with supplementary data about channel dimensions provided from the Jamuna River mdoern analogue (after Mitten et al., 2020).....	95
Table 5.2: Recommended number of realisations required for a statistically significant three-dimensional reservoir model suite to be developed for each the mean geobody thickness, standard deviation of geobody thickness and output target fraction for each of the studied geobodies for the Tuscher Canyon model using the SIS modelling algorithm. This shows significant variation across the different geobodies, with 68 realisations being shown to be the value for the channel elements standard deviation of geobody thickness value. ....	110
Table 5.3: Recommended number of realisations required for a statistically significant three-dimensional reservoir model suite to be developed for each the mean geobody thickness, standard deviation of geobody thickness and output target fraction for each of the studied geobodies for the Tuscher Canyon model using the OBM modelling algorithm. This shows significant variation across the different geobodies, with 27 realisations being shown to be the value for the channel elements standard deviation of geobody thickness value.....	110
Table 5.4: Recommended number of realisations required for a statistically significant three-dimensional reservoir model suite to be developed for each the mean geobody thickness, standard deviation of geobody thickness and output target fraction for each of the studied geobodies for the Tuscher Canyon model using the MPS modelling algorithm. This shows significant variation across the different geobodies, with 29 realisations being shown to be the value for the channel elements standard deviation of geobody thickness value.....	110

## List of Equations

Equation 2.1: Semi-Variogram Equation, where  $\gamma$  is the variance of the dataset at a given lag ( $h$ ),  $n$  is the number of values within a given lag distance,  $z(x_i)$  is the value with no lag distance, and  $z(x_i + h)$  is the value with lag distance of  $h$ . This  $\gamma$  value acts as the Y-value, and  $h$  denotes the lag distance (X-position) for the variogram (Figure 2.2). ..... 13

Equation 3.1: Periodicity equation used to determine the cyclicity of the random variable used to create the reservoir models (PERG value). ..... 50



## 1 Introduction

A reservoir model is a simplified numerical representation of the geology and geometries in the subsurface. Reservoir models are useful for characterising the subsurface within an area of interest. One of the common uses for reservoir modelling is to predict the geometry and distribution of facies (heterogeneity) in the subsurface in order to model fluid migration. Modeling the reservoir in this way is a particularly useful approach when applied to the strata of depositional settings in which the heterogeneity of facies (and, by inference, reservoir quality) varies over a range of scales that are below that of which can be imaged seismically (sub-seismic). One such example is strata deposited by fluvial systems.

Reservoir models can either be stochastic or deterministic. Stochastic models are models that are based upon a set of input parameters, but have a random variable incorporated into them. This variable is randomised each time a model is developed, creating a different version of the model for each realisation<sup>1</sup> (Renard et al., 2013). For stochastically developing a reservoir model, the input parameters will describe the general shapes of the architectural elements<sup>2</sup> within the reservoir model, and the random variable is used to describe the spatial distribution of the elements. This creates models comprising of comparable geobody shapes, but with different spatial positioning, which can lead to variation in the amount of channel stacking<sup>3</sup> across realisations. A deterministic model produces a result that is directly determined on the input parameters used (Renard et al., 2013). The same result will be generated regardless of the number of realisations developed (Renard et al., 2013). Well-to-well correlations can be used for deterministically developing a simple layer-cake reservoir model (Weber and van Geuns, 2005). Well-to-well correlations can be used to create deterministic reservoir models, but this is only possible with very close well spacing, which can be very expensive (Weber and van Geuns, 2005).

---

<sup>1</sup> Within this work, a realisation is described as being an individual representation of a model developed using a set of input parameters.

<sup>2</sup> When referring to a reservoir model, these architectural elements can be referred to as geobodies.

<sup>3</sup> Channel stacking represents the autogenic process of avulsion events within the reservoir model.

Where this close well spacing is not possible, probabilistic models can be made. These models 'bridge the gap' between stochastic and deterministic modelling processes, and create a variety of equiprobable scenarios (Weber and van Geuns, 2005). The wells can be used to create a framework for the model, where these act as pre-defined spatial anchors. Correlation between the wells is stochastically developed to create the reservoir model (Weber and van Geuns, 2005). The realisations developed from this approach will be different, but will preserve the spatial positioning of the pre-defined well positions. Probabilistic methods provide more accurate reservoir models than those created through stochastic models due to more information being known about the reservoir.

Reservoir models can also either be geocellular or surface models. Geocellular models are composed of a grid-like system of cells, whereby each cell represents a specified volume of a reservoir (this volume will depend on the cells dimensions) (Shepherd, 2009). Each cell contains information about that spatial position within the reservoir model (e.g., grainsize, and porosity and permeability characteristics). Geocellular models are particularly useful for producing petrophysical models, such as fluid flow and porosity-permeability models. This means that reservoirs can be better characterized and assessed for hydrocarbon extraction or carbon storage. Surface models are typically used to portray geological features such as horizons, faults and folds (de Kemp, 2021), which are useful for understanding the structural deformation history, and evolution of the flow field due to fracturing (Andersson and Hudson, 2004). This makes it ideal for exploration of minerals affected by dissolution and precipitation processes (Andersson and Hudson, 2004). Surface models are composed of layers that can bend, rather than cells that do not represent a continuous surface and cannot inherently bend, unless making use of an 8 corner point geocellular model. This makes surface models useful for representing structure within the subsurface, which makes them ideal for palinspastic reconstruction<sup>4</sup>.

---

<sup>4</sup> Restoring the cross-section of the subsurface to how it was prior to structural deformation (Vidal-Royo et al., 2015).

This study will focus on stochastic geocellular reservoir modelling, whereby all cells will represent the same volume, and use a center-point geometry since this is most commonly used within reservoir modelling. The high uncertainty of these stochastic three-dimensional geocellular reservoir models means that realisations generated with the same input parameters, are extremely unlikely to be identical. Each realisation may predict a variety of different reservoir volumes and quality, which will impact the economic viability of the reservoir. The generation of larger suites of reservoir models<sup>5</sup> typically decreases the uncertainty and increases the statistical significance<sup>6</sup> of the model suite. This decrease in uncertainty and increase in statistical significance enables a more informed decision to be made on the economic viability of a reservoir.

Current research shows that twenty realisations are required to develop a statistically significant two-dimensional reservoir simulation (Goovaerts, 1999), and consequently, twenty realisations are typically used to three-dimensionally model fluvial reservoir strata (Caers, Srinivasan and Journel, 2000; Tureyen and Caers, 2005; Benetatos and Giglio, 2021; Montero et al., 2021). A large number of studies make use of just ten realisations (Haldorsen and Damsleth, 1990; Seifert and Jensen, 1999; Liu et al., 2004; Falivene et al., 2006; Nordahl and Ringrose, 2008; Daly and Caers, 2010; Mitten et al., 2020), because ten realisations is the minimum number required to avoid ergodic fluctuations<sup>7</sup> (Falivene et al., 2006). The problem is further compounded by the fact that studies use several popular, and very different, methods for generating reservoir models. These reservoir modelling algorithms have been shown to develop realisations with differing characteristics using the same input values obtained from outcrop (e.g., Falivene et al., 2006).

One geological setting in which stochastic modelling in particular has been used extensively to predict the subsurface distribution of facies for economic appraisal, is the fluvial setting. The strata of fluvial systems comprise distinct elements each with distinct facies and very different

---

<sup>5</sup> Within this study, a suite of reservoir models (or suite of models) is described as a group of multiple realisations created with the same set of input parameters.

<sup>6</sup> In this study, statistical significance refers to a set of realisations (model suite) being representative of the reservoir being modelled.

<sup>7</sup> Variations between stochastic realisations (Falivene, 2006).

facies. The spatial distributions and geometries of the elements varies greatly over a range of scales and is governed primarily by the style of the fluvial system and by large-scale allogenic controls (e.g., basin subsidence rate, climatic variation, base level and sediment supply rate (Colombi, Limarino and Alcober, 2017)) and basin-scale autogenic controls (e.g., avulsion rates, grain size and sediment load (Postma, 2014)). All fluvial systems share the common characteristic that the variation of elements is below seismic resolution (sub-seismic).

Low sinuosity, bedload dominant (braided) systems are dominated by highly mobile sinuous- and straight-crested ripple- and dune-forms. Commonly, superimposition of these dunes can form barforms. Generally, this high channel mobility forms limited overbank deposits, however, mid-channel bars can become vegetated. In the subsurface, low sinuosity, bedload dominant systems are characterised by the dominance of planar and trough-crossbedded and cross-laminated sandstone fining-upwards sets. These systems will have an erosive base, with outsized clasts and larger, granule to cobble-sized clasts in the lowermost set, representing lower flow regime thalweg deposits. These systems are typically capped with upper flow regime ripples (from wash-over on top of the mid-channel bars. It is also possible, but unlikely to see overbank deposits preserved at the top of the succession, due to high channel mobility.

High Sinuosity, mixed load dominant systems are dominated by sinuous- and straight-crested dune-forms. These systems are generally stable, with the meanders generally getting steeper over time, and the formation of vegetated banks and levees. This leads to migratory point bars forming on the inside of meanders. The high channel stability leads to lateral accretion of the point bars, whereby sediment is deposited on the slope of the point bar, which is preserved as scroll bars in plan view. Ripples are likely to form on top of these point bars from wash-over. During times of higher discharge, chute channels may appear to cut through the point bars, and the levees can be breached, with crevasse splays forming. In the subsurface, high sinuosity, mixed load dominant systems are characterised by the dominance of planar and trough-crossbedded and cross-laminated sandstone fining-upwards sets. These systems will have an erosive base, with outsized

clasts in the lowermost section. Low-angle sets can appear throughout the succession and represent the lateral accretion from the point bars. The top of the channel fill succession is overlain by upper flow regime deposits due to gradual shallowing of the water. Typically, these are overlain by overbank deposits that may contain bioturbation and vegetation. It is also possible to find desiccation cracks, where floodwater has dried.

Whilst sediments deposited in fluvial systems don't necessarily always form the most productive hydrocarbon reservoirs, they can still be useful for the recovery of hydrocarbons (Tyler and Finley, 1991). When exploring the potential for carbon storage, channel interconnectivity and the ability for fluid flow within the preserved rock is important (Ringrose and Bentley, 2015). For an effective reservoir, the internal characteristics of the preserved structure must be known, and as this is highly variable (Ringrose and Bentley, 2015), stochastic reservoir modelling methods can be useful.

The research aims to determine the number of realisations required to model heterogeneity of elements in three-dimensional fluvial reservoir to a statistically significant level. Synthetic realisations are developed using three reservoir modelling algorithms and a range of realistic input parameters, and tested for statistical significance. Following analysis of the synthetic scenarios, a previously published three-dimensional reservoir model, from the fluvial strata of the Castlegate Sandstone formation exposed in Tuscher Canyon, Utah (Mitten et al., 2020) is used to determine the validity of the results obtained from this study.

## 1.1 Research aims and objectives

The overall goal of this project is to determine the number of realisations required for a statistically significant three-dimensional fluvial reservoir model suite. This project will be deemed a success if the two core aims are met:

**Aim 1:** Determine the average number of realizations required to develop a set of synthetic statistically significant three-dimensional fluvial reservoir models.

Objective 1: Develop a suite of synthetic reservoir models using a range of realistic, and non-realistic input parameters using a variety of modelling algorithms.

Objective 2: Determine the upper and lower limits of the search window.

Objective 3: Model the distributions of the sample population and compare it to the whole population to determine the optimal size of the sample population.

Aim 2: Determine the validity of the synthetic results in a real-world scenario.

Objective 1: Apply the developed methodology to a previously published geological model, specifically the model of Tuscher Canyon (with supplementary data supplied from the modern analogue of Jamuna River) as previously studied by Mitten *et al.*, 2020.

Objective 2: Determine the repeatability of the results from the synthetic dataset when applied to a real-world scenario.

Objective 3: Suggest any improvements or alterations needing to be made to the methodology.

## 1.2 Thesis signposting

This thesis details the creation of a representative suite of fluvial reservoir models along with their analysis using a novel methodology in order to determine the number of realisations required for a statistically significant three-dimensional reservoir model suite to be generated, along with a recommendation on how this research effects how fluvial reservoir modelling is carried out.

### 1.2.1 Chapter 2 – Literature Review

This chapter provides a comprehensive literature review on reservoir modelling, along with the techniques, and the challenges that are currently faced. This chapter will discuss: 1) the types of reservoir models available, 2) the types of fluvial rock model algorithms (SIS, OBM and MPS), 3) the uses of rock models for determining the characteristics of reservoirs, 4) general information about fluvial reservoir models, and 5) the current state of what is known about fluvial reservoir modelling.

### 1.2.2 Chapter 3 – Methodology

This chapter provides a detailed overview of methods by which the suites of reservoir models were generated, along with the methods and techniques used to analyze the properties that characterise the model suites. This is done by: 1) detailing the generation of the reservoir suites of models, and examining the input parameters and the different modelling algorithms used, 2) detailing the methods used to statistically model the properties characterising the reservoir models, 3) detailing the methods and workflow used to determine the optimal number of realisations required for a statistically significant three-dimensional reservoir model suite to be developed.

### 1.2.3 Chapter 4 – Analysis and Interpretation

This chapter provides analysis of the results achieved by applying the methodology outlined in Chapter 3 to synthetically generated suites of reservoir models. The chapter details the average number of realisations required for a statistically significant three-dimensional reservoir for the discrete variables produced from creating a large variety of synthetic fluvial reservoir models.

### 1.2.4 Chapter 5 – Application: Tuscher Canyon

This chapter provides application of the methodology and consequent results to the Tuscher Canyon reservoir model. The chapter details the: 1) geological background of the Lower Castlegate Sandstone, 2) results specific to the Tuscher Canyon models, with comparison to the suites of synthetic reservoir models 3) similarity percentages when a suite of 100 realisations are compared to suites of reservoir models containing: 20, 32 (average recommended number of realisations for the synthetic suites of reservoir models), and the recommended number of realisations for specific architectural elements of the Tuscher Canyon model, 4) recommended workflow for further three-dimensional fluvial reservoir modelling.

### 1.2.5 Chapter 6 – Discussion

The differences between the extensive suite of synthetic reservoir models and the application to the Tuscher Canyon model are discussed, with a final recommendation as to the best workflow to use. The limitations of the study are also considered.

### 1.2.6 Chapter 7 – Conclusion

This chapter covers the key points of the thesis and presents the further work that can be undertaken in the field of study. A short summary of the thesis is also provided.

## 2 Literature Review

Reservoir modelling enables geologists and reservoir engineers to generate three-dimensional representations of the subsurface (Ringrose and Bentley, 2015). These models can incorporate reservoir properties from two-dimensional reservoir simulators (Jacks, Smith and Mattax, 1973; Nilsen, Lie and Andersen, 2016). The type of reservoir model being used is dependent on several factors that need to be accounted for before it can be created. The first of these is the purpose for developing the model (e.g., visualisation, determining volumes, as an input for (fluid-flow) simulation, well planning, seismic modelling, enhanced oil recovery, or for carbon storage (Ringrose and Bentley, 2015)). Good reservoir design calls for a fit-for-purpose model, whereby flexible, faster, and tailored models are developed to solve a specific problem (Ringrose and Bentley, 2015). After this, the scale of the model is decided, followed by the amount of data (both hard and soft) that is required for a representative enough model to be developed (also known as determinism<sup>8</sup>). The required amount of determinism is strongly dependent on the purpose of the model (Ringrose and Bentley, 2015). The resolution of the model is important. Higher resolution models can incorporate significantly more geological detail and complexity than lower resolution models, but will also take significantly longer, and require far more computational power to construct (Gomez-Hernandez and Cassiraga, 1994). Higher resolution models will also take significantly longer to run computations on them (e.g., fluid flow) than other, lower resolution models. The user must consider both the size of the reservoir and the coarseness of the grid of cells being used to create the model as this will affect the computational demand to generate the model (Gomez-Hernandez and Cassiraga, 1994). In coarser gridded models, this usually means that smaller features will need to be re-scaled and representative, rather than being detailed (Nordahl and Ringrose, 2008).

---

<sup>8</sup> Increased amounts of hard and soft data will increase the determinism, but unless the geospatial distribution of the data is small, these models will be probabilistic and incorporate aspects of stochastic modelling.

## 2.1 Types of reservoir models

Reservoir modelling encompasses a range of properties related to the structural, stratigraphic, lithological and petrophysical properties of subsurface rocks (Mallet, 2002; Sacchi et al., 2016). Reservoir modelling has been used extensively to help predict the location, shape, and viability of hydrocarbon reservoirs or carbon sequestration potential, (Hosseini et al., 2013; Vo Thanh et al., 2019). There are three major types of reservoir model: rock models, petrophysical models (porosity and permeability), and stratigraphic forward models.

Rock models are a way of characterising the various relationships of subsurface structures, and facies present within a specific area of interest. These models are either 'conceptual', whereby the general characteristics (e.g. geometries and spatial distribution of facies) of the reservoir are modelled or 'conditioned' by making use of measured data (e.g., core logs), and interpreted data (e.g., seismic, drillers logs, geophysical logs or geological interpretations) inputs (e.g., Falivene et al., 2006; Martinius et al., 2017; Mitten et al., 2020; Carle and Fogg, 2020). This conditioning develops more realistic, and constrained reservoir models due to fewer cells needing to be determined.

Petrophysical models are developed from petrophysical data being applied to a facies model (Schlumberger Limited, 2022). They are used to calculate various reservoir characteristics e.g., shale volume, water saturation, porosity, effective porosity, and permeability (Schlumberger Limited, 2022). Porosity is a measure of the pore space to bulk volume ratio of a source rock and enables calculation of the total storage volume of a reservoir (Fisher et al., 2017), permeability is a measure of the ability of the flow of a fluid through a porous material (Fisher et al., 2017; Cannon, 2018; Ferguson, 2019), and effective permeability is the interconnected pore volume (Schlumberger Limited, 2022). Petrophysical models enable fluid-flow analysis (Pranter, Reza and Budd, 2006), volumetric calculations (Qadri, Islam and Shalaby, 2019) and production viability to be assessed (Jacobi et al., 2008), provide a visual representation of porosity-permeability

(Soleimani, Shokri and Rafiei, 2017), and are important for the determination of economic viability of a reservoir for hydrocarbon recovery, or carbon storage.

## 2.2 Rock model algorithms

Geostatistical methods of modelling rock models have previously fallen into three main groups: Pixel-based, Object-based, and Optimization methods (Tahmasebi, 2018), with methods making use of deep learning being recently added. Pixel-based methods are based on a set of points with defined properties (Tahmasebi, 2018). The methods are used to model both discrete (e.g., facies types) and continuous variables (e.g., porosity, permeability, fluid saturation) (Seifert and Jensen, 2000), and they aim to generate models that honor the input data to create a variogram which represents these values as a spatial two-point correlations (Strebelle and Journel, 2001). Object-based methods are considered as a group of stochastic objects defined by a specific statistical distribution (Haldorsen and Damsleth, 1990; Deutsch and Wang, 1996; Holden *et al.*, 1998; Skorstad *et al.*, 1999; Tahmasebi, 2018). Finally, Optimization methods rely on altering a model point-by-point, to iteratively produce a final model (Tahmasebi, 2018).

### 2.2.1 Neural Network Based Methods: GAN's

Generative Adversarial Networks (GANs) (Goodfellow *et al.*, 2014) are a type of deep learning algorithm to generate new content through competition between two neural networks called the generator and the discriminator (Sun, Demyanov and Arnold, 2023b). The generator is responsible for taking random noise and generating data that is representative of real data. The discriminator evaluates the data created by the generator alongside real data to determine which is real, and which is fake. Based on the response from the discriminator (and consequent feedback of whether the discriminator won or lost) both neural networks are trained using the loss function to minimize a 'loss' for both the generator and discriminator (Figure 2.1) (Sun, Demyanov and Arnold, 2023b). After multiple iterations, both neural networks can be trained to the point that the generator produces data that the discriminator finds indistinguishable from the real, training dataset.

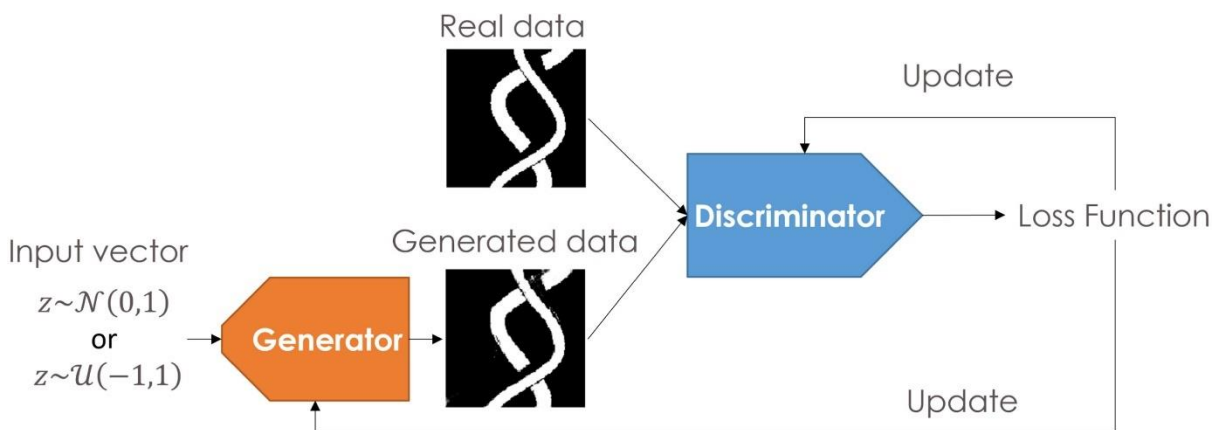


Figure 2.1: Flowchart of the GAN workflow, showing the generator create realistic data from an input vector (a set of elements with a uniform or normal distribution) which is then compared to the training dataset by the discriminator. The loss function is then used to train the neural networks until the discriminator is unable to distinguish between training data and the generated data (Sun, Demyanov and Arnold, 2023a)

GAN's have widespread usability, with them having such applications as image processing (Gu, Shen and Zhou, 2019), face detection and recognition (Zhao et al., 2019), medical image recognition (Kazemina et al., 2021), searching for new molecules (Blanchard, Stanley and Bhowmik, 2021), and reservoir modelling (Sun, Demyanov and Arnold, 2023a). GAN's such as FluvalGAN\_3DR (Sun, Demyanov and Arnold, 2023b) have successfully been used to model fluvial systems from stacking together multiple two-dimensional slices to create a three-dimensional volume.

Currently, the biggest benefits provided by using GAN's for reservoir modelling revolve around the increased realism between layers (when in a purely aggrading scenario) as previous layers can be used to condition subsequent layers, whilst also having a lower computational requirement due to the stacking of two-dimensional layers (Sun, Demyanov and Arnold, 2023b). The main drawback currently is the lack of application to any environment that is not purely aggradational since layers are stacked, and changes to previously modelled layers is not yet possible (Sun, Demyanov and Arnold, 2023b).

### 2.2.2 Pixel Based Methods: The Sequential Indicator Simulation

Sequential Indicator Simulation (SIS) is a type of modelling algorithm that uses variograms to populate a three-dimensional grid volume (Seifert and Jensen, 1999). A variogram (Figure 2.2, Equation 2.1) is a graphical depiction of the variance of a variable over a spatial random process, and it is composed of three main components: the nugget, the range, and the sill (Ringrose and Bentley, 2015). The nugget is the Y-intercept value of the graph and acts as a discontinuity value from below which values do not appear (Gill, 2009), and is a measure of the overall uncertainty in the variogram, the higher the value, the more uncertainty (Camana and Deutsch, 2019). The sill of the variogram is the point at which the variance of the values reaches 0 (Gringarten and Deutsch, 2003); and the range is the total lag distance required for the dataset to reach this sill, at which point the values of the variogram only incrementally increase (Li and Zhao, 2014).

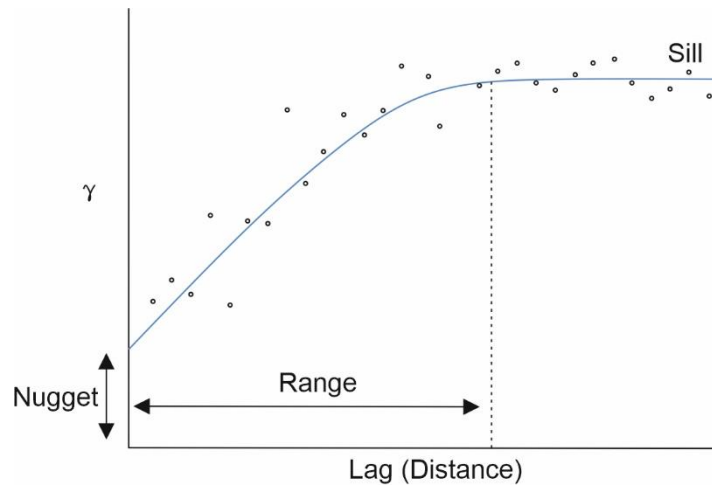


Figure 2.2: Synthetic variogram showing range, nugget, and sill. A variogram is a graphical depiction of the spatial variance of a variable. Variograms like this function as the basis for developing reservoir models using the sequential indicator simulation (SIS) algorithm after Ringrose and Bentley, 2015.

$$\gamma(h) = \frac{1}{2n} \sum_{i=1}^n (z(x_i) - z(x_i + h))^2$$

Equation 2.1: Semi-Variogram Equation, where  $\gamma$  is the variance of the dataset at a given lag ( $h$ ),  $n$  is the number of values within a given lag distance,  $z(x_i)$  is the value with no lag distance, and  $z(x_i + h)$  is the

*value with lag distance of  $h$ . This  $\gamma$  value acts as the Y-value, and  $h$  denotes the lag distance (X-position) for the variogram (Figure 2.2).*

The SIS algorithm uses both the indicator approach (Figure 2.3) and Monte Carlo simulation (Metropolis and Ulam, 1949) within its workflow (Deutsch, 2006; Zhou et al., 2018). The indicator approach (Figure 2.3) is where a random sequence of cells is selected rather than a more orderly row-by-row approach (Doyen, Psaila and Strandenes, 1994). For the Monte Carlo simulation, a CCDF (conditional cumulative distribution function) is used, meaning that after a cell within the model is determined, the new cell data is added to the dataset, and the probabilities are all recalculated (known as a backtransformation) (Journel and Alabert, 1990; Seifert and Jensen, 1999; Soares, 2001; Emery, 2004; Zhang, Switzer and Journel, 2006; Pyrcz and Deutsch, 2014; Ringrose and Bentley, 2015; Tahmasebi, 2018; Jika et al., 2020). This reliance of the distribution on the values regarding the distribution of values in the CCDF means that this backtransformation of data is crucial to the indicator approach used by the SIS algorithm (Figure 2.3) (Caers, 2000).

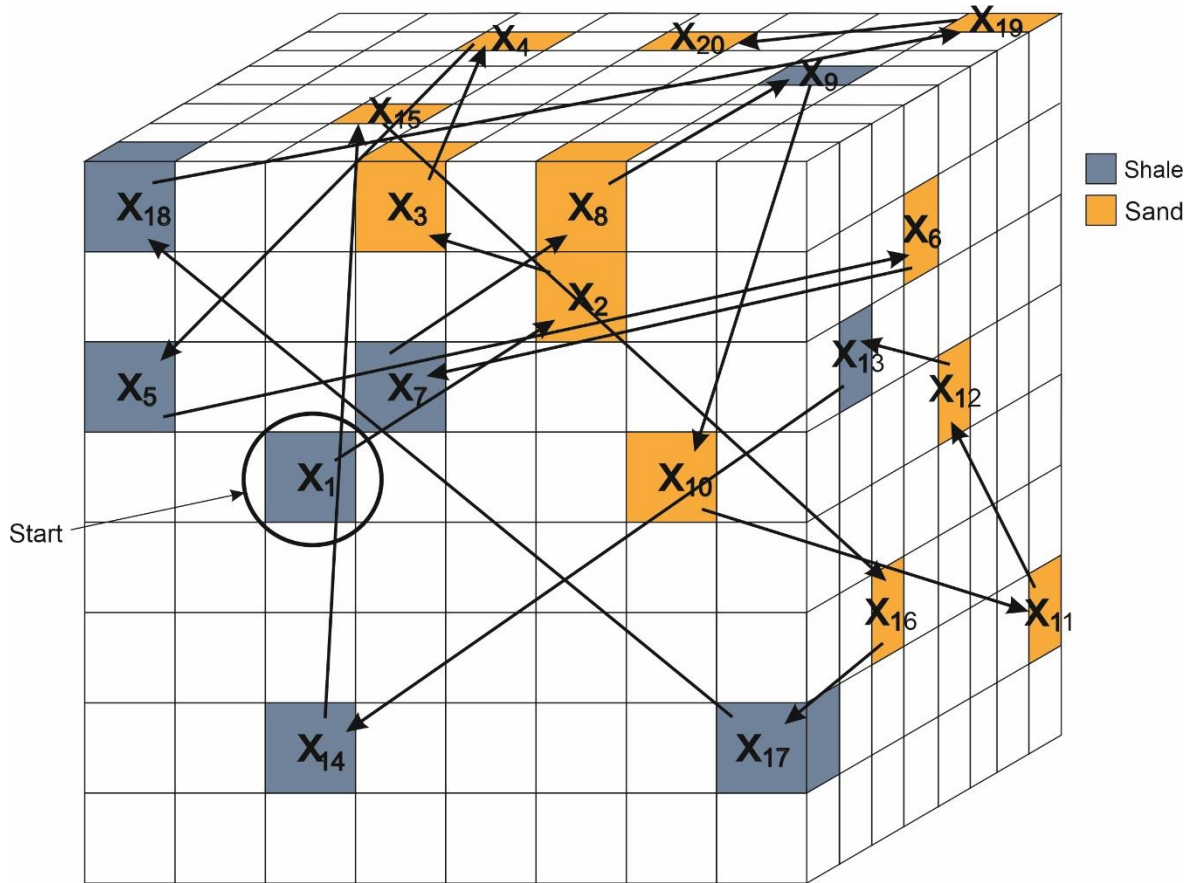


Figure 2.3: Graphical depiction of the indicator approach to the random nature of the selection of a cell for the SIS algorithm, with the random order of cells being visited, starting at  $X_1$  (circled). Once the cell has been visited, and its facies decided, in this case sand or shale, a backtransformation is applied to the conditional cumulative distribution function (CCDF). The next cell would then be randomly selected ( $X_2$ ), with this process repeating until all cells in the model have been visited.

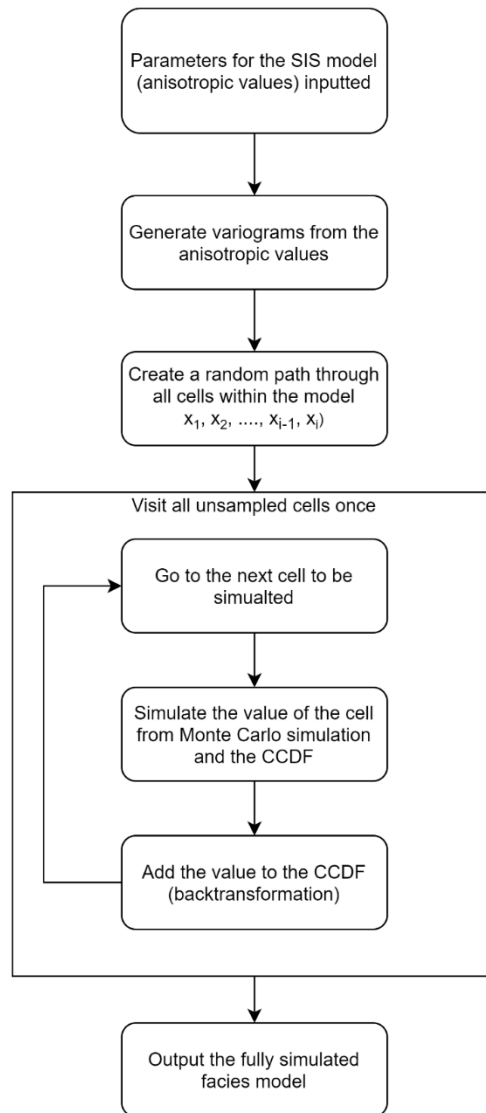


Figure 2.4: A generic flowchart for the SIS algorithm (adapted from Juang, Chen and Lee, 2004), detailing the workflow for the determination of the facies of each cell, backtransformation, and subsequently the creation of the reservoir model.

The SIS algorithm (Figure 2.4), has been used to model turbidites (Alabert and Massonnat, 1990), the Wilmington sand-shale sequence (Gomez-Hernandez and Journel, 1989), heavy-metal soil contamination (Juang, Chen and Lee, 2004), as a facies background of shallow marine, coastal plains and sheetflood bodies (MacDonald et al., 1992) and to model various rivers (Seifert and Jensen, 2000) such as the Jamuna River and Tuscher Canyon (Mitten et al., 2020). An example of an SIS-created reservoir model can be seen in Figure 2.5a.

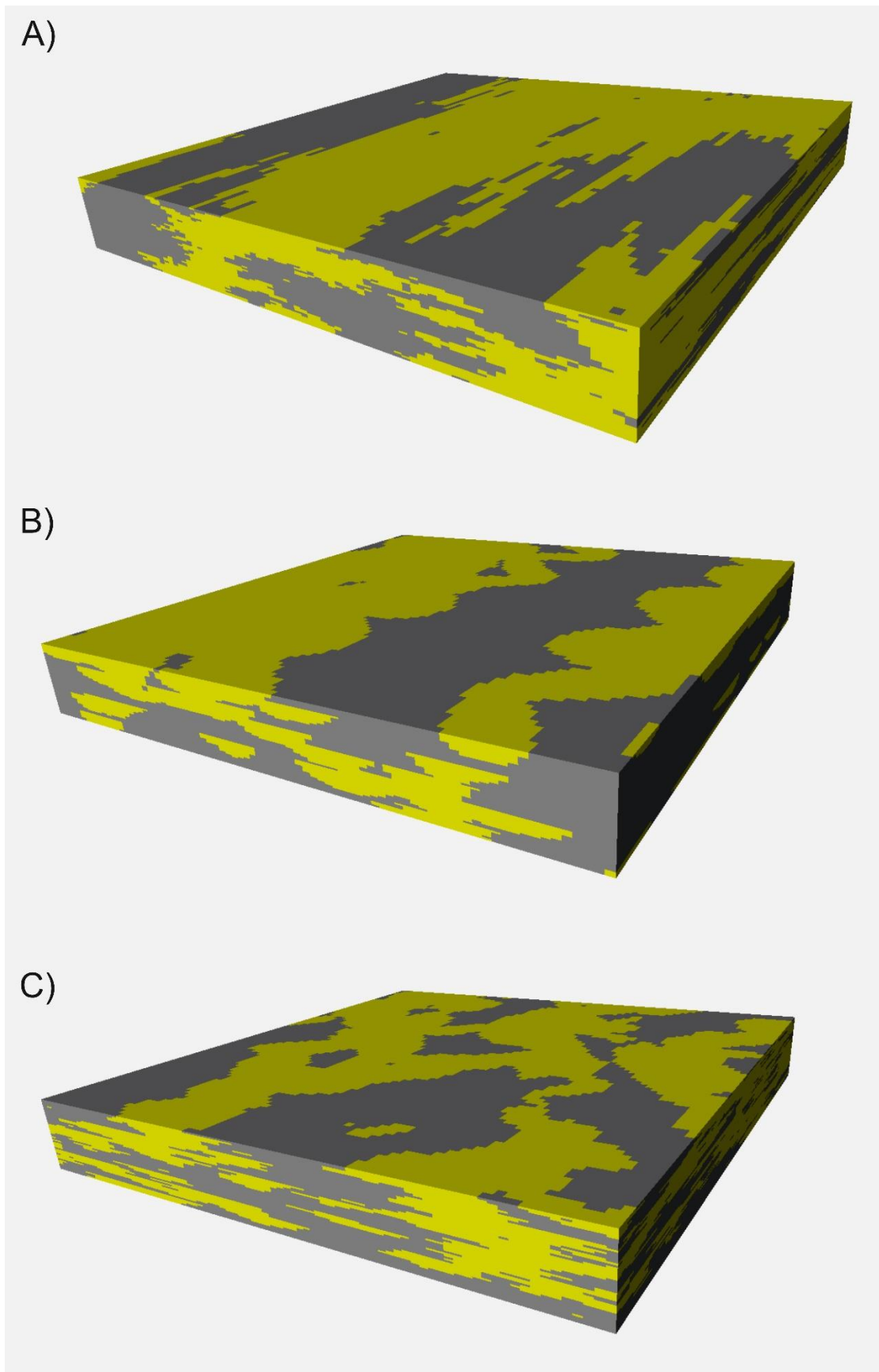


Figure 2.5: Comparison of equivalent synthetic reservoir models developed with the A) SIS, B) OBM, and C) MPS algorithm. The SIS model (A) was created using input parameters of 250 width, 2000m length, 10 vertical thickness, a nugget value of 0.0001, and target fraction of 50:50. The OBM model (B) was created

*using the input parameters of 250 amplitude, 500 wavelength, 250 width, 10 vertical thickness and target fraction of 50:50. The MPS model (C), was created using the OBM model (B) as a training image, and so effectively has the same input parameters. Models generated with the different modelling algorithms show distinct differences in both the representation, and style of the modelled geometries. The pixel-based algorithms (SIS – A and MPS – C) appear less clean than the object-based algorithm (OBM – B), with the individual cells being more prominently displayed. The SIS method appears far less realistic than the models generated with the other algorithms, and lacks any proper curvilinear, or naturalness. The OBM algorithm produces almost idealised geobodies, and represents nature, and curvilinear features better than the SIS algorithm. The models produced using the MPS algorithm are far more realistic, and enable both curvilinearity, and the randomness and chaos of nature to be captured within the model, producing by far the best, most realistic models.*

The main benefit of using this method for reservoir modelling is the ability to reproduce geological texture (Caers, 2000). SIS generated reservoir models also incredibly useful when there are either no clear genetic architectural shapes, or overly complex geobodies or facies interactions, that the OBM algorithm would struggle to model allow for the textural capabilities of the SIS algorithm to be fully utilised (Deutsch, 2006; Strebelle, 2012). Some models developed with the OBM algorithm have been used as a framework to create geological structure, with the facies distribution and texture being modelled using the SIS algorithm to provide a better distribution model (Cao, Zee Ma and Gomez, 2014). In comparison to OBM and the MPS algorithms, SIS more accurately represents the mean element proportions along with the mean element thickness and variability of downstream accretion elements (Mitten et al., 2020), and when the variograms are properly setup, better structure, and heterogeneity of inclined heterogeneous strata (IHS) can also be developed (Martinius et al., 2017). The SIS method also produces realisations that reproduce the mean element proportions far better than other methods (Mitten et al., 2020). With a large dataset (created from many model realisations being created), it is possible to assess the uncertainty within the resultant dataset, also allowing it to be quantified through analysis of standard deviation, mean geobody thickness and target fraction analysis. Usually this would be very time consuming, but pre-calculation of values is possible, for

them to be stored in a look-up table and called upon when required, consequently leading to shorter computational time (Tahmasebi, 2018; Gomez-Hernandez and Srivastava, 2021). Typically, the best usage of this model occurs when the architectural elements being recreated is unclear, when there are few curvilinear features, or when there is a high density of hard datapoints, such as close well spacing, or dense three-dimensional seismic data (Deutsch, 2006; Pycrz and Deutsch, 2014; Zhou et al., 2016). Finally, the SIS method benefits from a robust algorithm that is particularly easy to understand and can have the required statistical parameters being inferred from limited data (Deutsch, 2006) and can allow for better geological interpretation into reservoir modelling for flow simulation or reservoir management (Journel and Alabert, 1990).

The main drawback of the SIS algorithm comes with a lack of ability to accurately model complex geometries such as the sinuosity in fluvial channels (Seifert and Jensen, 1999, 2000), with this also extending to secondary fluvial channels, when misaligned from the main channel, ultimately becoming structureless blobs (Zhou et al., 2018). With the lack of being able to properly model channels in a direction differing from the main directions of the channels, lateral amalgamation of several channels is over-predicted, and subsequently skews data that could be returned from such models, such as net connectivity of the reservoir (Strebelle, 2012). Patchy and unstructured models also form due to the two-dimensional nature of the semi-variograms that are used to create the model, this can subsequently also lead to geologically unrealistic facies boundaries and transitional zones (Deutsch, 2006). The random sequence of the cells being visited can introduce ergodic periodicity into the dataset (Deutsch and Journel, 1992). SIS was also used as a training image for MPS modelling, but this proved to influence the resultant model too heavily with the removal of the ability to produce sinuosity (Ortiz and Deutsch, 2004; Ortiz and Emery, 2005).

### 2.2.3 Object-based Methods: Object Based Modelling

Object Based Modelling (Haldorsen and Chang, 1986; Haldorsen and MacDonald, 1987; Haldorsen and Damsleth, 1990; Deutsch and Wang, 1996; Lia et al., 1996; Holden et al., 1998; Visseur, 1999) represents different facies and objects distributed in space, using specific input parameters, such

as shape, channel size (width and thickness) and orientation (Dubrule, 1993, Holden *et al.*, 1998; Manzocchi *et al.*, 2007; Rezaee *et al.*, 2013; Vevle, Skorstad and Vonnet, 2018). This allows naturally occurring curvilinear features (Liu *et al.*, 2004) to be better modelled than some other methods. A drawback of this technique is that it is notoriously difficult to condition to data (Strebelle and Cavelius, 2014). OBMs are used solely for modelling discrete geological features such as facies types (Seifert and Jensen, 2000). OBMs tend to yield well confined channels, values such as lateral connectivity can be found to be reduced (unless a high net-gross is present, which is the total percentage of productive hydrocarbon volume within the model), hybrid methods of SIS and OBM methods have been utilized to counteract this. These hybrid methods create far more realistic, and natural models (Seifert and Jensen, 2000). The OBM method has been used to model the distribution of channels within fluvial reservoirs (Clemetsen *et al.*, 1990; Henriquez *et al.*, 1990; Pranter, Vargas and Davis, 2008), the distribution of crevasses and channels in the fluvio-deltaic Ness formation (Gundesø and Egeland, 1990), the Triassic Red Beds of Iberian Meseta (Yeste *et al.*, 2021), the Upper Cretaceous Blackhawk Formation, Utah (Villamizar *et al.*, 2015), the Beckwith Plateau, Utah, using the Mitchell Delta, Australia as a modern analogue (Nyberg *et al.*, 2019), and to model partially dolomitized remobilized carbonates, in the Gulf of Suez, Egypt (Corlett *et al.*, 2021).

An example of modeling software that utilizes the OBM algorithm is FLUVSIM (Deutsch and Tran, 2002), and it works through the following workflow. Sufficient channels to match the global proportions of each facies are placed randomly throughout the three-dimensional grid, with the number of crevasses attached to each channel dependent on the relative size of the channels being created, and the target proportions applied to crevasse splays. The sizes of the levees are also calculated and scaled to achieve the assigned proportion. Following this, four operations are defined: replace a channel object, add a channel object, remove a channel object, and correct a well interval. One of these operations is randomly called and applied to the model, and where it is involving the manipulation of a channel, it is picked randomly, and the various proportions are recalculated (Deutsch and Tran, 2002). This leads to the update of the model, whereby the

acceptance or rejection of that operation is decided by a simulated annealing schedule (Deutsch and Cockerham, 1994; Deutsch and Tran, 2002). Finally, the second step is repeated until the proportions match the user inputted values (Deutsch and Tran, 2002).

The process of creating the channels is iterated upon, with the multiple versions being used to constantly improve on the previous object, subsequently leading to the longer run times required (Figure 2.6) (Caers, 2001; Strebelle and Journel, 2001; Strebelle, 2002; Caers and Zhang, 2004; Liu et al., 2004). After the channels, and other objects are put into the three-dimensional model, the background fills any remaining cells.

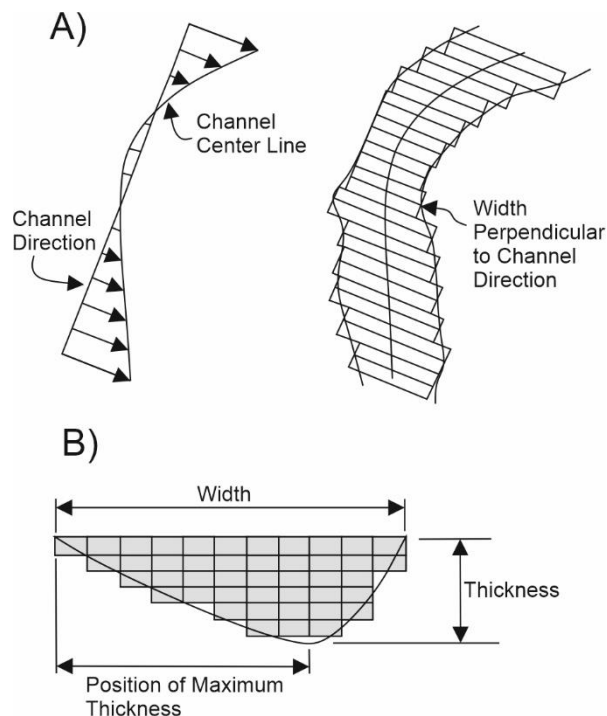


Figure 2.6: Aerial and cross-sectional view of the parameters used to define the channel structure within the object based modelling (OBM) algorithm. A) presents the aerial view, relating to channel direction and the central line of the channel, along with the width, whereas B) presents the cross-sectional view of the channel being presented in geocellular form, with relation to width, thickness, and position of the maximum thickness (dependent on the channel curvature) after Deutsch and Tran, 2002.

Whilst the OBM method is ideal for simulating realistic, curvilinear, geological structures (Figure 2.6b), there are some drawbacks, notably with the most realistic models requiring some sort of conditioning data, either hard well data or exhaustive secondary, but this proves to be a critical

limitation (Strebelle, 2012), as using hard data is very computationally taxing and requires a lot of time to simulate (Liu et al., 2004). This is also compounded by the fact that three-dimensional seismic cannot be used as a framework, with only two-dimensional seismic being compatible (Liu et al., 2004).

#### 2.2.4 Pixel Based Methods: Multiple-Point Statistics

The MPS (Multiple-Point Statistics) (Guardiano and Srivastava, 1993, and later developed upon by Strebelle, 2000, 2002) algorithm of modelling was developed to better model the complex curvilinear features found within nature (e.g., meanders and oxbow lakes), which previous modelling algorithms, such as SIS were unable to produce (Strebelle, 2002; Caers and Zhang, 2004; Strebelle and Cavelius, 2014; Tahmasebi, 2018). It combines the ability to realistically model curvilinear shapes (like object-based techniques) with the speed and ease of use of variogram-based techniques (such as SIS) (Strebelle, 2012). The MPS algorithm simultaneously uses multiple datapoints, which enable the modelling of complex shapes. Typically, since datasets are sparse and incomplete (Strebelle, 2012; Tahmasebi, 2018), a conceptual model of the expected structures found within the reservoir can be substituted in the form of a two- or three-dimensional numerical representation (Guardiano and Srivastava, 1993; Liu et al., 2004; Daly and Caers, 2010; Tahmasebi, 2018). These are referred to as TIs (training images) (Liu et al., 2004; Tahmasebi, 2018).

Typically, TIs are generated from process-based models, object-based models or from observed outcrop examples (Tahmasebi, 2018), but research has also created them from digital object models (DOM) originally created from Lidar scans, such as the work carried out in the Westwater Canyon Member of the Morrison Formation in New Mexico, USA (Pickel et al., 2015). Whilst it is common for these TIs to be images, they can also take the form of statistical properties (Tahmasebi, 2018), but these TIs must be representative of all of the possible shapes, dimensions, and relationships of geobodies thought to be present in the model (Strebelle and Journel, 2001; Caers and Zhang, 2004; Zhang, Switzer and Journel, 2006; Strebelle, 2012; Strebelle and Cavelius,

2014; Pickel et al., 2015). The biggest issue with the MPS algorithm is the lack of available training images, consequently, software such as TiGenerator was developed to create training images from the techniques used by the OBM algorithm (Maharaja, 2008), though it is still common that OBM models are used (Strebelle, 2002; Vevle, Skorstad and Vonnet, 2018). Notably, some examples of the usage of the MPS method include the Vadose zone of the Komadugu-Yobe River valley, southeastern Niger (Le Coz, Genthon and Adler, 2011), and Tuscher Canyon, Utah (Mitten et al., 2020).

Firstly, the algorithm searches for any available conditioning data (well data or previously simulated cell values) closest to the grid node that is currently being determined (Strebelle, 2000; Strebelle, 2012, Strebelle and Cavelius, 2014). A data event is then fully characterised by its geometrical configuration and its facies code (Strebelle, 2000; Strebelle, 2012). The training image is then scanned to find all similar structures within it (same geometric structure and facies code), and upon finding these will record the facies value at the central point of the training replicate (Figure 2.7) (Strebelle, 2000; Feyen and Caers, 2006; Zhang, Switzer and Journel, 2006; Strebelle, 2012; Strebelle and Cavelius, 2014).

After this, the estimated conditional probability is calculated for each facies at this point by the proportion of training replicates holding the same facies at the central location (Strebelle, 2000; Strebelle, 2012; Strebelle and Cavelius, 2014). Finally, the value of the specific cell being simulated is defined and determined from Monte Carlo sampling (Metropolis and Ulam, 1949) and assigned to the cell (Strebelle, 2000; Strebelle, 2012; Strebelle and Cavelius, 2014). Simply put, the method is a way of determining the probabilities of the occurrence of patterns (Okabe and Blunt, 2004), by using each of the various filters (Figure 2.7a), which then assign a probability to the cell (which is also added to a local conditional probability density function (CPDF) (Figure 2.7b) (Caers and Zhang, 2004; Zhang, Switzer and Journel, 2006). This process is repeated until all filters have been used, and the cell has a final probability (Caers and Zhang, 2004; Zhang, Switzer and Journel, 2006). This captures local patterns of the TIs, and enables points to be anchored onto the model

being built (Liu et al., 2004; Caers and Zhang, 2004; Zhang, Switzer and Journel, 2006). The indicator approach to this simulation is done by visiting each node in the current grid along a random path (Liu et al., 2004), with the gridding eventually getting finer and finer, to refine the value obtained in the coarser grid (Zhang, Switzer and Journel, 2006).

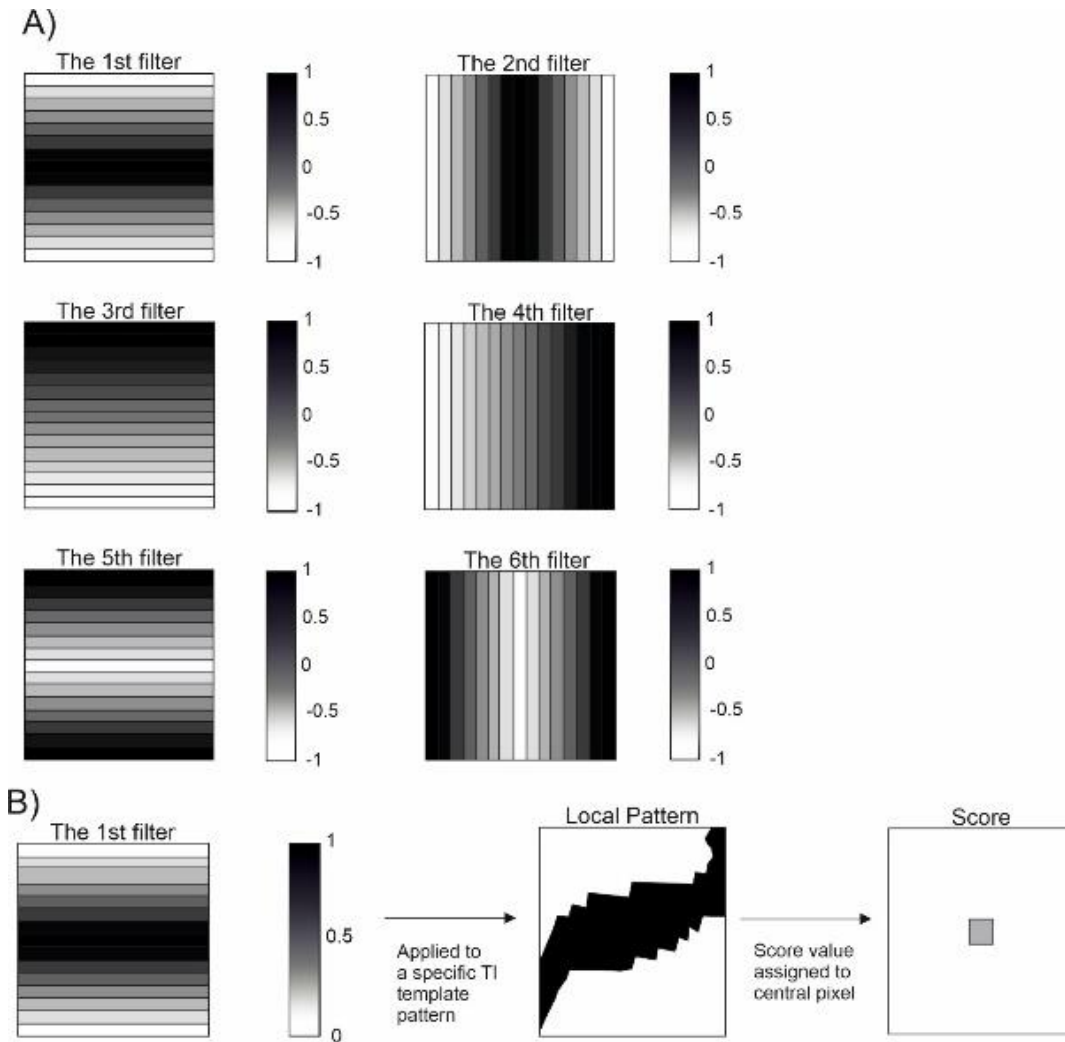


Figure 2.7: A) shows a variety of filters used on the local scale within the Multiple-Point Statistics (MPS) algorithm in order to transfer the general trends of the training image (TI) into the reservoir model. B) shows a worked example using the first filter presented in A) to provide a probability value to the cell, after Zhang, Switzer and Journel, 2006

One of the most notable variants of the MPS method is called SNESIM (Strebelle, 2000), where the MPS moments are stored within a search tree data structure allowing for quicker simulation, where the scanning phase is performed prior to simulation (Feyen and Caers, 2006; Strebelle,

2012). Sub-grids were also implemented to increase the relative proportion of previously simulated nodes in each nested grid (Strebelle, 2012). An example of a model generated using the MPS algorithm can be seen in Figure 2.5c (using an OBM model as a training image, Figure 2.5b), this has also been done to model the Triassic Red Beds of Iberian Meseta (Yeste *et al.*, 2021), which used the OBM method to create a training image of the outcrop/ behind outcrop (OBO) representation for the MPS algorithm to use. This helps to create geologically realistic models that honour the geostatistics created from the initial input parameters to be created (Caers and Zhang, 2004; Strebelle and Levy, 2008; Le Coz, Genthon and Adler, 2011; Hu *et al.*, 2014; Zhou *et al.*, 2018; Yeste *et al.*, 2021).

Whilst the MPS method is great at simulating the curvilinear geometry of natural formations, there are some drawbacks. A lack of similarity between internal patterns in the TI (Tahmasebi, 2018) is commonplace, but this can be solved by using OBM methods to develop the TI. Initially, the MPS algorithm made use of assuming homogenous distributions of facies proportions, geometries, and associations throughout the model, which doesn't work when applied to natural formations due to a lack of stationarity (Strebelle, 2012). Sparse well environments, or clustering of wells leads to a bias within the training image that would need to be corrected for (Strebelle, 2012), meaning that any TIs used must be densely populated (Strebelle and Journel, 2001; Tahmasebi, 2018). This subsequently means that there is a large strain on computational power when both analyzing TIs and informing the model based off of the results of the local CPDF (Strebelle and Journel, 2001). Finally, it is used slightly less than other methods due to increased complexity, run time and practical limitations, which include non-stationarity<sup>9</sup> (Strebelle and Zhang, 2004; Eskandari and Srinivasan, 2010; Zhou *et al.*, 2018), uncertainty in the geological scenario, and subjectivity in TI selection (Strebelle, 2002). The increased run time could be improved upon by using bunch simulation rather than pixel simulation, so as to increase the

---

<sup>9</sup> The mean and variance change throughout the modelled area due to a local conditional probability density function being constantly updated when using the filters to determine the probability of points in the TIs

efficiency of the entire simulation by a factor of the total bunch size (Figure 2.8) (Rezaee et al., 2013).

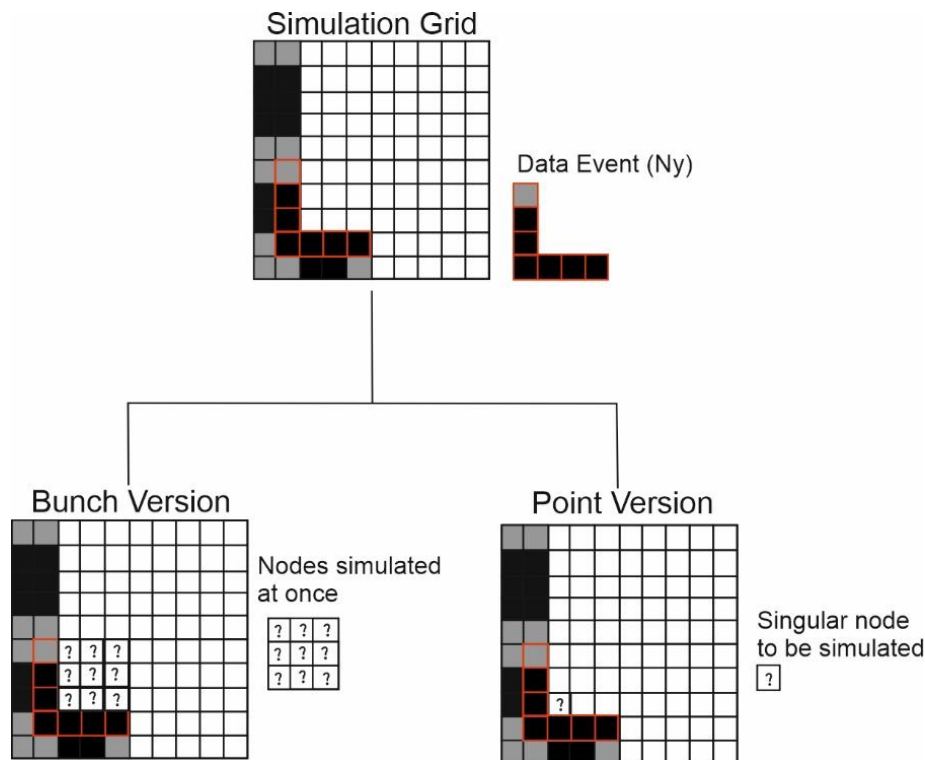


Figure 2.8: Pixel and Bunch Based approaches to the simulation process of Object Based Modelling (OBM).

The top depicts the original grid, with the left showing a 3x3 grid of cells being simulated at the same time (bunch processing), and the right showing a singular cell being simulated. This can improve the computational time required for the MPS algorithm to develop models, after Rezaee et al., 2013.

### 2.3 Rock model analysis

In terms of a reservoir, connectivity is the concept of the existence of a path-like structure within the subsurface of the same rock composition, through which fluids can migrate (Renard and Allard, 2013). This is essential for drainage of an oil or gas field, to the point where, if part of a reservoir is not connected to a producing well, then no hydrocarbons will be recovered (Larue and Hovadik, 2006; Hovadik and Larue, 2010). The connectivity structure of heterogeneous facies strongly influences the fluid flow (Renard and Allard, 2013), and ultimately the effectiveness, and efficiency of a reservoir. This property is split into two distinct versions – static and dynamic (Renard and Allard, 2013). The former of these cannot describe the connectivity, but instead

should be seen as more of a two-point statistical method of defining the probability of having a specific connectivity at a point (Renard and Allard, 2013) (such as how a semivariogram is used to describe the probability of a facies being present within a cell in the SIS modelling algorithm). Dynamic connectivity is instead reliant on a process-based approach, where the physics behind the creation of the sedimentary structures is considered. This requires knowledge about the geometry, and additional physical parameters, such as boundary types and reservoir saturation (Renard and Allard, 2013).

Geobody (also known as sand-body) connectivity is also used to describe the connectivity of a reservoir and is done by analyzing the structure of the geobody in its entirety rather than an instantaneous point (Renard and Allard, 2013), and is a measure of the total percentage of a reservoir that can be drained from a single well (Larue and Hovadik, 2006). In fluvial systems, there is usually low connectivity between the point-bar sand bodies, with far higher connectivity being found within the sand-rich (channel infill) intervals, where amalgamated sand bodies become more common (Pranter *et al.*, 2007).

It has also been found that after the proportion of sand within a system surpasses 50%, the degree of connectivity rises steeply, within a two-dimensional model (Allen, 1978). In a three-dimensional model, percolation theory has been used with a link to connectivity, from which, it was found that the percolation threshold occurs at approximately 25% net-to-gross ratio of sand (King, 1990; Allard and HERESIM Group, 1993), meaning that the connectivity of geobodies found within a modelled space is very low, until 25% net to gross, at which point connectivity dramatically increases. In models where net-to-gross is being incrementally increased, connectivity has been described to form a 'cascade zone', where the connectivity against net to gross ratio forms an S-curved graph (Figure 2.9) (Larue and Hovadik, 2006). This was also deemed to be the case for a two-dimensional slice (Figure 2.9a), but in a three-dimensional model (Figure 2.9b), the percolation threshold occurred at ~25%, the two-dimensional slice required ~60% net to gross (Larue and Hovadik, 2006).

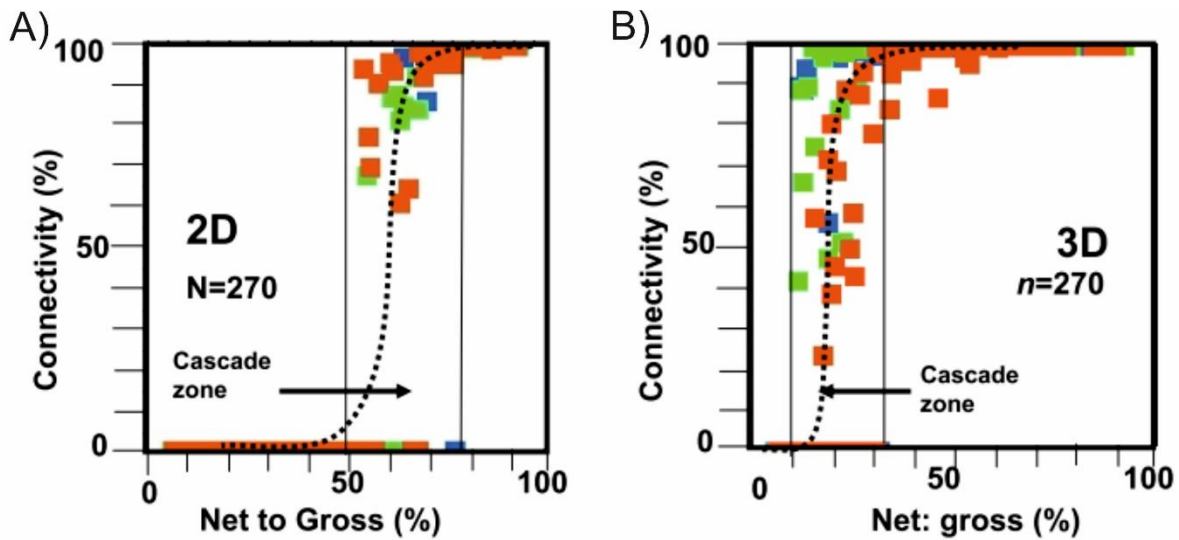


Figure 2.9: A) shows the two-dimensional representation of the connectivity-net to gross relationship, with the cascade zone appearing between 50% and 80%, whereas B) shows the same connectivity-net to gross relationship, with results being significantly shifted towards the left in the three-dimensional model. The drastic shift of the cascade zone of the connectivity of a three-dimensional model in comparison to a two-dimensional model suggests that two- and three-dimensional reservoir models should be treated as separate entities, with different characteristics (from Larue and Hovadik, 2006).

## 2.4 Fluvial reservoir models

When modelling fluvial systems, there are several characteristics that are needed to keep in mind to develop a representative model. Specifically, there are the: type of fluvial system, channel density, channel sinuosity, typical channel dimensions, single or multi-channel and the internal channel architecture (proportion of sand to mud within the main channel), though depending on the use of the reservoir, the model may neglect to show the internal channel architecture (Ringrose and Bentley, 2015). Such models as that of the Lower Castlegate Sandstone, Utah, describe the internal channel architecture (Mitten *et al.*, 2020). The Lower Castlegate Sandstone is composed of eight facies (one structureless conglomerate, six sandstone facies and one fine grained siltstone), along with four major geobodies (cut and fill channel elements, thalweg bedform complexes, downstream and laterally accreting barforms) (Miall, 1993, 1994; Yoshida, 2000; Mitten *et al.*, 2020).

Connectivity is arguably the most important property when it comes to fluvial reservoirs, and this can be modelled by the percolation theory, where channel connectivity is modelled based on probability (Ringrose and Bentley, 2015). The point at which the percentage of cells within a model needing to be filled (by a channel) in order to be connected is different for different models (Ringrose and Bentley, 2015), for example, the percolation threshold for overlapping sandstone object (as boxes in three-dimensional models) was seen to be approximately 0.25 (King, 1990), whereas stochastic models of intersecting sinuous channels has this value at between approximately 0.2 and 0.6 (Larue and Hovadik, 2006), ultimately suggesting that connectivity is proportional to channel sinuosity. Connectivity can be hampered by vertical or horizontal compartmentalization, arising from either a laterally extensive permeable depositional layer, faulting or even just from channel avulsions not linking up with previous channel deposits (Larue and Hovadik, 2006).

Alongside net to gross, reservoir architecture is also incredibly important for determining the total connectivity of the reservoir. For example, smaller, more sinuous channel deposits reduce the variance in connectivity of a reservoir (Larue and Hovadik, 2006). Higher channel sinuosity ultimately means that a channel occupies a larger horizontal width of the reservoir (Figure 2.10), consequently increasing the probability of vertical channel overlap, and ultimately the connectivity of a reservoir. The increase in reservoir connectivity is so large that the variation in connectivity is consequently decreased as connectivity reaches its upper limit of 100%.

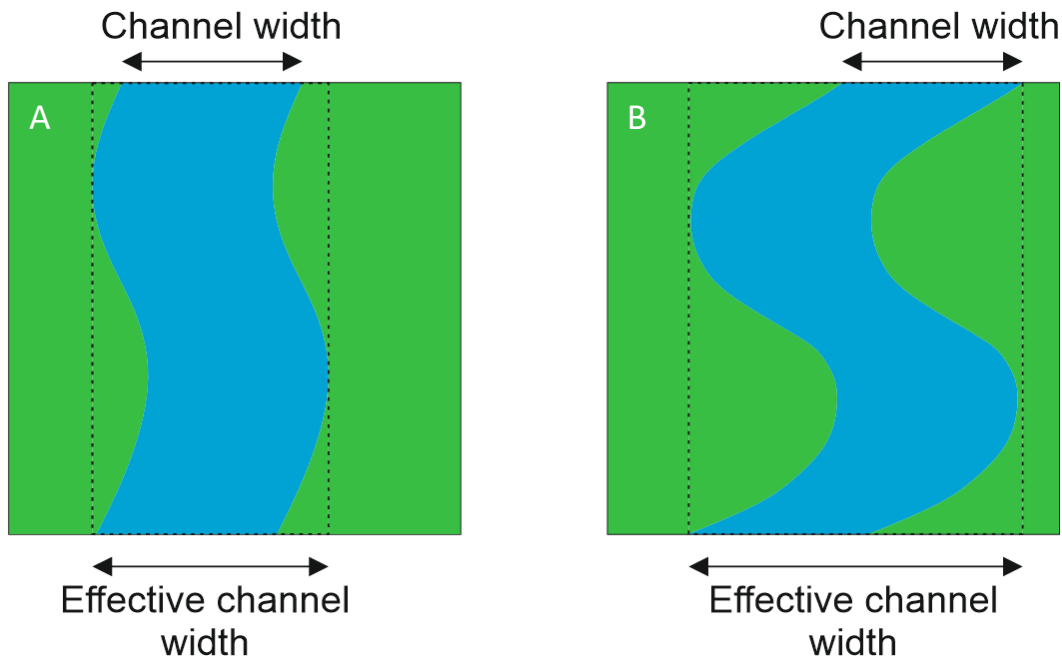


Figure 2.10: the effect of sinuosity on two channels of the same width. Channel A has far lower sinuosity than Channel B, and as such has a smaller effective channel width. Effective channel width in this case is the total width that the channel occupies. A higher effective channel width results in higher probability of channel stacking, and consequently a higher channel connectivity.

## 2.5 Model realisations – answers and problems

There are four main considerations to be made when rock models are developed: the statistical significance, the reproducibility, efficiency, and the detail and resolution of the models being simulated. a statistically significant rock model in a two-dimensional section is produced when there are approximately 20 realisations/ realisations created (Figure 2.9). More realisations than this this decrease the size of the uncertainty marginally, meaning that a larger dataset will produce diminishing returns after a certain point (Goovaerts, 1999). This approach was used to predict flow properties for water cuts and oil recovery, with 80 sample permeabilities being randomly selected from a possible 1600 minipermeater measurements to act as conditioning data (40 x 40 minipermeater measurements taken from a 2 by 2-foot vertical section of Berea sandstone), with 100 realisations developed from this, making use of p-field, sequential Gaussian, and sequential indicator simulation (Goovaerts, 1999).

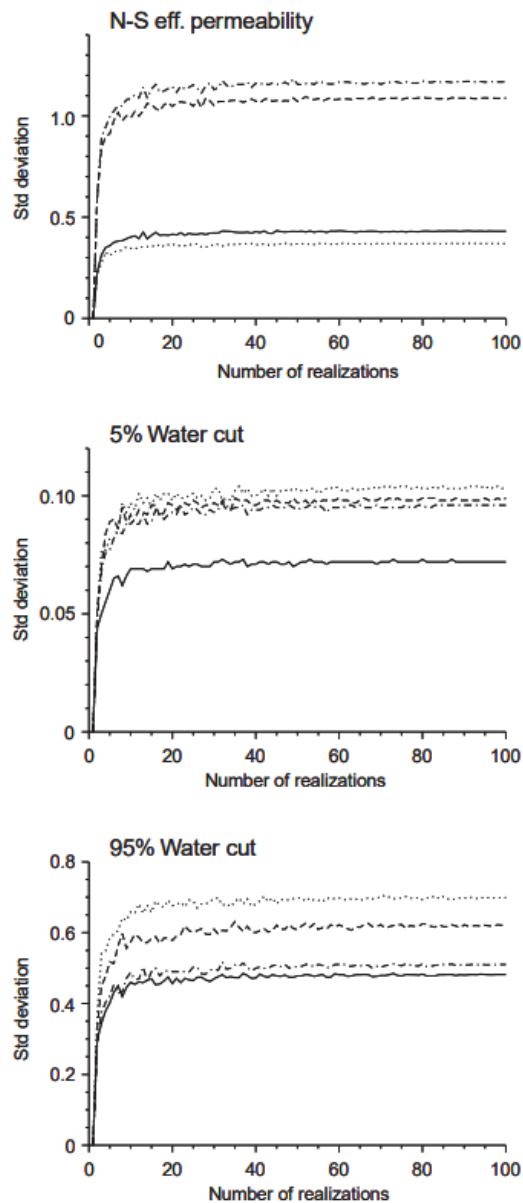


Figure 2.11: The minipermeater data being used to create porosity permeability models, and the standard deviation of these models being plotted against number of realisations (lag), to produce variograms. The standard deviation values plateau at approximately 20 realisations, suggesting diminishing returns, when it comes to total variation of the models past this number of realisations (after Goovaerts, 1999).

The time taken to generate reservoir models is not the only concern, another major factor is the accuracy of the resultant rock model. A larger pool of data will create more reliable and realistic reservoir models, since these hard data acts as a framework to condition surrounding values (Falivene et al., 2006). Any soft data uncertainties, such as those presented from using geologic interpretation, driller's logs, geophysical logs, or imaging (Carle and Fogg, 2020) are minimal over

an average of 10 realisations (Falivene et al., 2006). The workflow (Figure 2.12) centered around the use of as much hard and soft data that could be extracted from a sandstone filled turbidite channel, from a Quarry outcrop in the Ainsa basin (Falivene et al., 2006). The analysis of the results (Figure 2.12) showed that the SIS, TGS (truncated Gaussian simulation) and OBM algorithms struggled to represent the three-dimensional nature of the undulating beds, with the MPG (also known as MPS) algorithm representing these undulations well (Falivene et al., 2006).

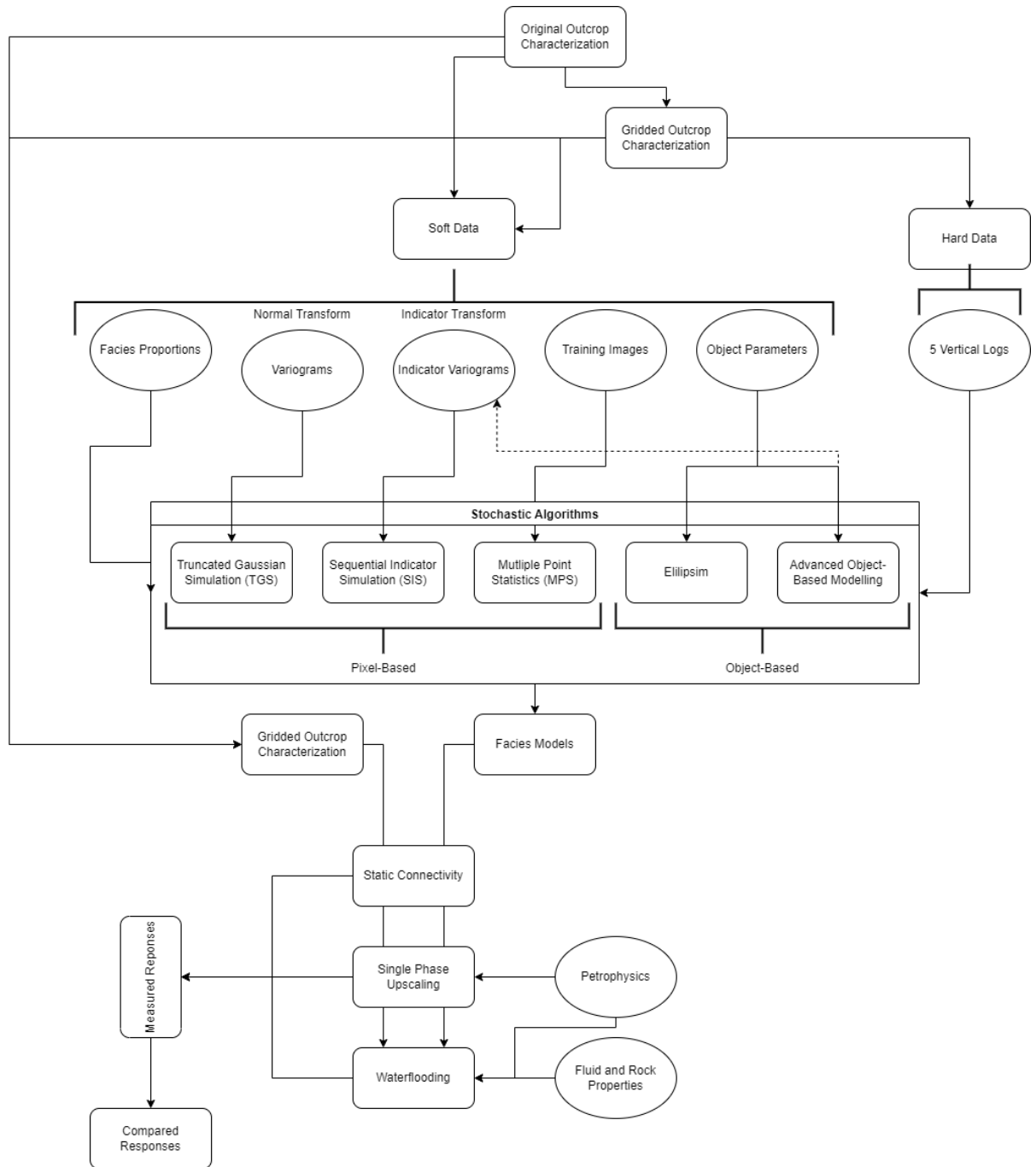


Figure 2.12: Flowchart showing the processes used to develop reservoir models from outcrop behind outcrop (OBO) models (after Falivene et al., 2006)

Where the algorithm was set up to expect undulations, very realistic models were produced, with continuous sandstones being modelled when unaccounted for (Falivene et al., 2006). Even though this was carried out on a two-dimensional section, the results from this study show that the discrepancies between outcrop and the models appeared to be algorithm based rather than data dependent, variogram based methods struggling to represent sinuosity or undulations (Falivene

et al., 2006).

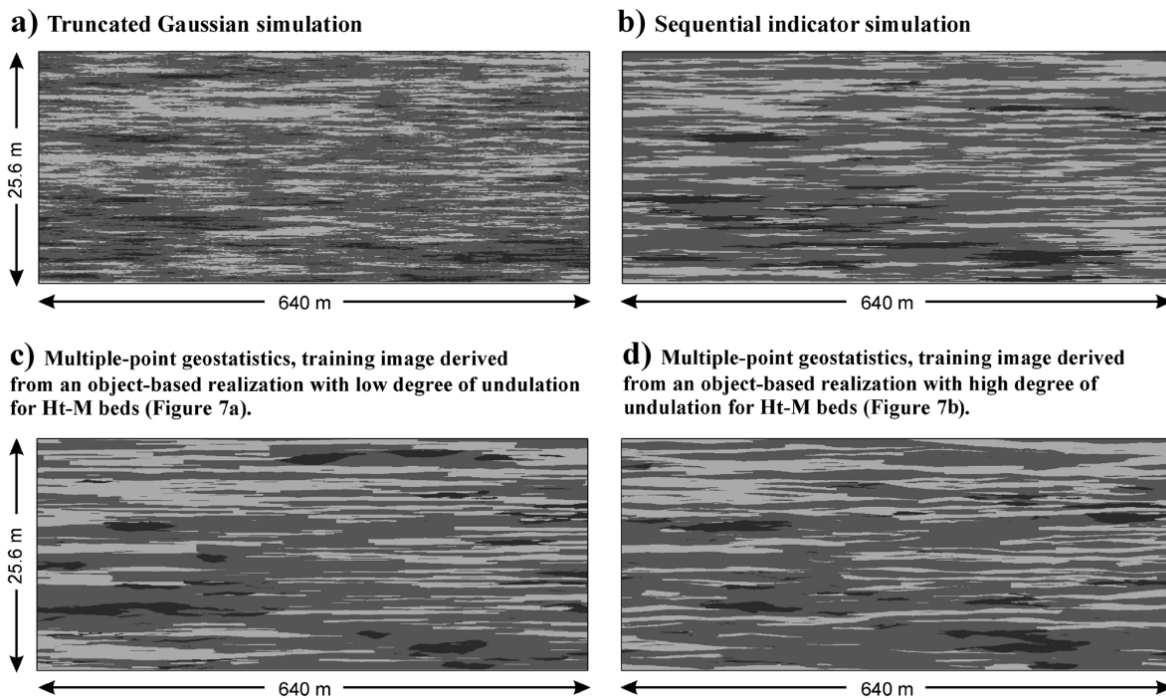


Figure 2.13: Examples of the different two-dimensional panels achieved from the workflow in Figure 2.12, displaying the variation of different algorithms using similar input parameters. This hints at discrepancies in model representation being present (Falivene et al., 2006).

What is currently not known, is how many realisations are required to create a statistically significant three-dimensional reservoir model suite, with a variety of algorithms, and with various parameters, such as target fractions, major and minor directions, and vertical values.

## 2.6 Summary and Discussion

Previous work focuses on a variety of different modelling types and methods, with the earlier, and more primitive, methods paving the way for huge advancements in the field of reservoir modelling. Prior work in the fields of statistical significance, and realism of reservoir models (Goovaerts, 1999; Falivene et al., 2006), coupled with the differences in static connectivity between two-dimensional and three-dimensional models (Larue and Hovadik, 2006), suggests that the approximate 20 realisations required for a statistically significant two-dimensional reservoir model may not be correct for an equivalent three-dimensional model. The difference in static connectivity between two-dimensional and three-dimensional models suggests that the

three-dimensional nature of reservoir modelling completely changes a model's fundamental properties, and as such, suggests that the number of realisations required for a statistically significant three-dimensional reservoir model suite should also change - this is the focus of this research.

## 3 Methodology

This chapter will outline three main sections of the methodology being used within this study:

- The creation of suites of fluvial reservoir models;
- The initial statistical modelling methods of the generated reservoir models;
- The statistical analysis of the datasets obtained from the initial statistical modelling.

### 3.1 Data Collection

The synthetic suites of reservoir models used in this study were created by using the Schlumberger™ Petrel v.2020 software. The models were developed within a 2,000m x 2,000m x 50m grid, composed of 320,000 cells per model, with a cell resolution of 25m x 25m x 1m to reflect the homogeneity in the X and Y direction in sedimentary systems, with more of a focus to capture high resolution detail in the Z axis (Enge et *al.*, 2007). This grid design provides a balance between the duration of time for the models to be developed, whilst also providing a large enough area to effectively visualise heterogeneity.

The focus of this study is to determine the number of realisations required in order to develop a statistically significant three-dimensional reservoir model suite. One hundred realisations (as previously used by Goovaerts, 1999) were generated for each set of input parameters for each of the SIS, OBM and MPS algorithms. The realisations were repeated across a range of sand to shale ratios of 20:80, 30:70, 40:60, 50:50, 60:40, 70:30 and 80:20, presented as a percentage target fraction of the total model volume. Together, the realisations provide a representative sample of model suites that ensure wider ranging applicability of the study.

#### 3.1.1 Reservoir Models

To provide wider scale applicability of this study, three of the most popular reservoir modelling algorithms are used:

- Sequential Indicator Simulation (SIS)
- Object Based Modelling (OBM)

- Multiple-point Statistics (MPS)

Each of these modelling algorithms requires a distinct set of input parameters, which can make it difficult to compare results from different algorithms. Since the suite of models will be analysed with respect to each other, it is important that the input parameters used with each algorithm create realistic models of fluvial systems, with a mixture of bedload and suspended load styles, that are comparable across algorithms.

#### *Sequential Indicator Simulation - SIS*

In order to develop the synthetic suites of models, the SIS algorithm requires input values for:

- Major Direction (fluvial channel length)
- Minor Direction (fluvial channel width)
- Vertical Height (fluvial channel thickness)
- Nugget value (the y-intercept of the variogram used to create the model and effects the variability of the models being produced) (see Figure 2.2)

The proposed variogram parameters for the SIS modelling algorithm were selected to provide a wide range of both 'realistic', 'fringe-case', and 'unrealistic' fluvial reservoir models. Realistic input parameter values provide proof that the methodology has real-world viability; fringe-case and non-realistic input parameter models provide proof of widescale applicability, whilst also increasing the pool of test-cases. Channel width to thickness (W/T) ratios of fluvial systems is very variable dependent on the style of fluvial system, and the characteristics of the channel (e.g. discharge rate, sediment load, and slope steepness) (Gibling, 2006). Generally, braided and low-sinuosity rivers will have a W/T value between 50-1000, meandering rivers will have a W/T ratio between 30-250, and distributary systems will have a W/T ratio between 5-30 (but this becomes more variable at 1-250 for distal alluvial fans and aprons) (Gibling, 2006). Whilst the generation of sinuosity is a limitation of the SIS algorithm, the wide range of channel width to thickness ratios (given by the variation of the channel width and channel thickness input parameters) should

provide a good compromise for modelling a wide range of fluvial systems, whilst also providing comparison to the OBM and MPS modelling algorithms.

To create a represented suite of models a wide range of input parameters is required. The ranges of parameters used in this work are detailed in Table 3.1 below.

Major Direction	Minor Direction	Vertical Height	Nugget
500	125	5	0.0001
1000	250	10	
1500	375	15	
2000	500	20	
3000			

*Table 3.1: SIS input values showing major direction, minor direction, vertical height, and nugget values used to create the suite of fluvial reservoir models.*

The range of major directions (Table 3.1) is defined such that it will not produce models with channels lengths extend beyond the model. This was done to see what affect, if any, major direction had upon the reproducibility of such models. To account for more realistic geological features, the major direction value of 3000m is also included. This enables channels to be projected beyond the 2000m reservoir model grid, providing a continuous geobody, thus a more realistic comparison to the OBM and MPS algorithms can be made, where the channels are more readily projected through the grid.

The ranges of values used for the minor and vertical directions (Table 3.1) are designed to generate a wide variety of channels with realistic properties. These geometric input parameters together with target fractions generating 560 different model sets being generated.

The wide ranges of values for both the channel width (125 to 500) and the vertical thickness (5 to 20) are summarised within Figure 3.1, where all other input parameters are the same. The channel width and vertical thickness values lead to large variations in the generated models. It is

important to use a wide range of input parameters to encompass the broad range of possible real-world scenarios.

## SIS Algorithm

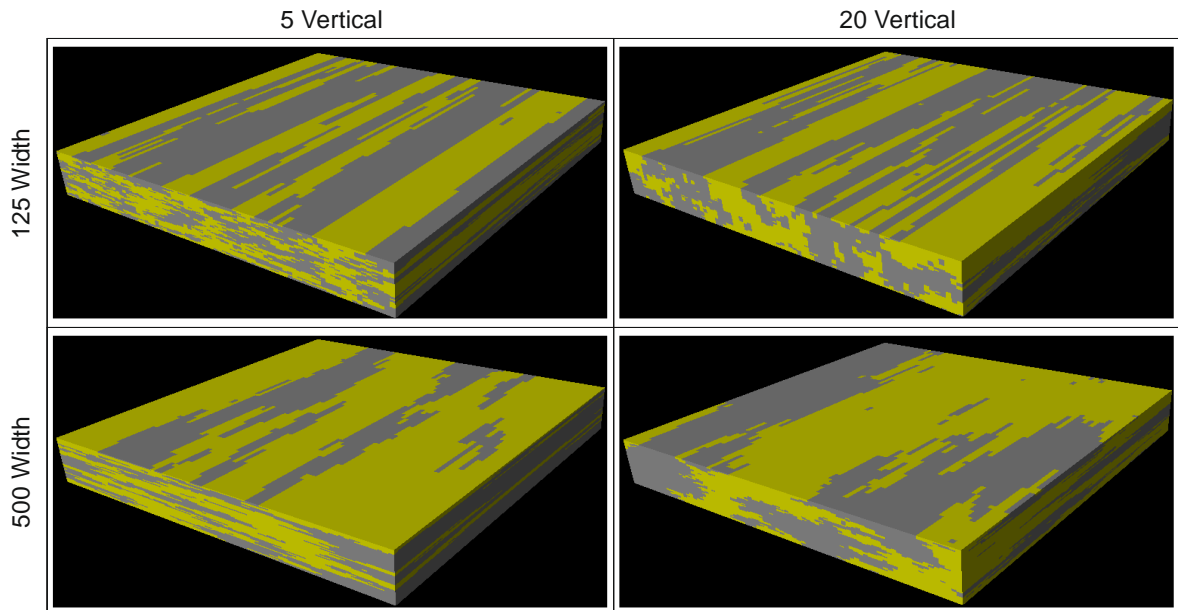


*Figure 3.1: Example synthetic fluvial reservoir models generated using the SIS modelling algorithm, using the same input parameters for the major direction (3000) and the nugget value (0.0001), with the width (minor direction) and the vertical thickness being altered (125 and 500, and 5 and 20 respectively), showing the differences between the models generated using the edge cases of some of the input values.*

### *Object Based Models - OBM*

In order to develop the synthetic suites of models, the OBM algorithm needs input values for:

- Channel Width (fluvial channel width)
- Wavelength (distance between meanders of the fluvial channel)
- Amplitude (the extent of the meander of the fluvial channel)
- Vertical Height (fluvial channel thickness)

The proposed variogram parameters for the OBM modelling algorithm were selected to provide a wide range of both 'realistic', 'fringe-case', and 'unrealistic' fluvial reservoir models. Realistic input parameter values provide proof that the methodology has real-world viability; fringe-case and non-realistic input parameter models provide proof of widescale applicability, whilst also

increasing the pool of test-cases. Channel width to thickness (W/T) ratios of fluvial systems is very variable dependent on the style of fluvial system, and the characteristics of the channel (e.g. discharge rate, sediment load, and slope steepness) (Gibling, 2006). Generally, braided and low-sinuosity rivers will have a W/T value between 50-1000, meandering rivers will have a W/T ratio between 30-250, and distributary systems will have a W/T ratio between 5-30 (but this becomes more variable at 1-250 for distal alluvial fans and aprons) (Gibling, 2006). Whilst the sinuosity (given by the amplitude and wavelength parameters) is highly variable for a wide range of channel width to channel thickness ratios, this should help to capture the wide variation of W/T ratios for a given sinuosity.

To create a represented suite of models a wide range of input parameters is required. The ranges of parameters used in this work are detailed in Table 3.2 below.

Channel Width	Wavelength	Amplitude	Vertical Height
125	250	125	5
250	500	250	10
375	750	375	15
500	1000	500	20

*Table 3.2: OBM input values showing channel width, wavelength, amplitude, and vertical height values used to create the suite of fluvial reservoir models.*

The range of channel widths (Table 3.2) will produce models with channels of various sizes and represent more classical mature and immature fluvial systems respectively. The range of values used for the wavelength and amplitude (Table 3.2) generate models with varying degrees of sinuosity. The vertical height (Table 3.2) was selected so that the Z-value (lower vertical extent) of the model wouldn't be exceeded, nor too easily connected by the stacking of just a few modelled channels.

This array of input parameters generates 256 different models for each of the 7 sand to shale ratios (target fractions) used within this study. This generates 1,792 different models. The wide

ranges of values for both the amplitudes of the sinusities of the channels (125 to 500) and their vertical thicknesses (5 to 20) are summarised within Figure 3.2, where all other input parameters are the same. This leads to large variations in the models being developed. It is important to use a wide range of input parameters during the generation of a suite of synthetic reservoir models since outcrops used to create the models will have varying channel parameters. Consequently, this suite of synthetic reservoir models study is required to be as comprehensive as possible, to ensure applicability to real-world examples.

## OBM Algorithm

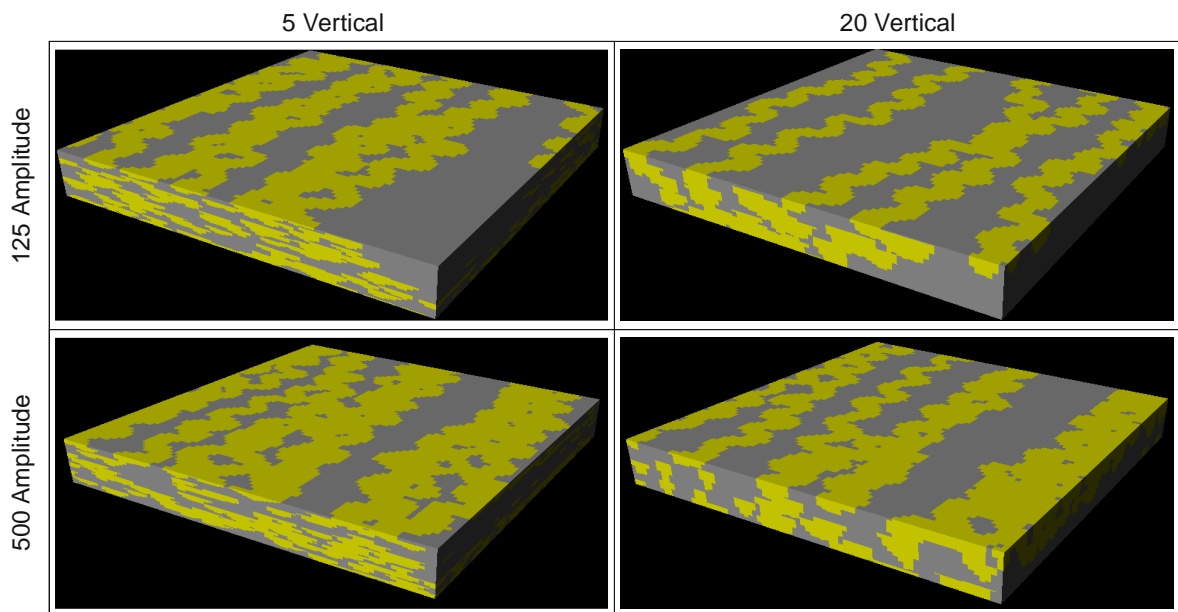


*Figure 3.2: Example synthetic fluvial reservoir models generated using the OBM modelling algorithm, using the same input parameters for the channel width (125) and the wavelength (250), with the amplitude (minor direction) and the vertical thickness being altered (125 and 500, and 5 and 20 respectively), showing the differences between the models generated using the edge cases of some of the input values.*

### *Multiple-Point Statistics - MPS*

In order to develop the synthetic suites of models, the MPS algorithm requires an input in the form of a training image (TI). Typically, these are generated from OBMs that are in turn generated from the input parameters that are intended to be modelled by the MPS algorithm. Subsequently, the same input parameters are required as with the OBM models:

- Channel Width (fluvial channel width)
- Wavelength (distance between meanders of the fluvial channel)
- Amplitude (the extent of the meander of the fluvial channel)
- Vertical Height (fluvial channel thickness)

To create a represented suite of models a wide range of input parameters is required. The ranges of parameters used in this work are detailed in Table 3.2 below.

Channel Width	Wavelength	Amplitude	Vertical Height
125	250	125	5
250	500	250	10
375	750	375	15
500	1000	500	20

*Table 3.3: MPS input values showing channel width, wavelength, amplitude, and vertical height values used to create the suite of fluvial reservoir models.*

In order to prevent bias when selecting the OBM realisation being used as the MPS TI, a random number generator was used to select a random number between 1 and 100. This number was selected to be 77, meaning that the 77<sup>th</sup> realisation of each model suite is used as the TI for that suite of MPS models.

This array of input parameters used to create the OBM models created 256 different MPS models for each of the 7 sand to shale ratios (target fractions) used within this study, generated 1,792 different models. The wide range of values for both the amplitude of the sinuosity of the channel (125 to 500) and the vertical thickness (5 to 20) is summarised within Figure 3.3, where all other input parameters are the same, leading to relatively large variations in the models being developed. It is important to use a wide range of input parameters since models developed to portray actual reservoirs will have a bespoke set of input parameters, with no two reservoirs being the same. Consequently, this study is required to be as wide-reaching as possible, to ensure applicability to real-world examples.

## MPS Algorithm

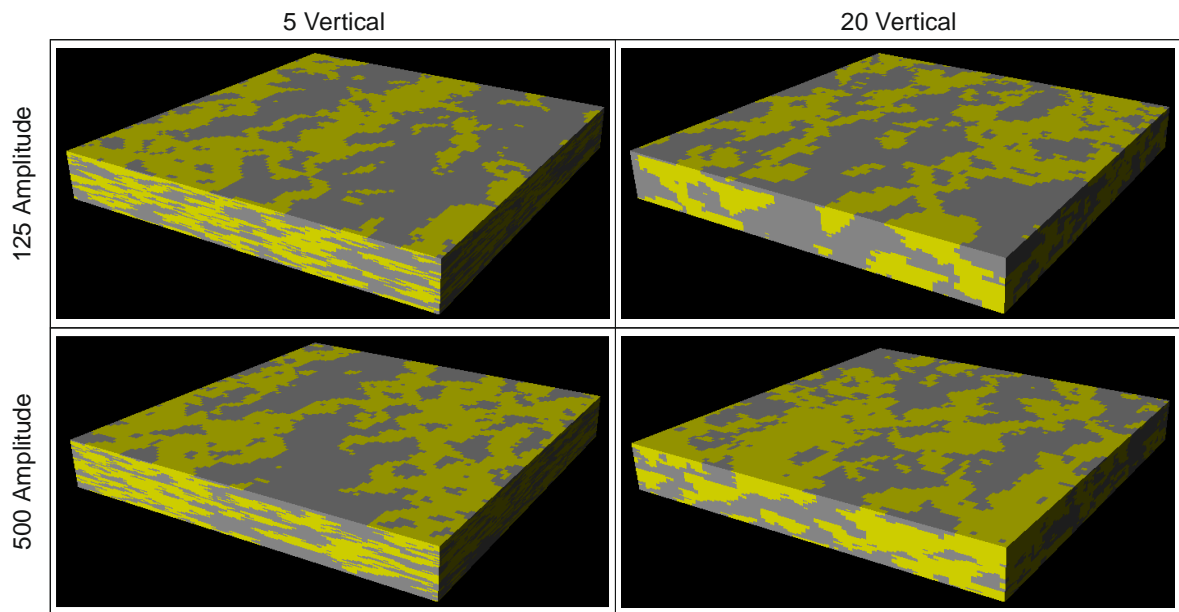
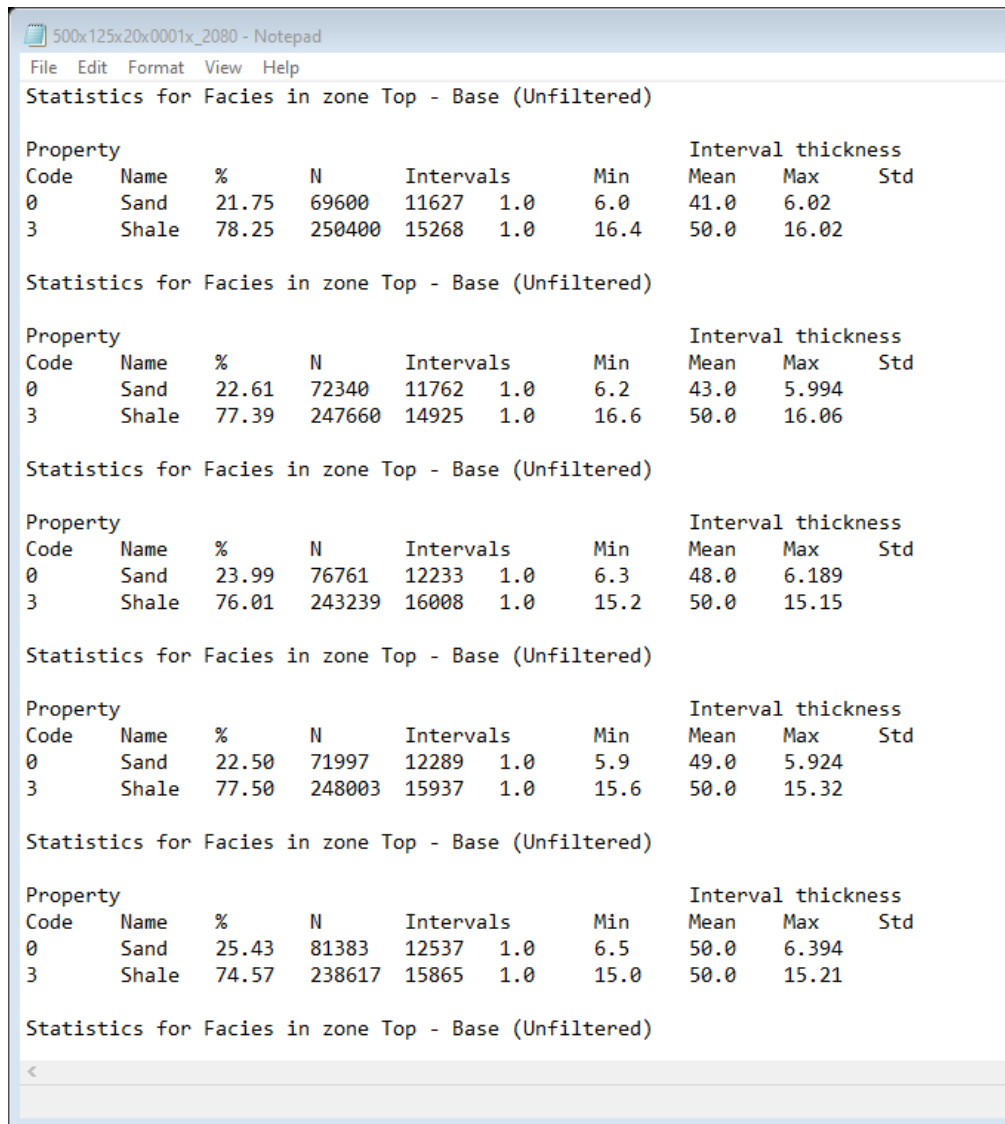


Figure 3.3: Example synthetic fluvial reservoir models generated using the MPS modelling algorithm, using the same input parameters for the channel width (125) and the wavelength (250), with the amplitude (minor direction) and the vertical thickness being altered (125 and 500, and 5 and 20 respectively), showing the differences between the models generated using the edge cases of some of the input values.

### 3.2 Statistical Modelling

The Schlumberger™ Petrel v.2020 software returns a set of values for each of the realisation within the synthetic suite of models. The outputs can be seen within Figure 3.4, and include Code (Facies Code), Name (Facies Name), % (Target Fraction), N (Number of cells), Intervals (Number of discrete groups of cells described by the same facies), Min (Minimum interval thickness), Mean (Average interval thickness), Max (Maximum interval thickness) and Std (Standard Deviation of geobody thickness within the model).



500x125x20x0001x\_2080 - Notepad

File Edit Format View Help

Statistics for Facies in zone Top - Base (Unfiltered)

Property							Interval thickness		
Code	Name	%	N	Intervals	Min	Mean	Max	Std	
0	Sand	21.75	69600	11627	1.0	6.0	41.0	6.02	
3	Shale	78.25	250400	15268	1.0	16.4	50.0	16.02	

Statistics for Facies in zone Top - Base (Unfiltered)

Property							Interval thickness		
Code	Name	%	N	Intervals	Min	Mean	Max	Std	
0	Sand	22.61	72340	11762	1.0	6.2	43.0	5.994	
3	Shale	77.39	247660	14925	1.0	16.6	50.0	16.06	

Statistics for Facies in zone Top - Base (Unfiltered)

Property							Interval thickness		
Code	Name	%	N	Intervals	Min	Mean	Max	Std	
0	Sand	23.99	76761	12233	1.0	6.3	48.0	6.189	
3	Shale	76.01	243239	16008	1.0	15.2	50.0	15.15	

Statistics for Facies in zone Top - Base (Unfiltered)

Property							Interval thickness		
Code	Name	%	N	Intervals	Min	Mean	Max	Std	
0	Sand	22.50	71997	12289	1.0	5.9	49.0	5.924	
3	Shale	77.50	248003	15937	1.0	15.6	50.0	15.32	

Statistics for Facies in zone Top - Base (Unfiltered)

Property							Interval thickness		
Code	Name	%	N	Intervals	Min	Mean	Max	Std	
0	Sand	25.43	81383	12537	1.0	6.5	50.0	6.394	
3	Shale	74.57	238617	15865	1.0	15.0	50.0	15.21	

Statistics for Facies in zone Top - Base (Unfiltered)

<

Figure 3.4: Example Petrel Output File showing all of the possible characteristics to analyse within the study, whilst also showing the output format.

From these outputs the following are of relevance to this study:

- The target fraction (directly informs the number of cells that are assigned to each facies, and in theory shouldn't deviate much from the input target fraction data). Whilst the broad value (i.e., approximately 30) is informed by the inputted target fraction, the actual value (i.e., 29.62) is determined by the random property values assigned to the channel element (i.e., channel thickness, channel width, and the sinuosity values), with the cells representing each facies summed and divided by the total number of cells to derive the total percentage of each facies within the model.

- The average geobody thickness defines the overall static connectivity of the model. In a real-world scenario, it would help to define the economic viability of a hydrocarbon reservoir. This average geobody thickness is the average geobody thickness of all geobodies of each of the facies represented within the model. Not only does this account for and represent channel stacking (which can help to represent the overall connectivity of the reservoir model), but it also helps to represent the values for the channel thickness, since an average values is given as an input, along with  $\pm 20\%$  of that value (i.e., an average of 15 would have a minimum of 12 and a maximum of 18).
- The standard deviation of geobody thickness is also important as it demonstrates the distribution of the geobody thickness data and helps to illustrate the variety of results found within the models. The spread of data for the geobody thickness values is important since two realisations modelled with the same input parameters could have the same average geobody thickness (i.e., 12.5), but could have completely different ranges of values (i.e., 10-15 and 5-35). These distributions are widely varied and will create completely different reservoir models, but looking at just the outputted target fraction and the average geobody thickness would suggest otherwise.

The other outputs provided by the Schlumberger™ Petrel v.2020 were deemed to either be irrelevant or repetitive of other values. For example, the % column is the percentage equivalent of N, and both give a representation of the target fraction. The intervals column shows the number of geobodies, which would be a weaker measure of channel connectivity than the average geobody thickness (mean thickness). Finally, min thickness (minimum geobody thickness) is too heavily influenced by the input vertical thickness, and max thickness is usually 50, and is too heavily influenced by the height of the three-dimensional grid. Both of these values show minor variation to be useful within this study, and the average geobody thickness has been selected instead.

The histogram, periodogram and Goovaerts plot have been selected to analyse the trends of the target fraction, average geobody thickness and standard deviation of geobody thickness values.

This enables us to understand the spread of results, and ultimately determine the statistical significance of model sets, and how many model realisations this occurs at. This work follows the generalised workflow shown in Figure 3.5.

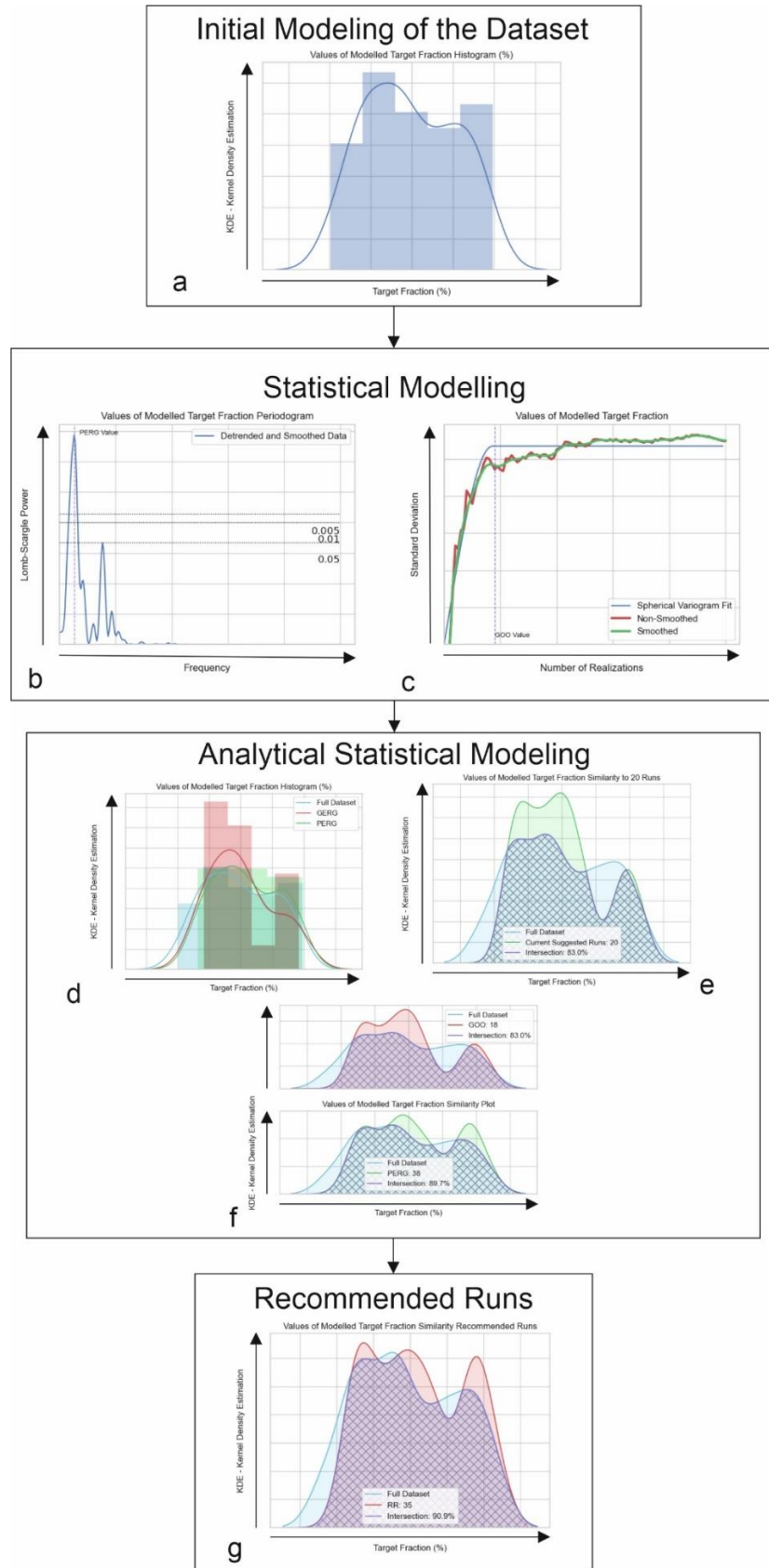


Figure 3.5: Generalised workflow of the methodologies for this study, starting with the creation of histograms a) to highlight dataset distributions. This is followed by the creation of a periodogram b) and Goovaerts plot c) in order to find the PERG and GOO values to be used when comparing restricted model

*suite distributions to the initial model suite of 100 realisations d) overlain distribution histogram of all three, e) initial model suite of 100 realisations compared to 20 realisations, and f) similarity plot between the initial model suite of 100 realisations and GOO (top) and the initial model suite of 100 realisations and the PERG (bottom)). Finally, finding the optimal realisations and comparing this restricted model suite to the initial model suite of 100 realisations (g).*

### 3.2.1 Histograms

The Kernel Density Estimations (KDE) of histograms (Figure 3.6) is used in this study to show the general distribution, spread of data, mean, skew and kurtosis (how flat or peaked the curve is) can be quantified. Kernel Density Estimation (KDE) has been used rather than the Probability Density Function (PDF) as the KDE provides a smoother curve when estimating the PDF of a random variable since the entire distribution is broken down into smaller segments based on a sliding window and modelled as a Gaussian distribution (bell curve). This later enables a more reliable data overlap to be quantified when comparing dataset results.

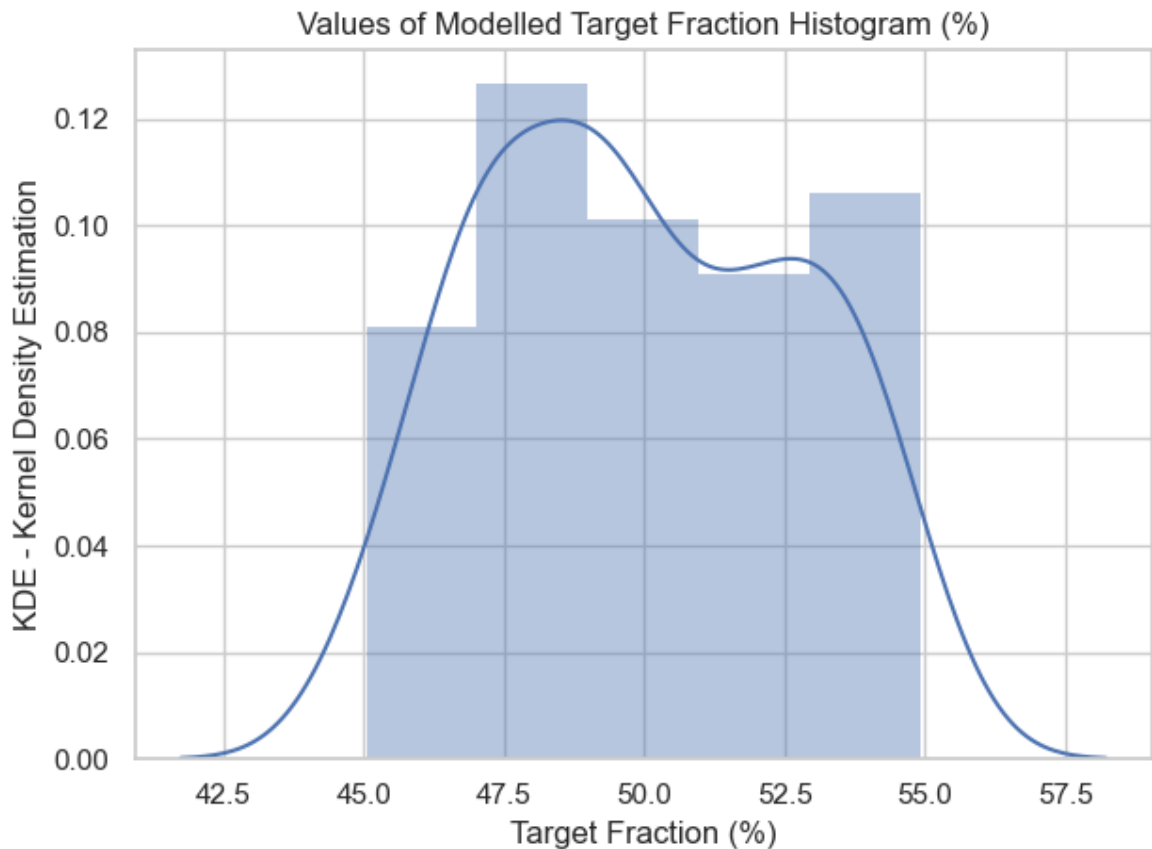


Figure 3.6: synthetic histogram showing the dataset distribution of target fraction values.

### 3.2.2 Periodogram

The Lomb-Scargle periodogram (Lomb, 1976; Scargle, 1982) (Figure 3.7) is a method of time-series analysis, for detecting periodicity within unevenly sampled signal data (Lomb, 1976; Scargle, 1982). This requires that the dataset is treated as a timeseries, where the discrete statistic undergoing analysis (outputted target fraction, average geobody thickness or standard deviation of geobody thickness) provides the amplitude variation (Lomb-Scargle Power), and the realisation number provides the time (frequency). This resultant timeseries is then smoothed and detrended, removing the any trends or cyclicity occurring past 100 realisations. This enables the amplitude of the ergodic fluctuation to be: 1) more obvious and 2) more statistically significant. A white noise model (linear least squares) has been used for measuring probable noise-ergodic signal as it is both computationally inexpensive, and commonly used when measuring noise significance in Lomb-Scargle periodograms. The plotted graph should show some peaks occurring at specific

frequencies – these frequencies are caused by an increased power spectral density value (PSD), which is the total contribution of a specific frequency to the entire signal (VanderPlas, 2018).

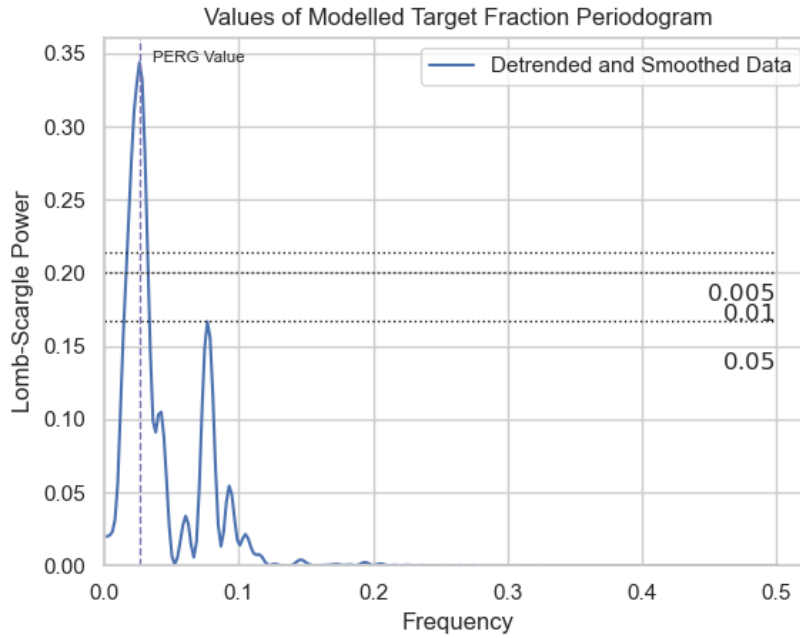


Figure 3.7: synthetic Lomb-Scargle periodogram showing one predominant peak (showing short-term periodicity), with a few smaller peaks which show longer term cyclicity within the dataset.

A heightened PSD is usually common of either background noise, or periodicity within a dataset. Within this study, the periodicity here is provided by the random variable being used when creating a set of stochastic reservoir models. As such, the periodicity of this random variable is useful to estimate at which point repeat sampling of data begins to occur. The frequency at the peak PSD value can be returned as a realisation number, when the equation:

$$Period = \frac{1}{Frequency}$$

Equation 3.1: Periodicity equation used to determine the cyclicity of the random variable used to create the reservoir models (PERG value).

is applied. This periodicity is referred to as the PERG within this study and is the periodicity of the ergodic nature of the random variable for the stochastic reservoir models, which is the total

number of realisations required for repeat sampling of the analytical value (outputted target fraction, average geobody thickness or standard deviation of geobody thickness).

### 3.2.3 Goovaerts Plot

The Goovaerts plot (Figure 3.8) is based off of the work of Goovaerts (1999), where the standard deviations of an ever-growing dataset were plotted in order to find the point at which an increase in the number of values being analysed leads to only an incremental improvement to the spread of data. In variograms, this is referred to as a sill, which is the plateauing of the dataset. When fitted with a spherical variogram fit, the Goovaerts plot allows for a specific point at which this incremental improvement in the spread of data occurs. The point at which this point occurs is called the GOO value. This is important as it depicts the point at which the standard deviation of the dataset is large enough to encapsulate the true value of the analytical value (outputted target fraction, average geobody thickness and standard deviation of geobody thickness). If fewer realisations were used, then it is possible that the true value would not be represented, and would lead to an unrepresentative reservoir model suite being developed.

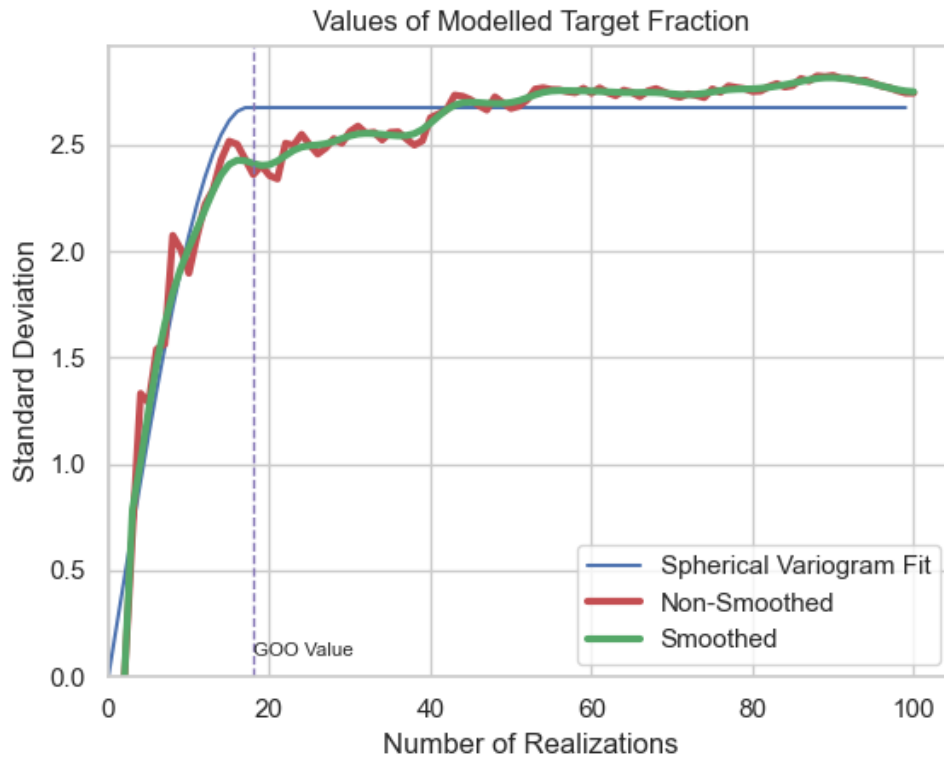


Figure 3.8: synthetic Goovaerts plot showing the creation of a sill when the standard deviations of an ever-increasing dataset (lag) is plotted, showing negligible changes to the distribution of the dataset.

### 3.3 Analytical Statistical Modelling

In addition to the statistical modelling techniques mentioned within Chapter 3.2, the following additional methods are used to build upon and make use of the previous results of the methods already used. These analytical methods utilise the values for the GOO and the PERG, to determine the number of realisations are actually required to return a statistically significant sample. In order for the GOO and the PERG values to be used, they must be determined to be independent of one another, that is, the value of one of the GOO or the PERG does not rely on, or show correlation to the value of the other. If this is the case, then these values are not independent, and as such cannot be used to find the recommended number of realisations for a statistically significant three-dimensional synthetic suite of reservoir models.

### 3.3.1 Comparison Plot

The comparison plot (Figure 3.9) is a slight variation of the histogram and differs by overlaying the initial model suite of 100 realisations with two restricted model suites. These restricted model suites are based on the values of the PERG and the GOO retrieved from the periodogram and Goovaerts plot respectively. This is done to provide a visual comparison of the distribution of data from the first X number of values within the dataset. This comparison makes a good reference point on the way to finding the optimal number of realisations required for a restricted input dataset to still show the same general data distributions as that of the initial model suite of 100 realisations.

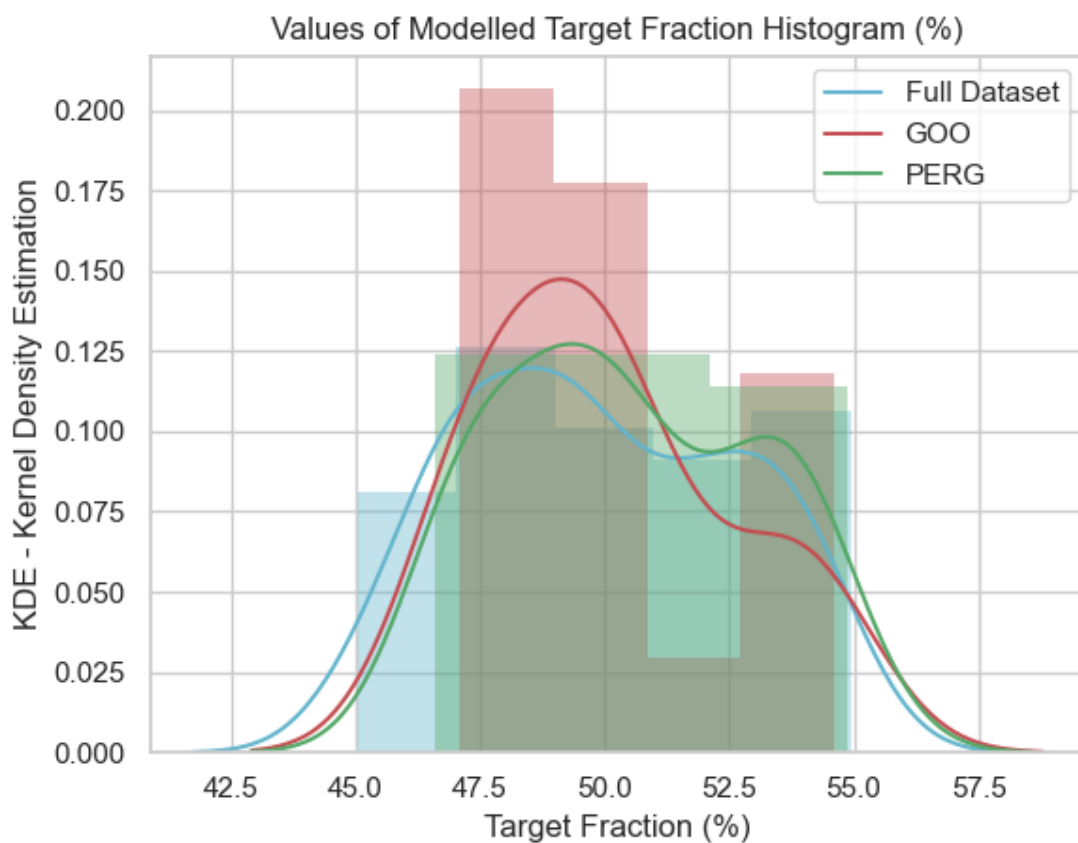


Figure 3.9: synthetic comparison plot of the initial model suite of 100 realisations with the restricted ones created when using the PERG (periodic ergodicity) and GOO (point at which the standard deviation of an increasing dataset forms a plateau) values.

### 3.3.2 Similarity Plot

The similarity plot (Figure 3.10) is also similar to the histogram, but with extra steps – the main difference being that the GOO and the PERG restricted model suites are being directly compared to the distribution of the entire dataset. This is done by finding the intersectional area (overlap) of the two distributions, and provides not only a visual approximation, but an accurate numerical value to quantify the ‘goodness of fit’.

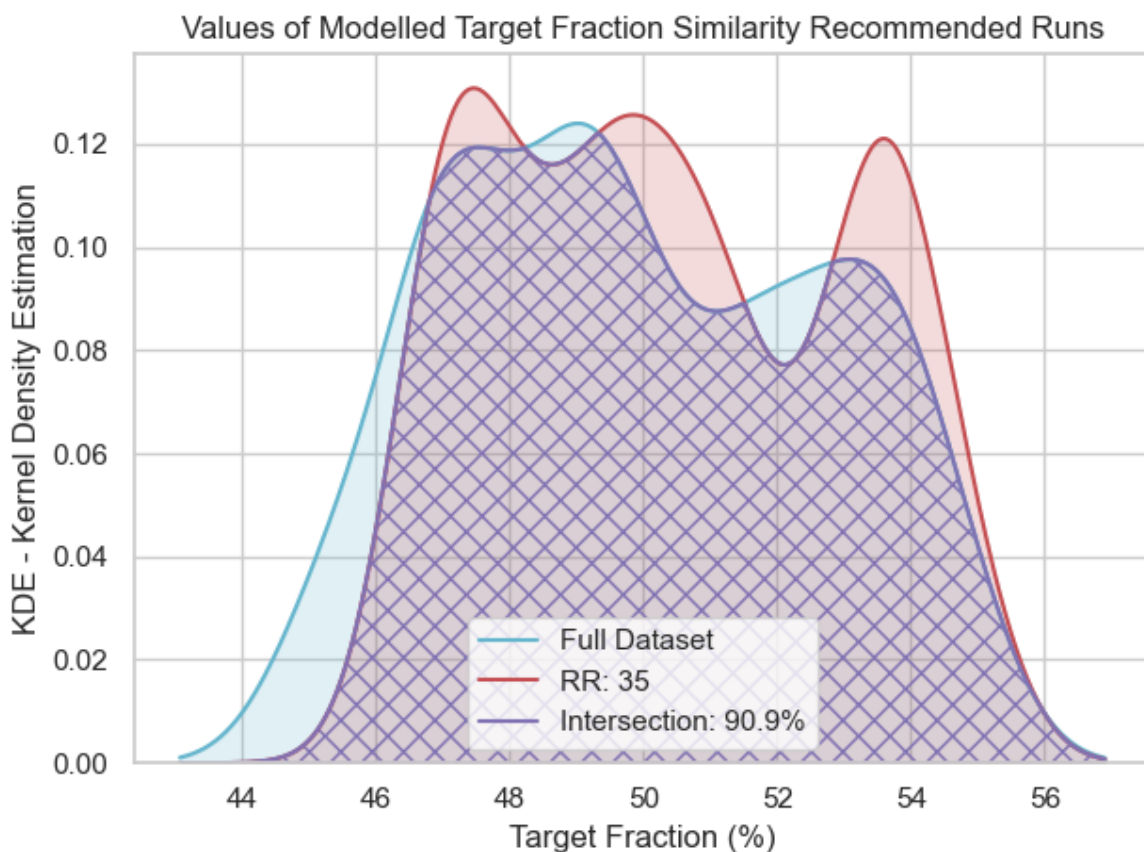


Figure 3.10: synthetic similarity plot using a restricted model suite (in this case, the first 35 realisations) to be compared to the initial model suite of 100 realisations (100 realisations), with the intersectional percentage being calculated. This is a numerical representation of how well a restricted model suite represents the variety of reservoir models present within a larger suite of models.

### 3.3.3 Previously Used Realisations

To properly compare and demonstrate the need for a tailored approach to fluvial reservoir modelling, the industry standard value (20 realisations) is used as the restricting factor to the

entire dataset. This is plotted as a similarity plot and compared to the distribution of the initial model suite of 100 realisations, where the intersection percentage can be calculated (Figure 3.11).

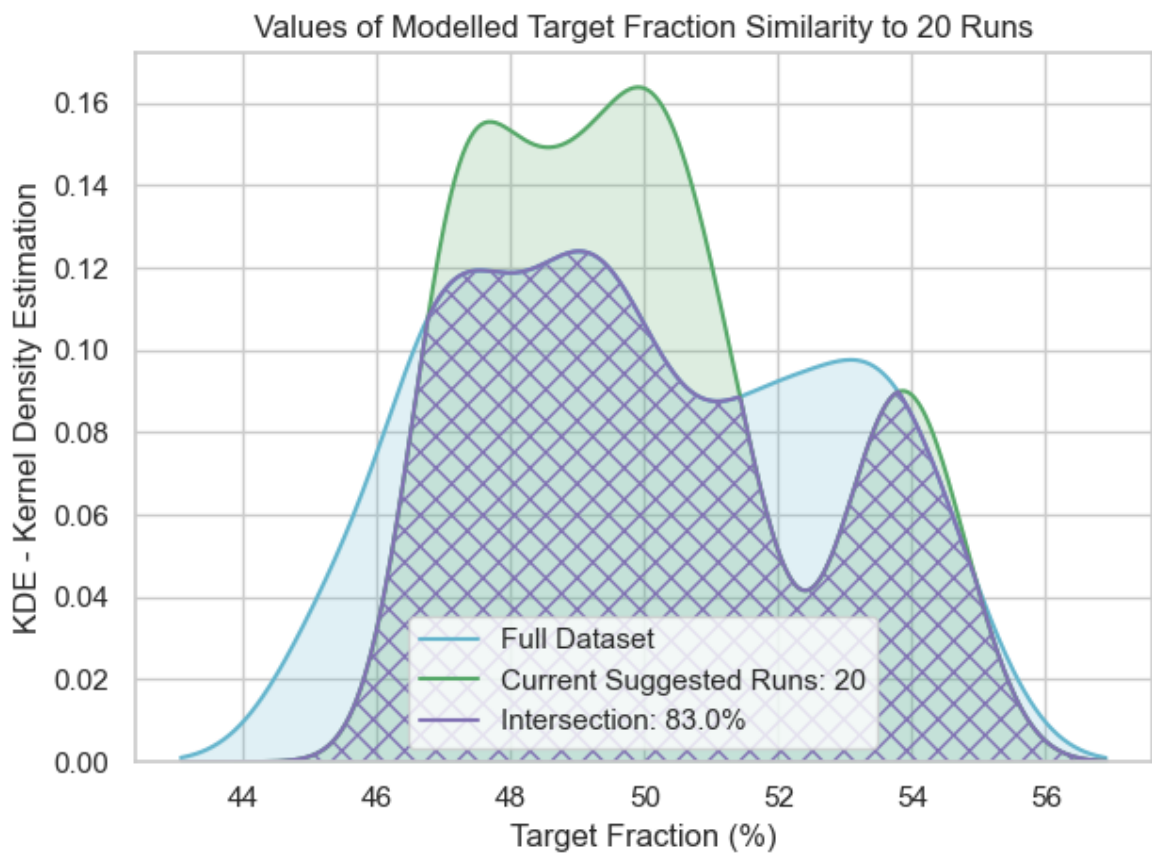


Figure 3.11: synthetic similarity plot comparing the initial model suite of 100 realisations (100 realisations) to the restricted model suite of the previously used number of realisations used (the first 20 realisations), with the intersection percentage being plotted. This is a numerical representation of how well a restricted model suite represents the variety of reservoir models present within a larger suite of models.

### 3.3.4 Realisations Required

In order to find the required number of realisations of a model for it to be classified as statistically significant, we must first consider the constraints upon which this value is found within.

1. The value must be below the total number of realisations being run within the dataset
2. The value must not exceed the point at which resampling of data is occurring – i.e., it must be lower than the PERG

3. The value must exceed the sill created by the Goovaerts plot since the standard deviation becomes negligibly different as the number of values held within the dataset is increased
4. The intersectional percentage of the dataset must be the closest fit to the entire dataset as is possible within the constraints above

From this set of 'rules', the workflow described in Figure 3.12 is then followed to produce a meaningful analytical procedure for the recommended number of realisations to be determined.

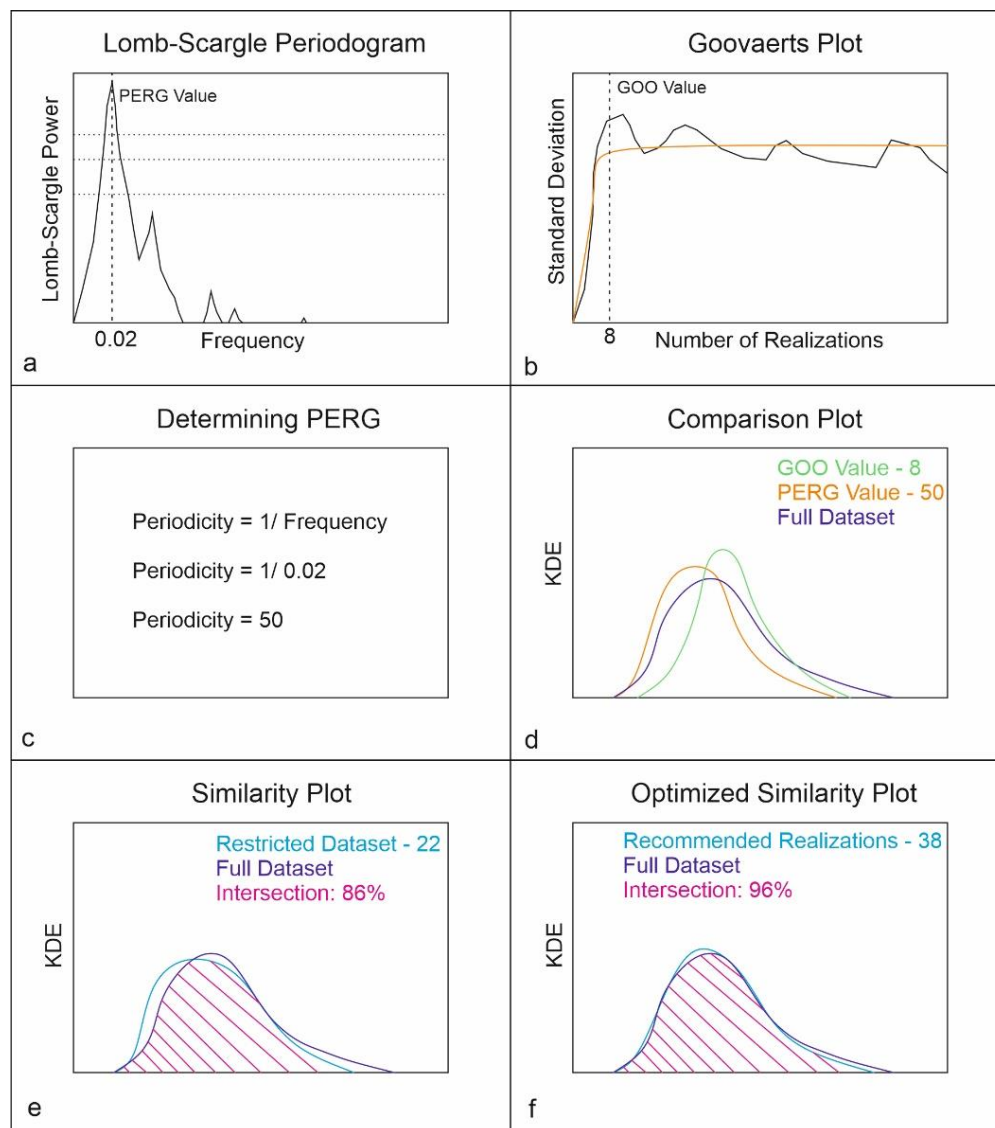


Figure 3.12: generalised workflow for finding the PERG (a and c) and GOO (b) values, and then these being used to compare restricted model suites with the initial model suite of 100 realisations (d) to then find the intersection percentages of increasing realisations numbers (e), until the optimal value is found (f) which is the largest intersectional percentage, giving the best representation of variety of reservoir models.

Once the PERG value (Figure 3.12a and c) and the GOO value (Figure 3.12b) have been determined, these values can then be used as 'limits' that are used to restrict the dataset to the first  $X^{10}$  number of realisations. These datasets are then compared to the initial model suite of 100 realisations by way of a histogram, allowing for the distribution and values held within the restricted model suites to be further compared to the initial model suite of 100 realisations (Figure 3.12d).

The number of required realisations must fall between the point at which repetition of the random variable used when creating the suites of models (PERG) and the point at which the spread of data between an ever-increasing dataset becomes insignificant (GOO). For this 'ideal' value to be determined, the overlap percentage (intersection) of a restricted model suite, and the initial model suite of 100 realisations can be calculated. First, this is done with the PERG (Figure 3.13 bottom) and GOO (Figure 3.13 top) values, and then for all of the values within the search area. This allows for an iterative search to occur between the bounds of the GOO and the PERG,

---

<sup>10</sup> X is classified as a dynamic value, which is wholly dependent on the number of realisations that produces the best intersectional (similarity) percentage when compared to the original model suite of 100 realisations in the search area between the GOO and the PERG. This number represents the point at which the variability of the model suite is best represented.

whereby the restricted model suite will incrementally increase (Figure 3.12e), and the intersection percentage can be compared to previous values, to determine the new 'best fit' distribution.

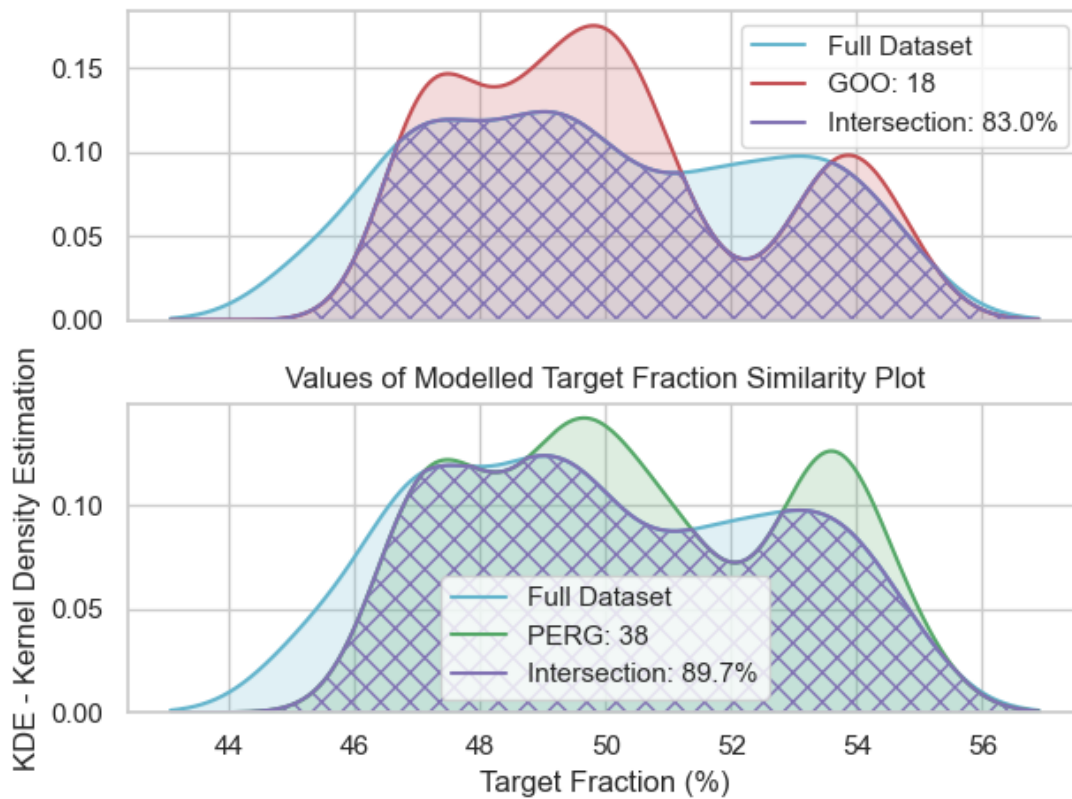
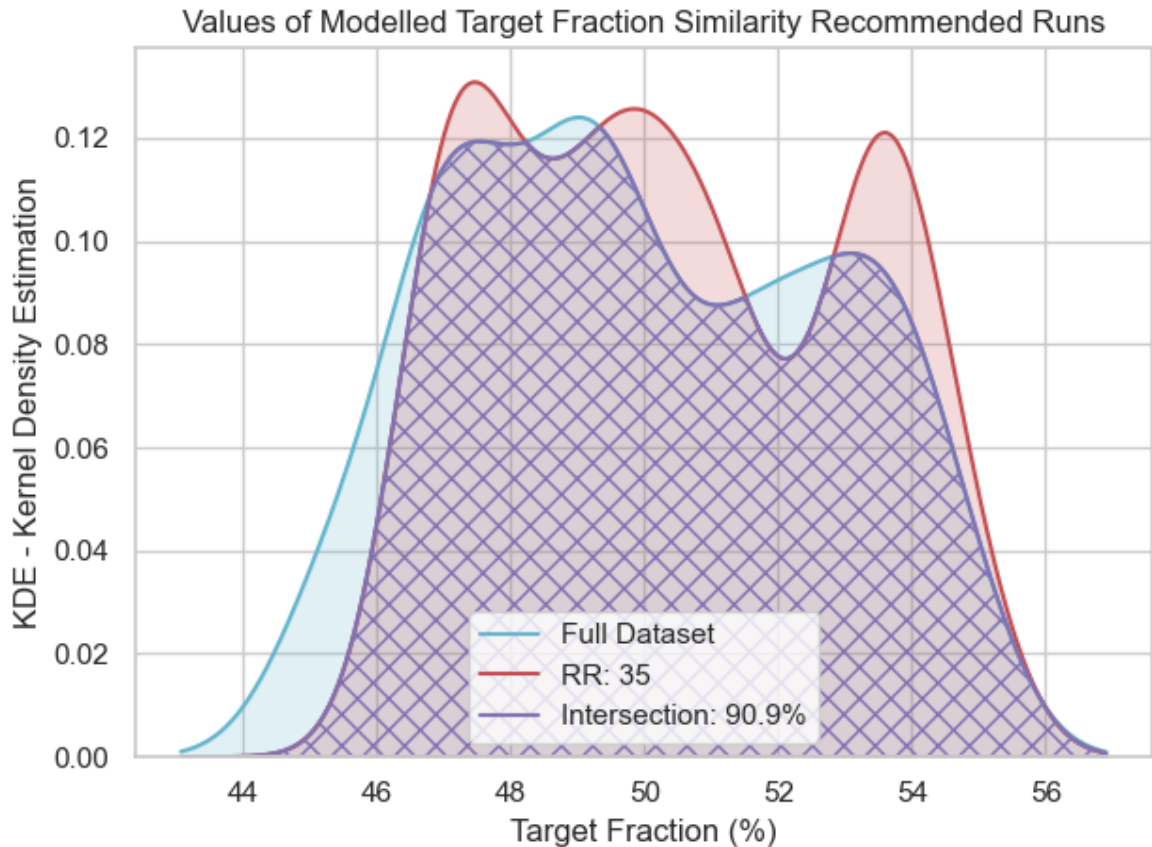


Figure 3.13: synthetic version of the similarity plot comparing the distributions of the restricted model suite to the first 18 realisations as given by the GOO value (top) and the first 38 realisations as given by the PERG value (bottom) to the initial model suite of 100 realisations, and then finding the intersection percentage of both to the initial model suite of 100 realisations.

Once all values between the GOO and the PERG inclusive have been queried, it will be deemed that the number of realisations being used within the highest intersectional percentage value is the best fitting dataset (Figure 3.12f and Figure 3.14), and as such is the optimal number of realisations to represent the entire dataset, whilst preventing resampling.



*Figure 3.14: synthetic similarity plot of the initial model suite of 100 realisations compared to the recommended number of realisations (35), showing the highest intersection percentage of all of the values for realisations between the GOO and the PERG. This produces the largest variety of reservoir models from the initial model suite of 100 realisations.*

This recommended number of realisations can be compared to the standard 20 realisations (Figure 3.15), to demonstrate the increased accuracy and the need for this increased number of realisations to be carried out to develop a better, more statistically significant, and more accurate end result. This value is representative of the number of realisations that produces the optimal variety of reservoir models found within the initial suite of 100 realisations, whilst not repeating characteristic properties, or being below the point at which the standard deviation of the dataset is still increasing, and has not formed a plateau.

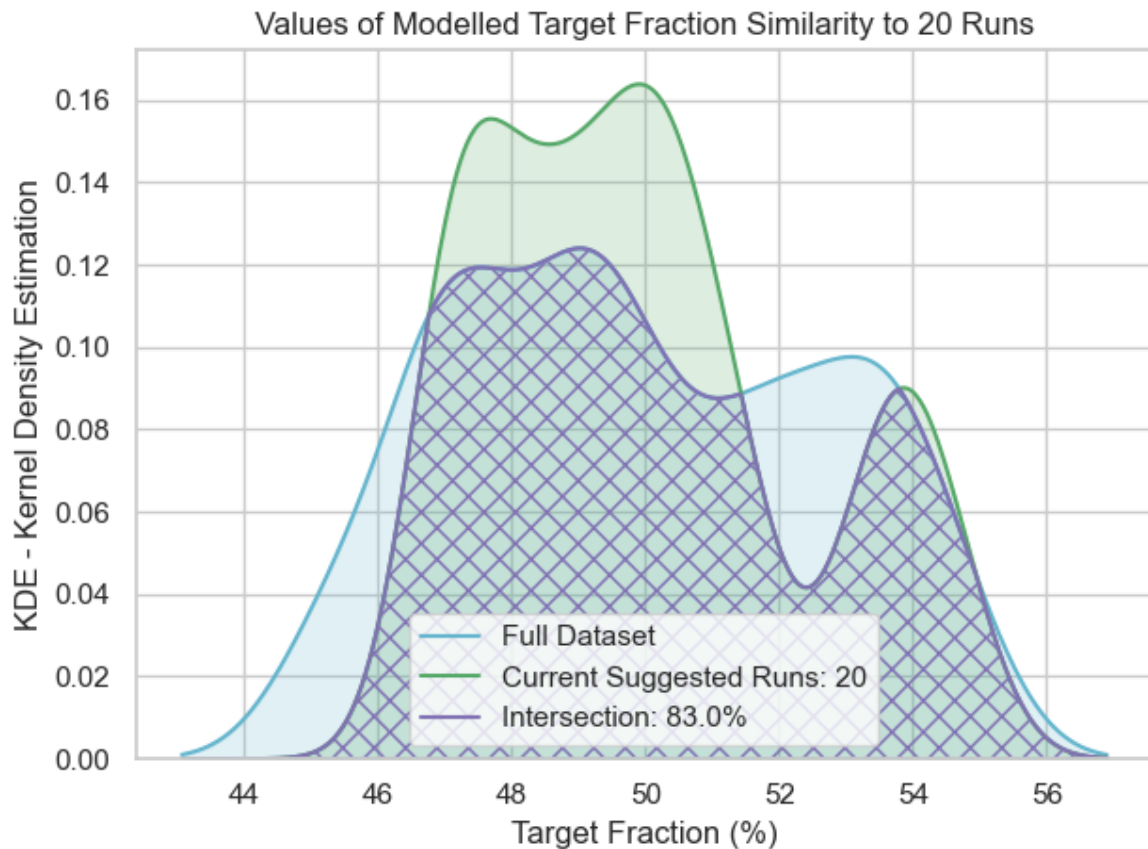


Figure 3.15: synthetic similarity plot comparing the initial model suite of 100 realisations to the restricted model suite of the previously used number of realisations used (the first 20 realisations), with the intersection percentage being plotted, giving a numerical value to the representation of the variety of reservoir models within the initial model suite of 100 realisations.

### 3.4 Summary

The workflows and methods detailed in this chapter determine the number of realisations required to produce a statistically significant three-dimensional reservoir model suite. This workflow provides solid statistical reasoning, and numerical expression as to why that many models are required in the form of intersection percentage, which can be later compared to the current industry standard to provide another level of evidence to support a more tailored approach to the number of models run.

## 4 Analysis and Interpretation

The input parameters outlined within Chapter 3 led to the generation of a variety of synthetic model suites. Upon processing the raw statistical data returned from these suites of reservoir models. There are trends and patterns that can be seen across the results from all three modelling algorithms. This chapter will analyse the following relationships:

1. The average number of realisations required to produce a statistically significant three-dimensional reservoir model suite for each modelling algorithm, and how this value changes with the mean geobody thickness values, standard deviation of geobody thickness values, and outputted target fraction, across a variety of input target fractions.
2. The spread (standard deviation) of the suites of reservoir models, and consequently their reproducibility.
3. How well the recommended number of realisations represents the initial 100 realisations of the suite of reservoir models for each set of input parameters for the generated reservoir models.

Within this chapter, these trends and patterns will be explored and explained, and a number for the number of realisations required for a statistically significant suite of fluvial reservoir models to be developed.

### 4.1 Number of realisations

The number of realisations refers to three different values:

- The number of realisations required for the standard deviation of values to become negligibly different in an ever-increasing dataset, following the same methodology as Goovaerts (1999), so is referred to as the 'GOO' value,
- The number of realisations at which point the resampling of data occurs, also known as the Periodic Ergodicity, or 'PERG value',

- The number of realisations that gives the optimal representation (highest intersectional percentage) of 100 realisations, leading to this being the Recommended number of Realisations to be used by the end user, or 'RR' value.

Analysed within this section are the values for:

- The mean geobody thickness of the sand geobody,
- The standard deviation of the thicknesses of sand geobodies within the realisations,
- The outputted target fraction represented within the models.

The aim of this analysis is to find the number of realisations required to develop a 'representative suite of realisations' for a specific set of input parameters across all three of the modelling algorithms. The analysis of these parameters will help to pinpoint how many realisations, on average, are required for a statistically significant three-dimensional reservoir model suite to be generated. Within this chapter, the opaque lines are representative of the raw average values for the PERG (green), GOO (blue) and RR (red). The faint lines are representative of the average values with the residuals removed (values outside of  $\pm 2$  standard deviations) for the PERG (green), GOO (blue) and RR (red).

#### 4.1.1 Mean geobody thickness

For the SIS (Figure 4.1a), OBM (Figure 4.1b) and MPS (Figure 4.1c) algorithms, different values and trends are produced for the PERG, GOO and RR values across all input target fractions. For the majority of PERG values fall within the values of 35 to 38 realisations, with the only exceptions being 42, 40 and 33 realisations for the SIS algorithm (within the 50, 60 and 80 input target fractions respectively). When the residuals are removed, all PERG values drop by a single realisation, and the peak at the 50 input target fraction is lost for the SIS algorithm. This marginal change suggests that the values for the PERG are representative and include few anomalous or boundary values. The GOO values are also consistent, and all are found within the range of 11 to 14 realisations irrespective of the input target fraction or modelling algorithm, with values dropping by an insignificant amount (less than a realisation) when the residuals are removed.

Finally, the RR values also stay consistent, with values ranging from 30 to 34 for the majority of values, with this peaking at 35 realisations for the SIS algorithm at the 60 input target fraction. Upon the residuals being removed, all RR values drop by a single realisation. All the RR values mimic the PERG values that correlate with the same input target fraction.

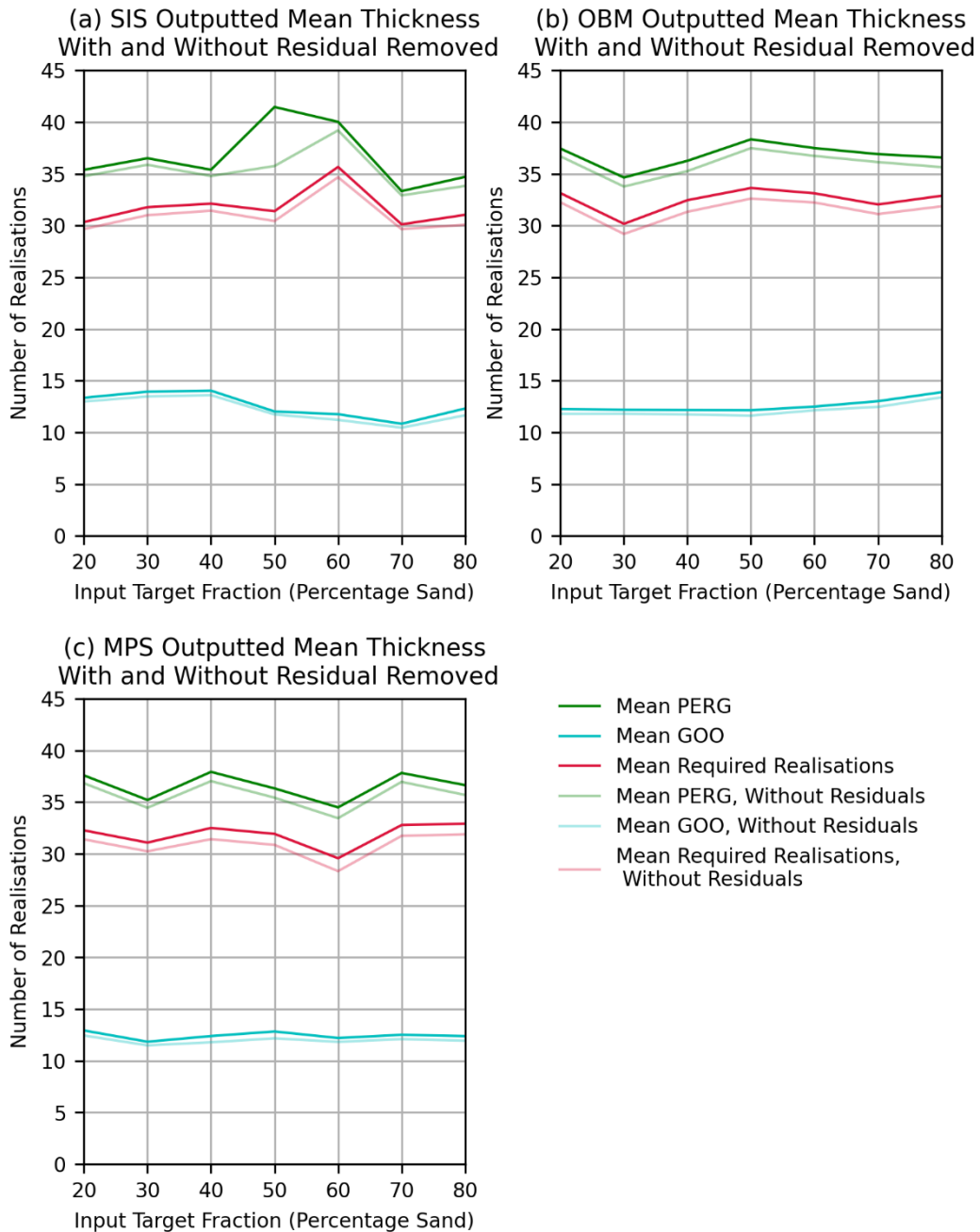


Figure 4.1: Comparison of the PERG, GOO and RR values for the mean geobody thickness values (bold lines), with the outlier values (residuals) removed (faint lines), across the (a) SIS, (b) OBM, and (c) MPS modelling algorithms, with values shown for all input target fractions.

#### 4.1.2 Standard deviation of geobody thickness – StDev Thickness

For the SIS (Figure 4.2a), OBM (Figure 4.2b) and MPS (Figure 4.2c) algorithms, different values and trends are produced for the PERG, GOO and RR values across all input target fractions. All PERG values fall within the values of 35 to 38 realisations, and when the residuals are removed, all PERG values drop by a single realisation. This marginal change suggests that the values for the PERG are representative and include few anomalous or boundary values. The GOO values are also consistent, and all are found within the range of 12 to 14 realisations irrespective of the input target fraction or modelling algorithm, with values dropping by an insignificant amount (less than a realisations) when the residuals are removed. Finally, the RR values also stay consistent, with values ranging from 30 to 35 for all values, with this being limited to 33 realisations for the MPS algorithm. Upon the residuals being removed, all RR values drop by a single realisations. All the RR values mimic the PERG values that correlate with the same input target fraction.

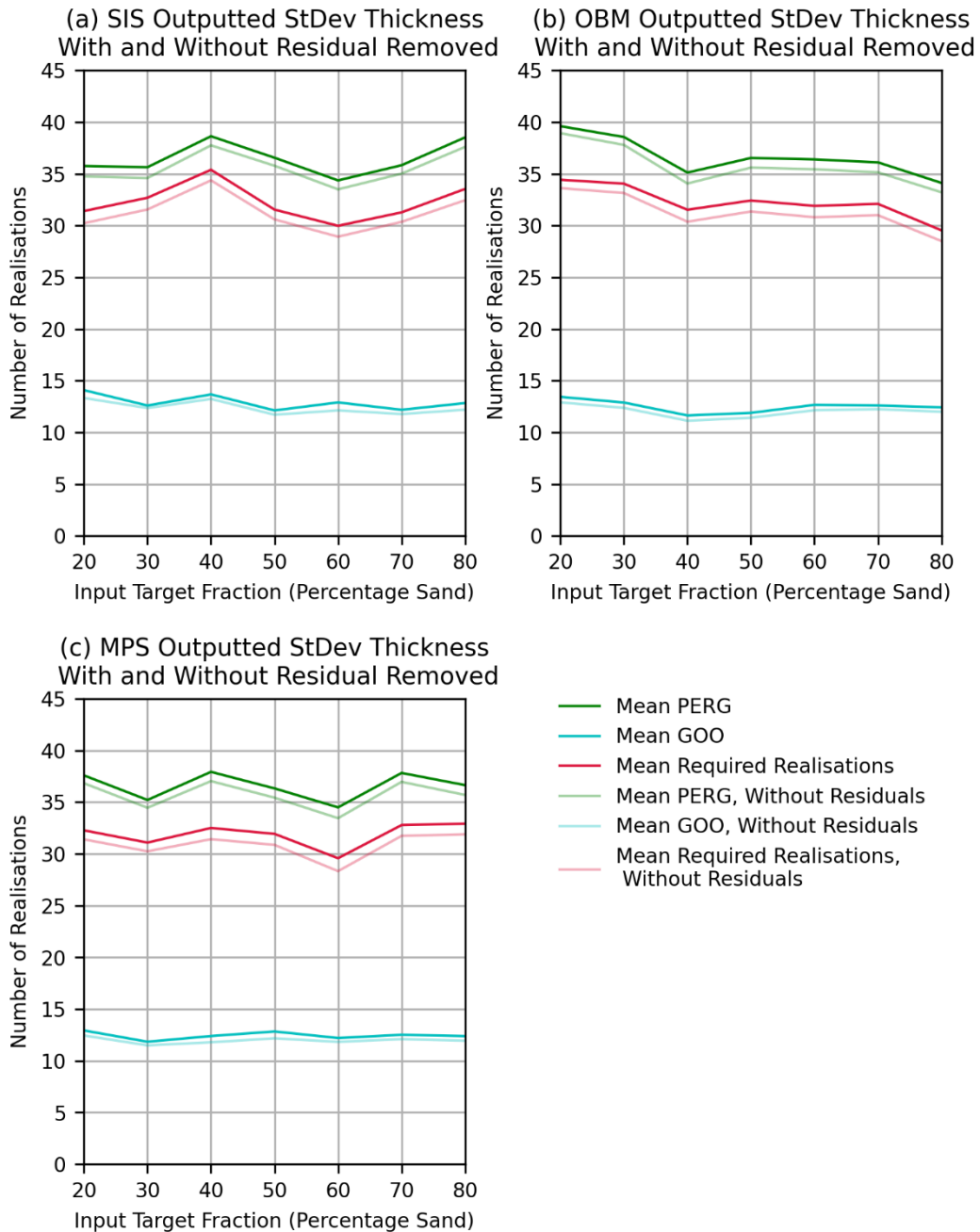


Figure 4.2: Comparison of the PERG, GOO and RR values for the standard deviation of geobody thickness values (bold lines), with the outlier values (residuals) removed (faint lines), across the (a) SIS, (b) OBM, and (c) MPS modelling algorithms, with values shown for all input target fractions.

#### 4.1.3 Target Fraction

For each the SIS (Figure 4.3a), OBM (Figure 4.3b) and MPS (Figure 4.3c) algorithms, different values and trends are produced for the PERG, GOO and RR values across all input target fractions.

For the most part, all PERG values fall within the values of 33 and 38 realisations, with the only

exceptions being 42 realisations at the 50 input target fraction for the SIS algorithm. When the residuals are removed, all PERG values drop by a single realisation, and the peak at the 50 input target fraction is lost for the SIS algorithm, dropping to 37 realisations. This marginal change suggests that the values for the PERG are representative and include few anomalous or boundary values. The GOO values are also consistent, and all are found within the range of 10 to 15 realisations irrespective of the input target fraction or modelling algorithm, with values dropping by an insignificant amount (less than a realisations) when the residuals are removed. Finally, the RR values also stay consistent, with values ranging from 30 to 34 for the majority of values, with the SIS algorithm having values as low as 28 realisations at the 70 input target fraction. Upon the residuals being removed, all RR values drop by a single realisations. All the RR values mimic the PERG values that correlate with the same input target fraction.

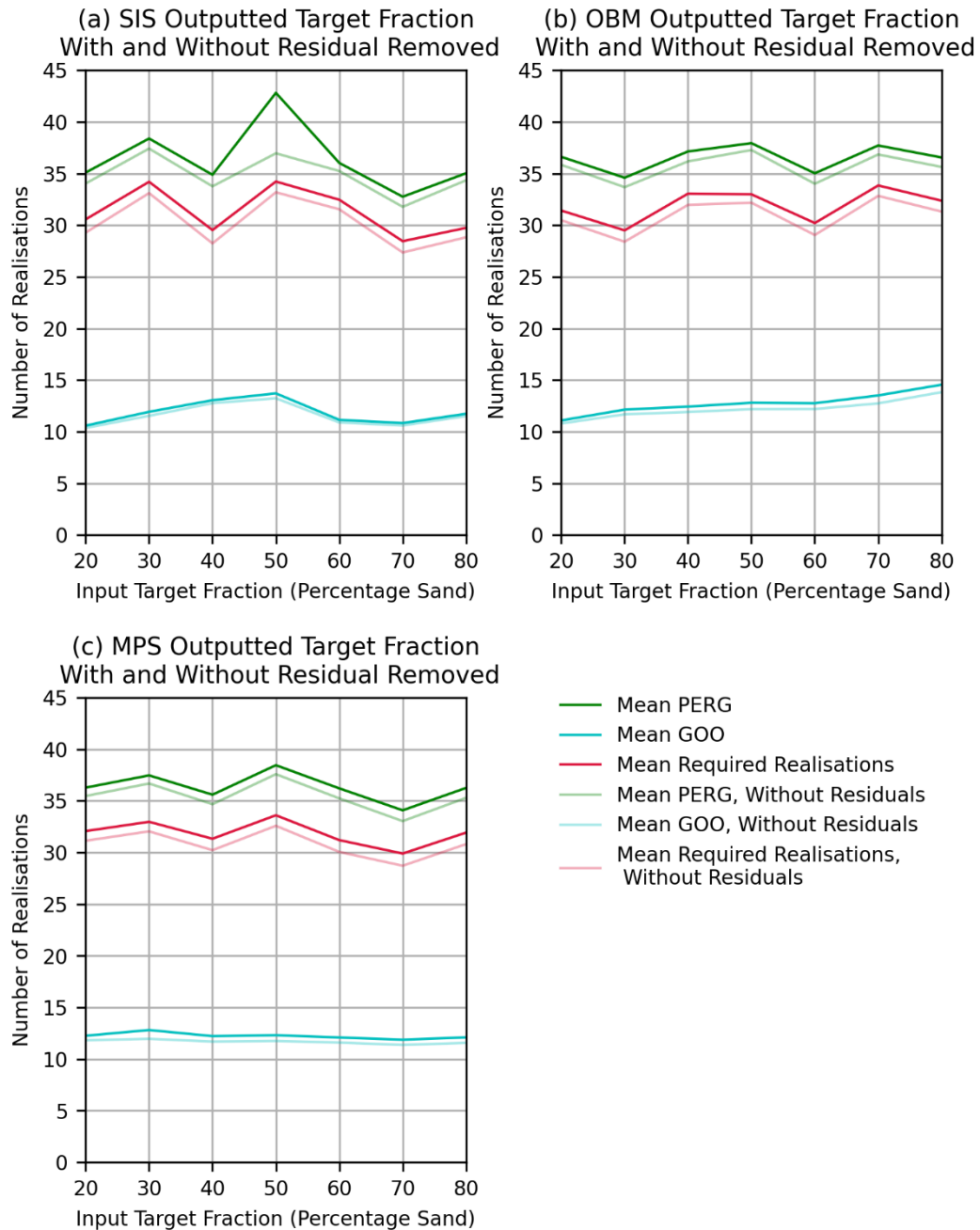


Figure 4.3: Comparison of the PERG, GOO and RR values for the output target fraction values (bold lines), with the outlier values (residuals) removed (faint lines), across the (a) SIS, (b) OBM, and (c) MPS modelling algorithms, with values shown for all input target fractions.

#### 4.1.4 PERG, GOO and RR Values

Direct comparison of the PERG (Figure 4.4a, Figure 4.5a and Figure 4.6a), GOO (Figure 4.4c, Figure 4.5c and Figure 4.6c) and RR (Figure 4.4e, Figure 4.5e and Figure 4.6e) values highlight the general similarity of values across each of the modelling algorithms, and whilst the different algorithms

show differing trends, the generally tight grouping of each of the average values for each input target fraction suggests that there is more of a statistical similarity than is immediately suggested by the produced suites of fluvial reservoir models. The relatively consistent (and large) standard deviation values for the PERG (Figure 4.4b, Figure 4.5b and Figure 4.6b) and RR (Figure 4.4f, Figure 4.5f and Figure 4.6f) values, suggests a relatively large dispersion of the values that contribute to this average value, and would suggest a high degree of variability. This is to be expected from what is essentially a random value, such as the PERG, where the value is controlled by the periodicity of the random variable being used to create the suites of fluvial reservoir models, and since the PERG heavily influences the RR value (as can be seen in Figure 4.4, Figure 4.5 and Figure 4.6), this also extends to the RR value. The GOO (Figure 4.4d, Figure 4.5d and Figure 4.6d) values have a much lower standard deviation however (approximately 8), which is likely the effect of the GOO value representing the number of values required for the standard deviation of a group of values to form a plateau in the dataset.

### Mean Thickness PERG, GOO and RR Values Across All Algorithms

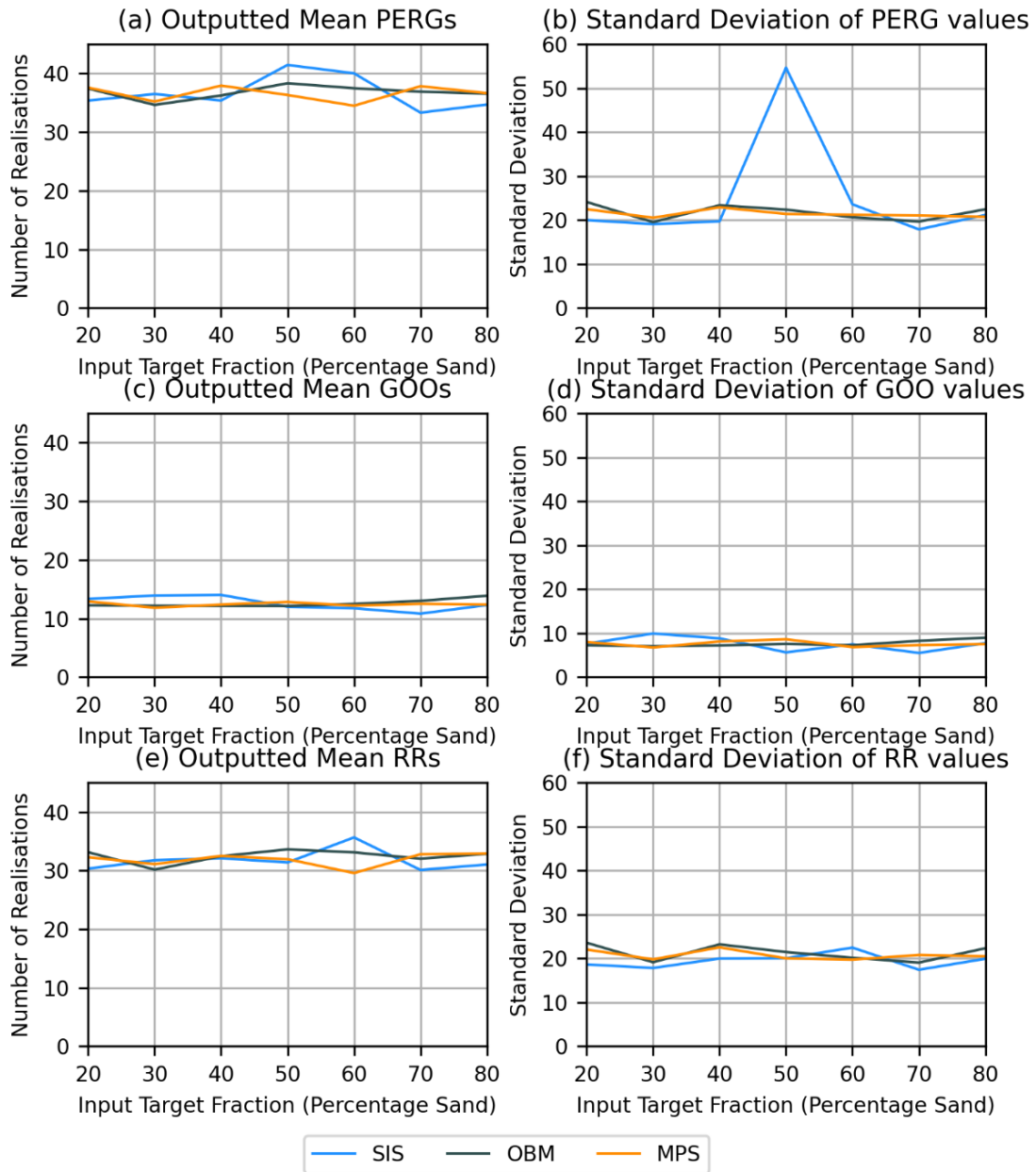


Figure 4.4: Comparison of the (a) PERG, (c) GOO and (e) RR values for the mean geobody thickness values, for each of the SIS, OBM, and MPS modelling algorithms, with values shown for all input target fractions. The standard deviations of these average results (detailing how spread out the values are) is given for the (b) PERG, (d) GOO, and (f) RR values.

### Standard Deviation of Thickness PERG, GOO and RR Values Across All Algorithms

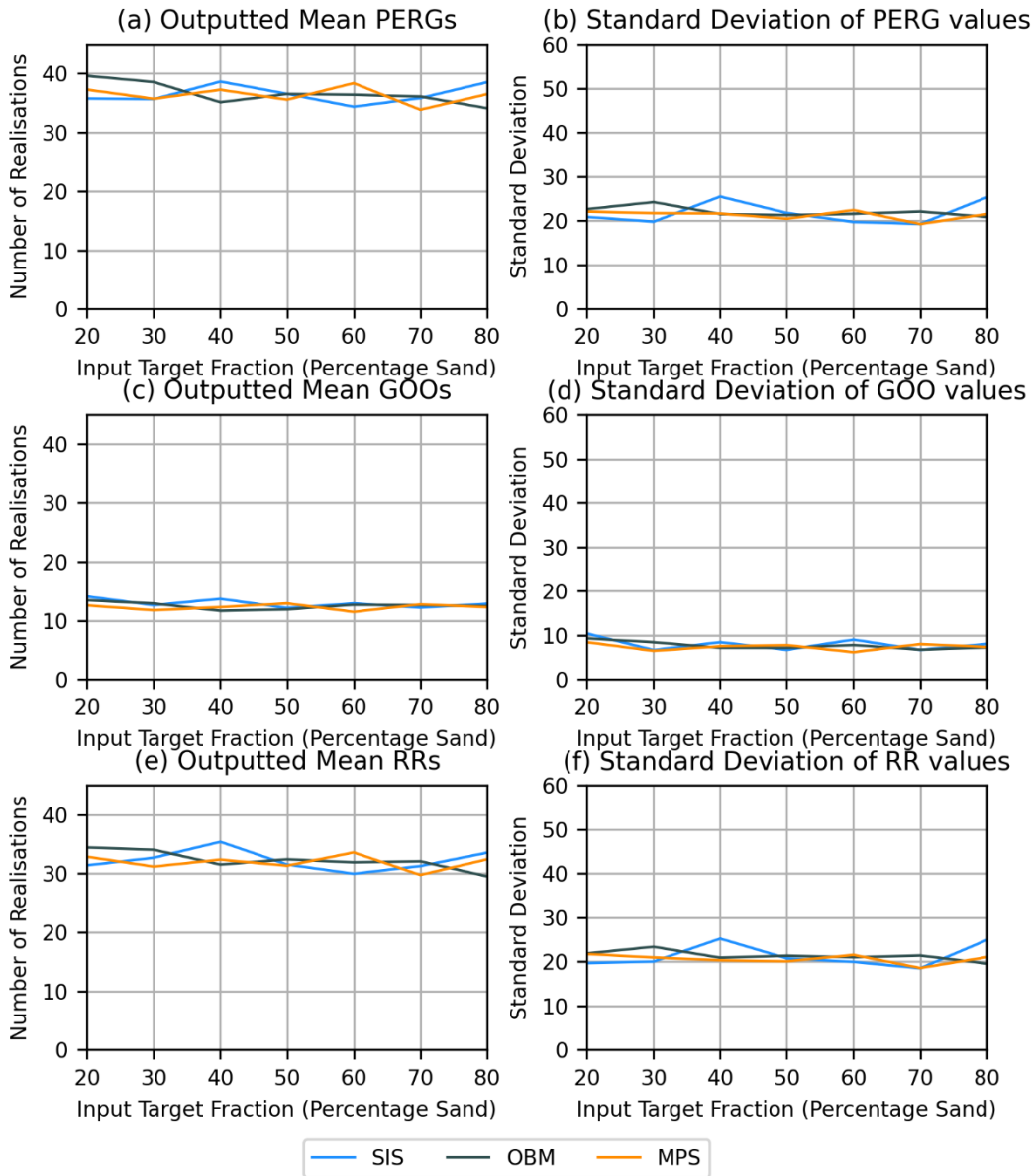


Figure 4.5: Comparison of the (a) PERG, (c) GOO and (e) RR values for the standard deviation of geobody thickness values, for each of the SIS, OBM, and MPS modelling algorithms, with values shown for all input target fractions. The standard deviations of these average results (detailing how spread out the values are) is given for the (b) PERG, (d) GOO, and (f) RR values.

### Outputted Target Fraction PERG, GOO and RR Values Across All Algorithms

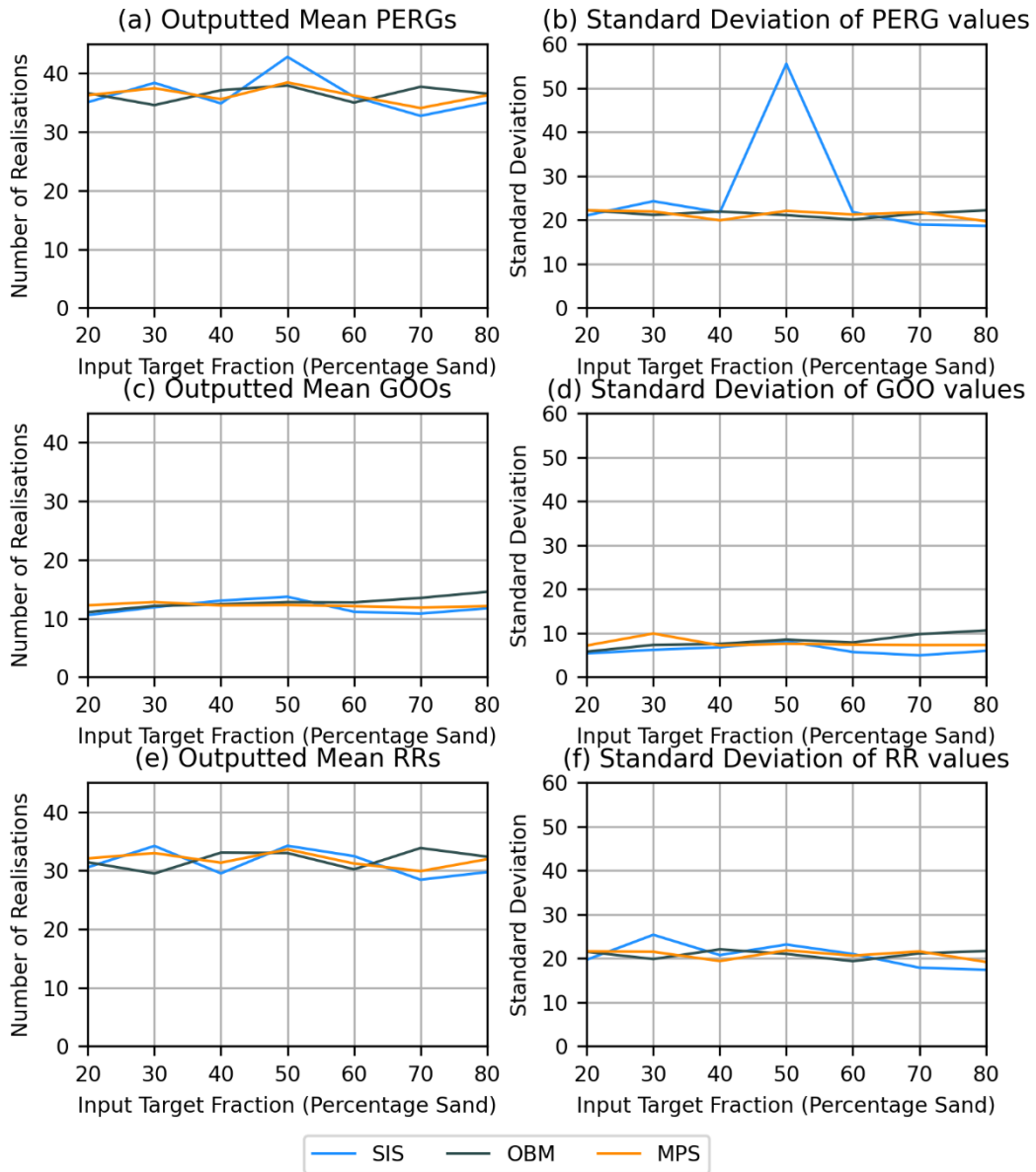


Figure 4.6: Comparison of the (a) PERG, (c) GOO and (e) RR values for the outputted target fraction values, for each of the SIS, OBM, and MPS modelling algorithms, with values shown for all input target fractions. The standard deviations of these average results (detailing how spread out the values are) is given for the (b) PERG, (d) GOO, and (f) RR values.

Illustrated within Figure 4.7, Figure 4.8 and Figure 4.9 are the total distributions of the PERG values for the SIS, OBM and MPS modelling algorithms respectively. These figures demonstrate the approximate 20 standard deviation as shown in Figure 4.4b, Figure 4.5b and Figure 4.6b. Whilst a standard deviation of about 20 would be considered to be large for the dataset, the

actual spread of data shows that the main core of PERG values is focussed rather centrally to values near to 30 for each the mean geobody thickness (Figure 4.7a, Figure 4.8a and Figure 4.9a), standard deviation of geobody thickness (Figure 4.7b), and outputted target fraction (Figure 4.7c, Figure 4.8c and Figure 4.9c) for each the SIS (Figure 4.7), OBM (Figure 4.8) and MPS (Figure 4.9) algorithms.

The PERG values for the SIS algorithm (Figure 4.7) shows two distinct peaks in values, occurring at the 15 and 65 bins. The first of these peaks (15 realisations) is generally much larger at a frequency of approximately 30, in comparison to the second discrete peak (65 realisations), which generally has a frequency of 10, which is a significant decrease from the frequency of the largest peak. Furthermore, immediately after the 15 realisations bin, there is a constant decrease in frequency across the 30 (frequency of 25), 40 (frequency of 10) and 55 (frequency of 5) bins. Inclusive of the 15 realisations bin, this equates to approximately 87.5% of the entire dataset for the SIS algorithm having a PERG value of less than 65 realisations, with the approximate average being found within the 30 realisations bin.

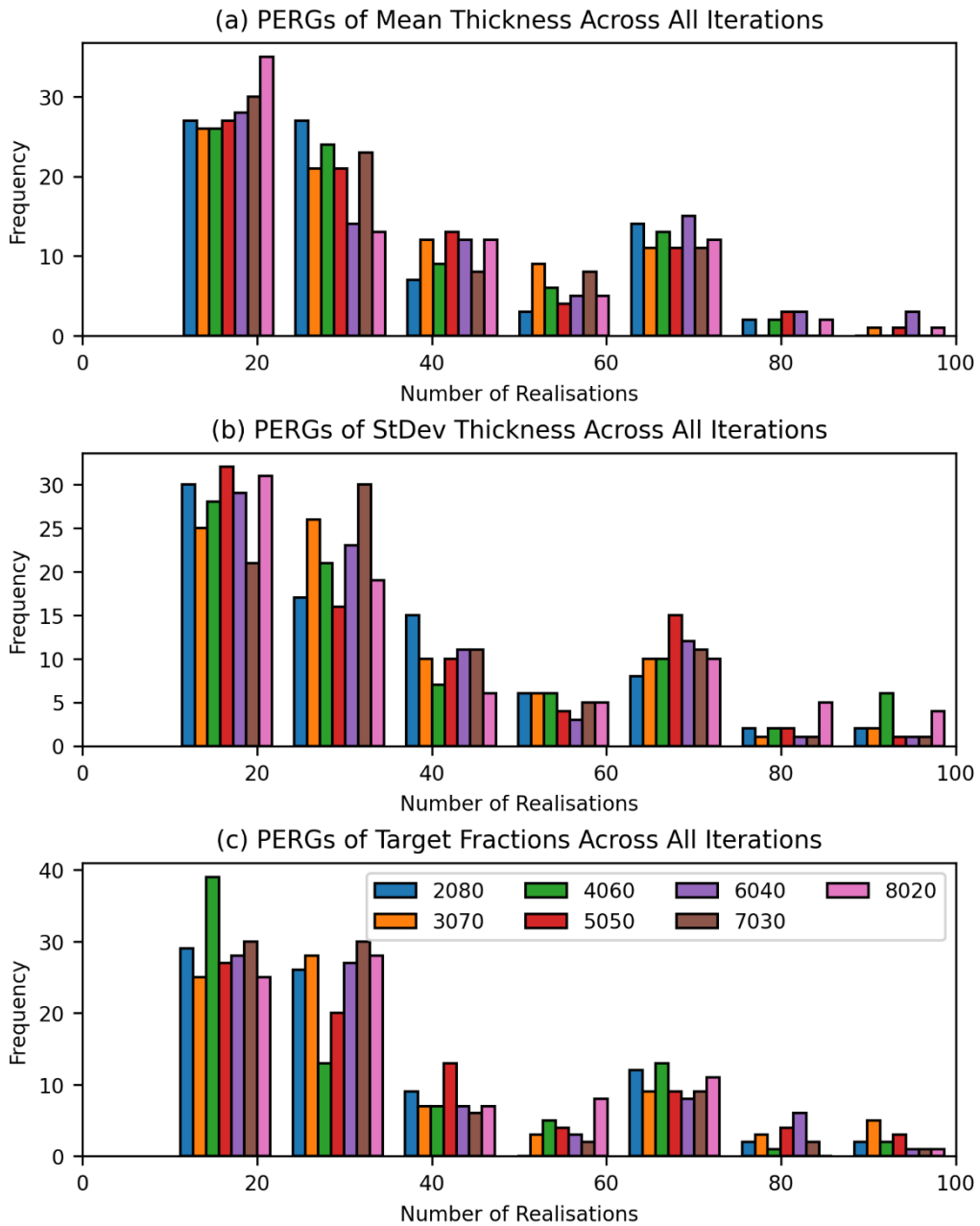


Figure 4.7: Distribution of the PERG values for the (a) mean geobody thickness, (b) standard deviation of geobody thickness, and (c) output target fraction, for the SIS algorithm.

The PERG values for the OBM algorithm (Figure 4.8) shows two distinct peaks in values, occurring at the 20 and 65 bins. The first of these peaks (20 realisations) is generally much larger at a frequency of approximately 90, in comparison to the second discrete peak (65 realisations), which generally has a frequency of 30, which is a significant decrease from the frequency of the largest peak. Furthermore, immediately after the 20 realisations bin, there is a constant decrease in frequency across the 35 (frequency of 60) and 50 (frequency of 25) bins. Inclusive of the 10 and

20 realisations bins, this equates to approximately 77% of the entire dataset for the SIS algorithm having a PERG value of less than 65 realisations, with the approximate average being found within the 30 realisations bin.

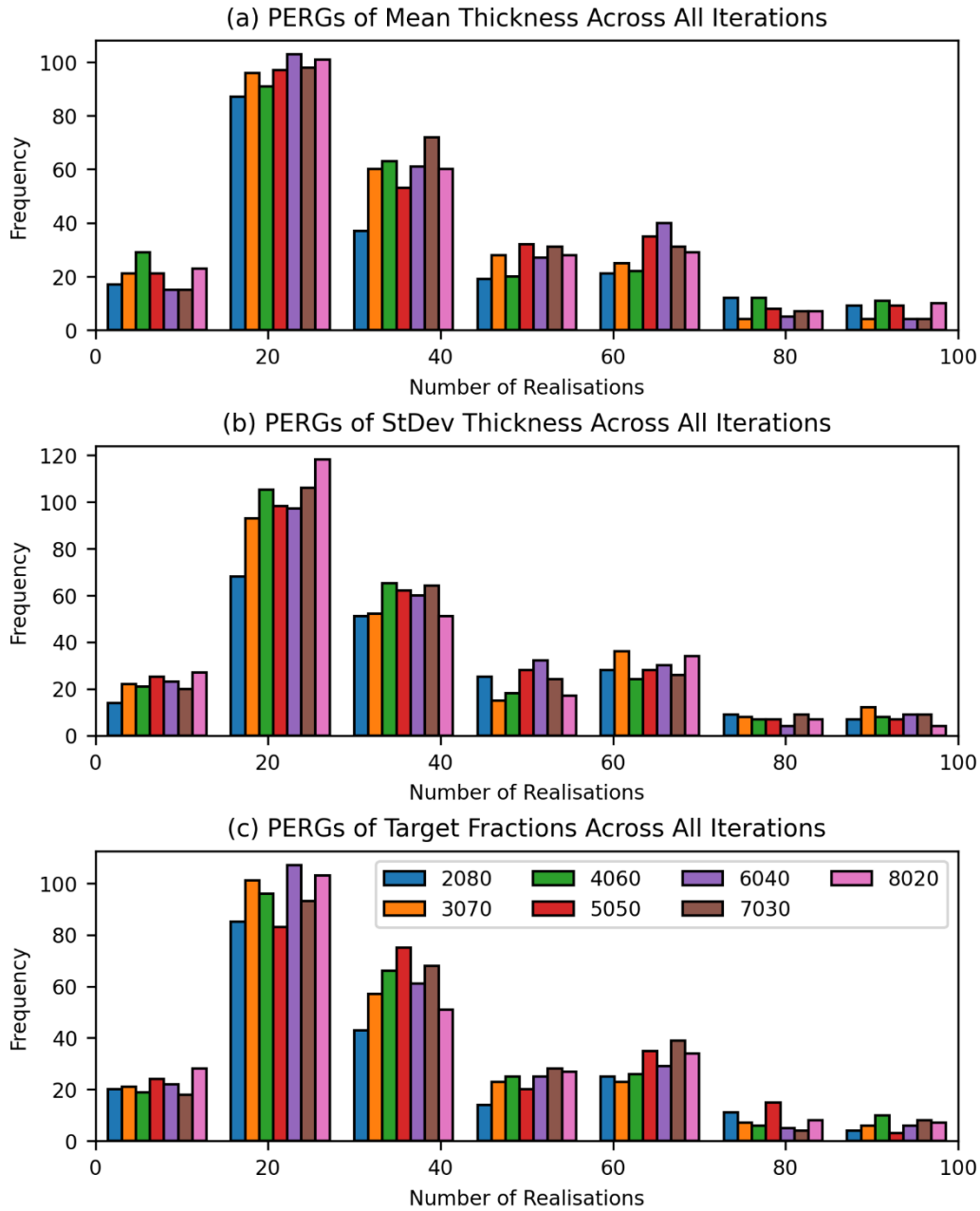


Figure 4.8: Distribution of the PERG values for the (a) mean geobody thickness, (b) standard deviation of geobody thickness, and (c) output target fraction, for the OBM algorithm.

The PERG values for the MPS algorithm (Figure 4.9) shows two distinct peaks in values, occurring at the 18 and 65 bins. The first of these peaks (18 realisations) is generally much larger at a frequency of approximately 70, in comparison to the second discrete peak (65 realisations), which generally has a frequency of 30, which is a significant decrease from the frequency of the largest peak. Furthermore, immediately after the 18 realisations bin, there is a constant decrease in frequency across the 30 (frequency of 70), 40 (frequency of 40) and 55 (frequency of 20) bins. Inclusive of the 18 realisations bin, this equates to approximately 78% of the entire dataset for the SIS algorithm having a PERG value of less than 65 realisations, with the approximate average being found within the 30 realisations bin.

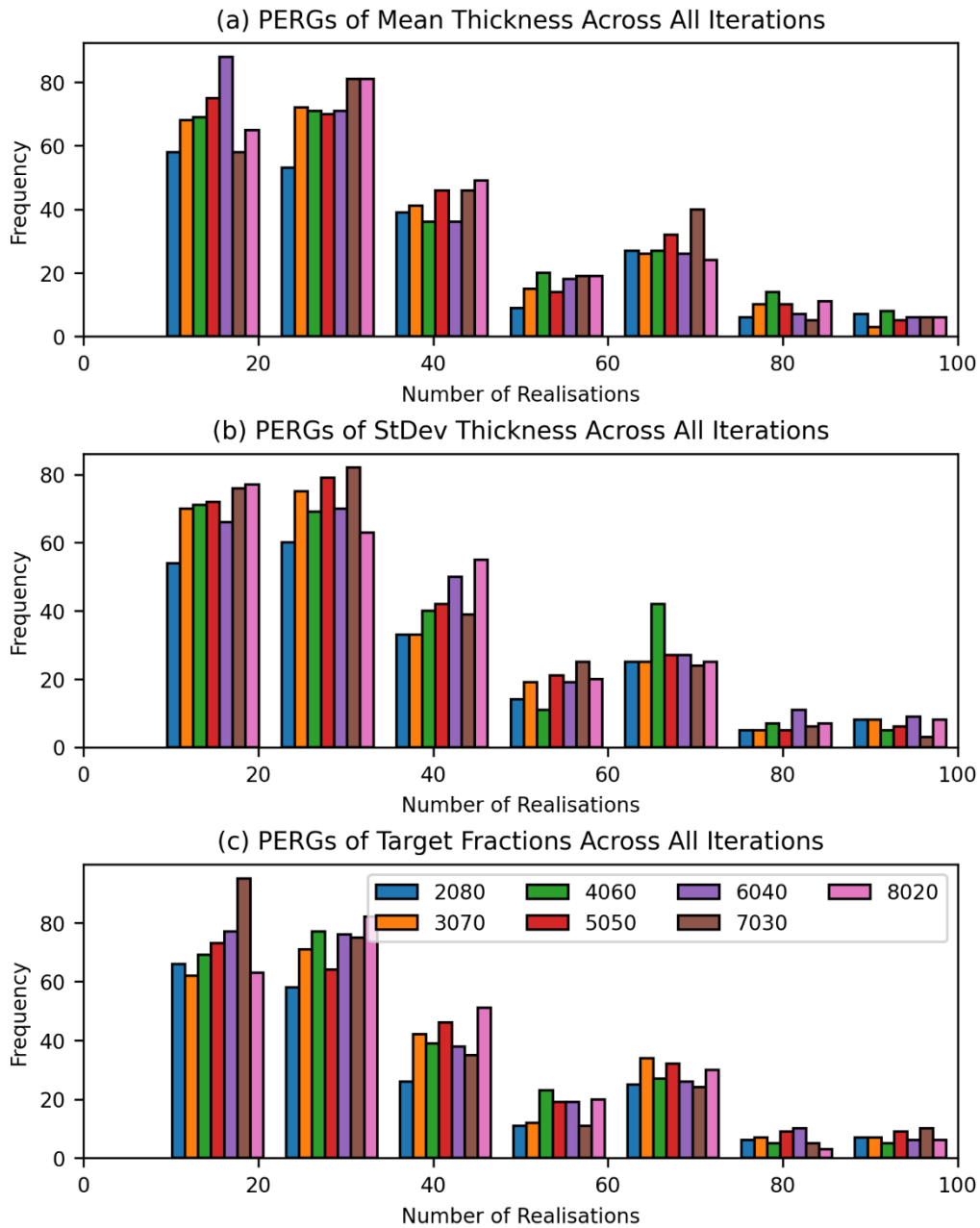


Figure 4.9: Distribution of the PERG values for the (a) mean geobody thickness, (b) standard deviation of geobody thickness, and (c) output target fraction, for the MPS algorithm.

The CDF graph of the average PERG values (Figure 4.10) corresponds to the histogram plots (Figure 4.4d, Figure 4.5d, and Figure 4.6d). The effect of the modelling algorithm is relatively negligible (as seen within the CDF), with the different reservoir modelling algorithms all showing the same general trends for the discrete variable being analysed. This similarity also extends to the general distribution of values. Across all of the plotted lines, 20 realisations (Goovaerts, 1999) only encompasses one quarter of all results (25<sup>th</sup> percentile), and as such is high unlikely to create

a representative sample of values. Furthermore, the median value occurs at approximately 30 realisations, whilst the 60<sup>th</sup> percentile occurs at 35, and the final 20 percent of results fall above 50 realisations. Notably, just 5% of all values occur at values over and inclusive of 80 realisations.

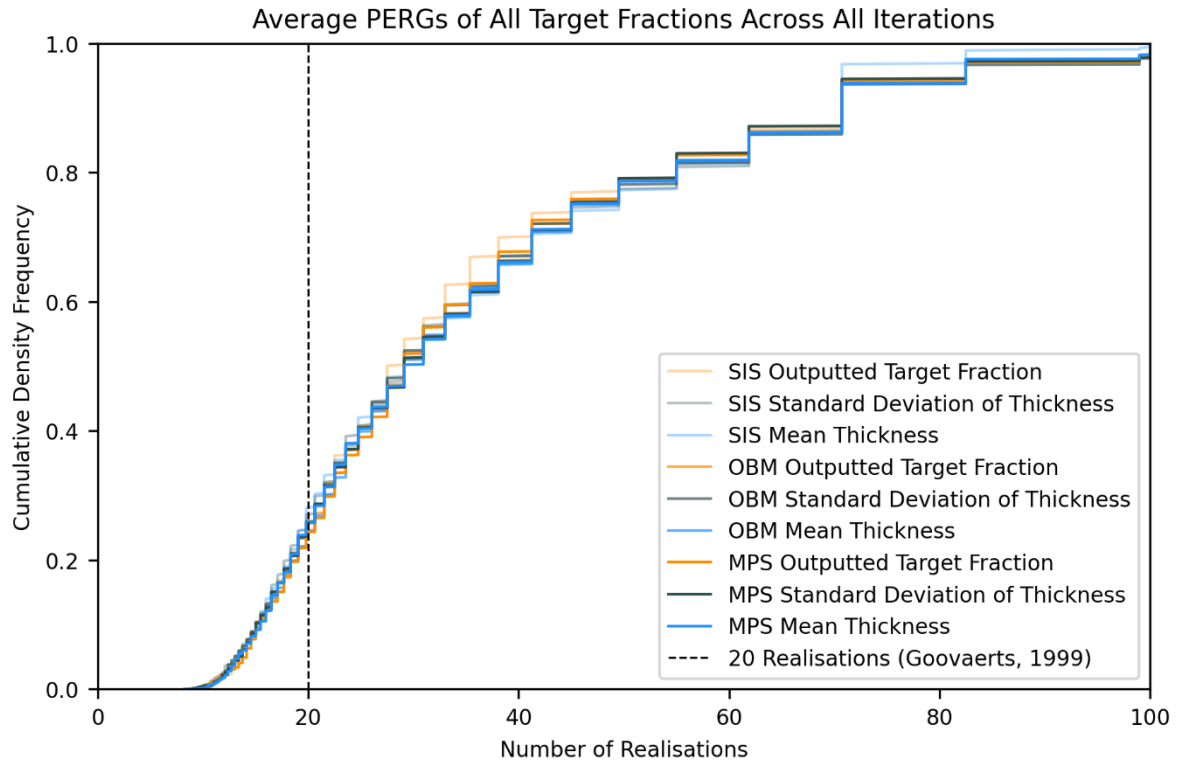


Figure 4.10: Cumulative distribution function (CDF) of the PERG values for the mean geobody thickness, standard deviation of geobody thickness, and outputted target fraction, for each the SIS, OBM and MPS modelling algorithms, with the previously used 20 realisations marked on the graph.

Illustrated within Figure 4.11, Figure 4.12 and Figure 4.13 are the total distributions of the GOO values for the SIS, OBM and MPS modelling algorithms respectively. These figures demonstrate the approximate 20 standard deviation as shown in Figure 4.4d, Figure 4.5d and Figure 4.5d. A standard deviation of about 8 would be considered to be relatively average for a dataset of this size. The spread of data shows that the main core of GOO values is focussed rather centrally to values near to 10 for each the mean geobody thickness (Figure 4.11a, Figure 4.12a and Figure 4.13a), standard deviation of geobody thickness (Figure 4.11b, Figure 4.12b and Figure 4.13b), and outputted target fraction (Figure 4.11c, Figure 4.12c and Figure 4.13c) for each the SIS (Figure 4.11), OBM (Figure 4.12) and MPS (Figure 4.13) algorithms.

The GOO values for the SIS algorithm (Figure 4.11) shows a singular peak at the 8 realisations bin. After this peak (with an approximate frequency of 40-45), is an immediate decrease in frequency across the other bins, with approximately half of the frequency of the previous bin being represented. Approximately 70% of all GOO values are held across the first two bins for each the mean geobody thickness, standard deviation of geobody thickness and output target fraction. This leads to the mean value being found within the 8 realisations bin.

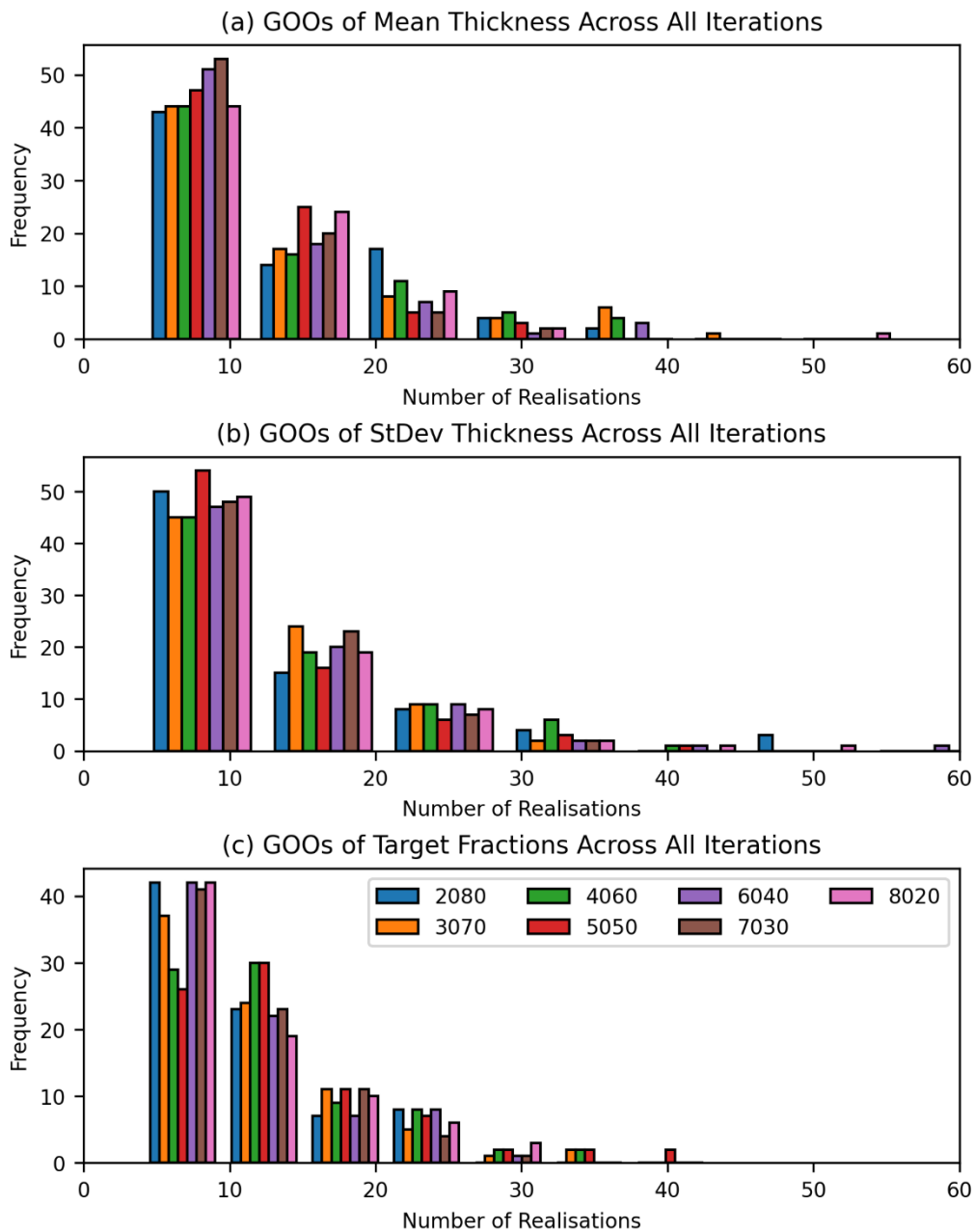


Figure 4.11: Distribution of the GOO values for the (a) mean geobody thickness, (b) standard deviation of geobody thickness, and (c) output target fraction, for the SIS algorithm.

The GOO values for the OBM algorithm (Figure 4.12) shows a singular peak at the 8 realisations bin. After this peak (with an approximate frequency of 150), is an immediate decrease in frequency across the other bins, with approximately half of the frequency of the previous bin being represented (excluding the output target fraction graph, Figure 4.12c), which shows this as a quarter rather than half. Approximately 85% of all GOO values are held across the first two bins for each the mean geobody thickness, standard deviation of geobody thickness and output target fraction, suggesting that a very strong bias for lower realisations results. The average value is located within the 8 realisations bin.

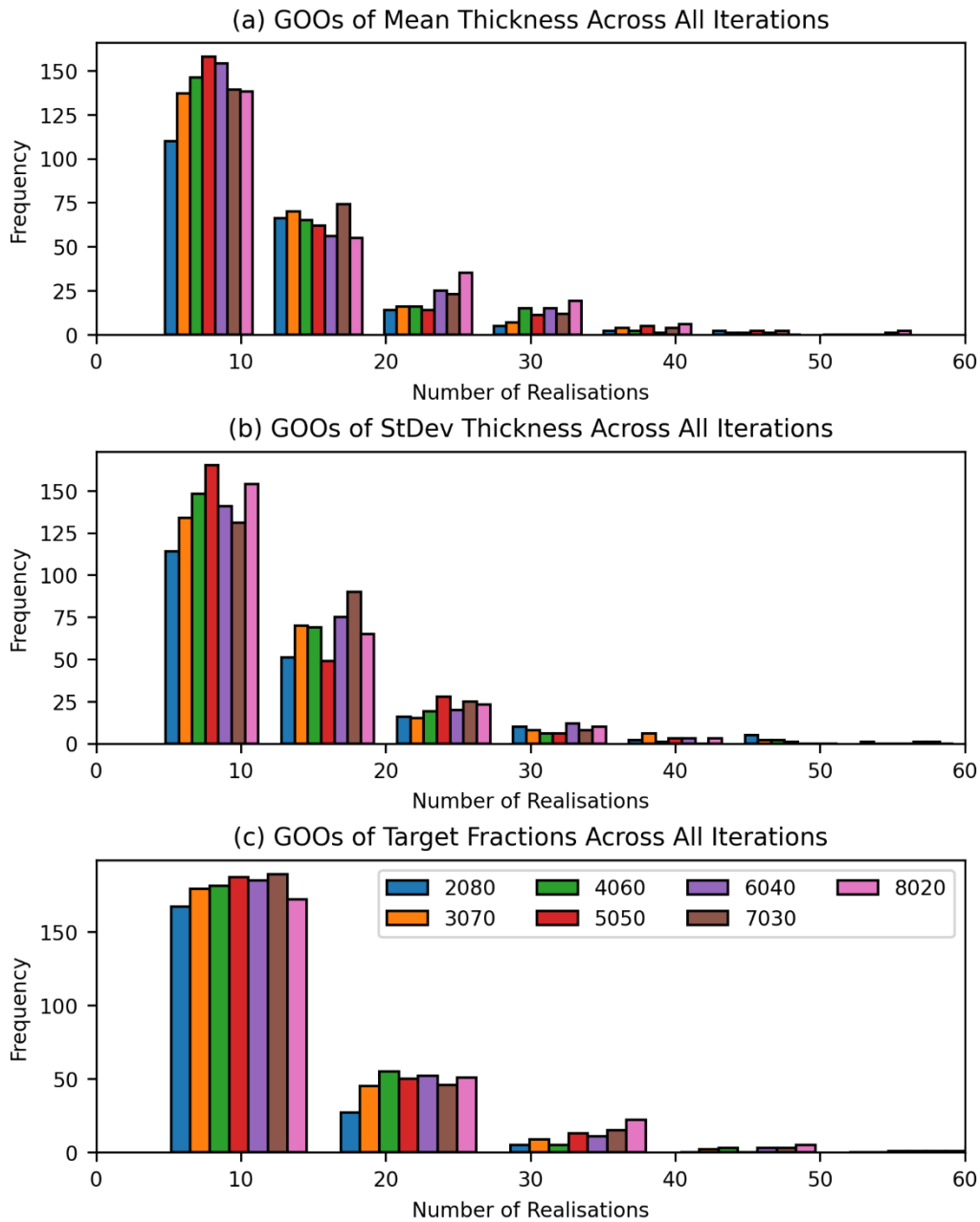


Figure 4.12: Distribution of the GOO values for the (a) mean geobody thickness, (b) standard deviation of geobody thickness, and (c) output target fraction, for the OBM algorithm.

The GOO values for the OBM algorithm (Figure 4.13) shows a singular peak at the 8 realisations bin. After this peak (with an approximate frequency of between 125 and 175), is an immediate decrease in frequency across the other bins, with approximately half of the frequency of the previous bin being represented (excluding the outputted target fraction graph, Figure 4.13c),

which shows this as a quarter rather than half. Approximately 90% of all GOO values are held across the first two bins for each the mean geobody thickness, standard deviation of geobody thickness and output target fraction, suggesting that a very strong bias for lower realisations results. The average value is located within the 8 realisations bin.

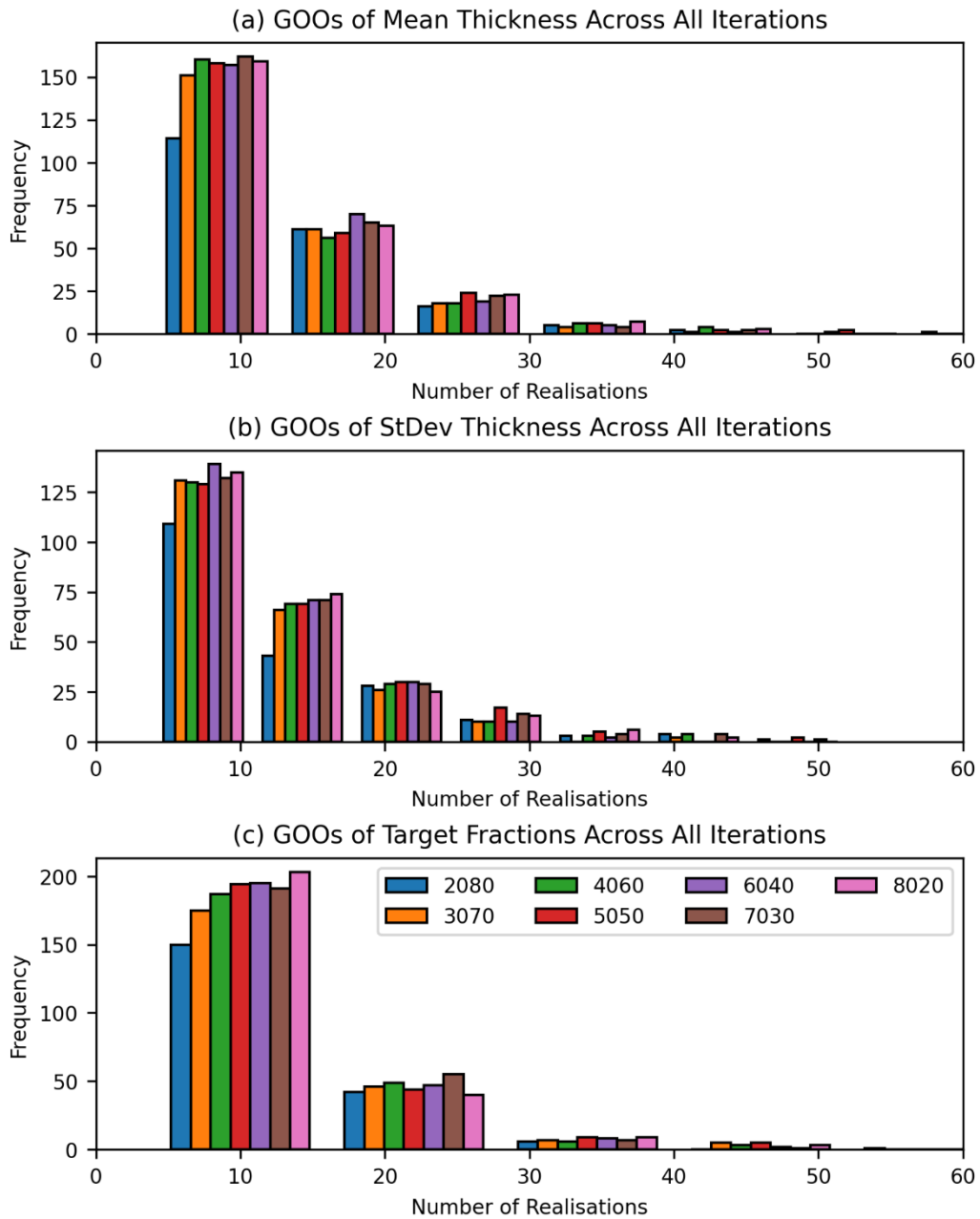


Figure 4.13: Distribution of the GOO values for the (a) mean geobody thickness, (b) standard deviation of geobody thickness, and (c) output target fraction, for the MPS algorithm.

The CDF graph of the average GOO values (Figure 4.14) corresponds to the histogram plots (Figure 4.11, Figure 4.12 and Figure 4.13). The effect of the modelling algorithm is relatively negligible (as seen within the CDF), with the different modelling algorithms all showing the same general trends, along with roughly the same distribution of values. Across all of the plotted lines, 20 realisations (Goovaerts, 1999) encompasses 85 percent of all results, and as such is high likely to include a representative sample of values. Furthermore, the median value occurs at approximately 10 realisations, whilst the 60<sup>th</sup> percentile occurs at 12, and the final 20 percent of results fall above 20 realisations. Notably, just 5% of all values occur at values over and inclusive of 30 realisations.

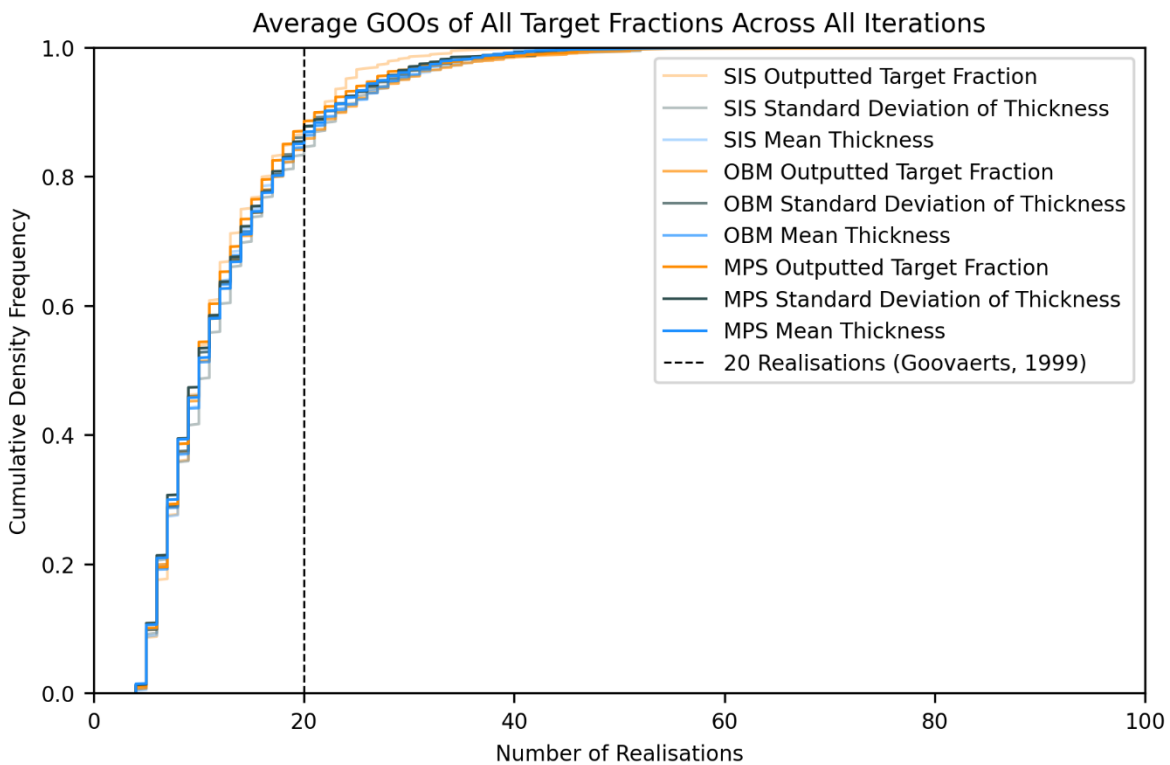


Figure 4.14: Cumulative distribution function (CDF) of the GOO values for the mean geobody thickness, standard deviation of geobody thickness, and outputted target fraction, for each the SIS, OBM and MPS modelling algorithms, with the previously used 20 realisations marked on the graph.

Illustrated within Figure 4.15, Figure 4.16 and Figure 4.17 are the total distributions of the RR values for the SIS, OBM and MPS modelling algorithms respectively. These figures demonstrate the approximate 20 standard deviation as shown in Figure 4.4f, Figure 4.5f and Figure 4.6f. Whilst

a standard deviation of about 20 would be considered to be large for the dataset, the actual spread of data shows that the main core of PERG values is focussed rather centrally to values near to 30 for each the mean geobody thickness (Figure 4.15a, Figure 4.16a and Figure 4.17a), standard deviation of geobody thickness (Figure 4.15b, Figure 4.16b and Figure 4.17b), and output target fraction (Figure 4.15c, Figure 4.16c and Figure 4.17c) for each the SIS (Figure 4.15), OBM (Figure 4.16) and MPS (Figure 4.17) algorithms.

The RR values for the SIS algorithm (Figure 4.15) shows two distinct peaks in values, occurring at the 15 and 65 bins. The first of these peaks (15 realisations) is generally much larger at a frequency of approximately 25, in comparison to the second discrete peak (65 realisations), which generally has a frequency of approximately 8, which is a significant decrease from the frequency of the largest peak. Furthermore, immediately after the 15 realisations bin, there is a relatively stable decrease in frequency across the 25 (frequency of 20), 40 (frequency of 10) and 55 (frequency of 5) bins. This equates to approximately 75% of the entire dataset for the SIS algorithm having a PERG value of less than 65 realisations, with the approximate average being found within the 25 realisations bin.

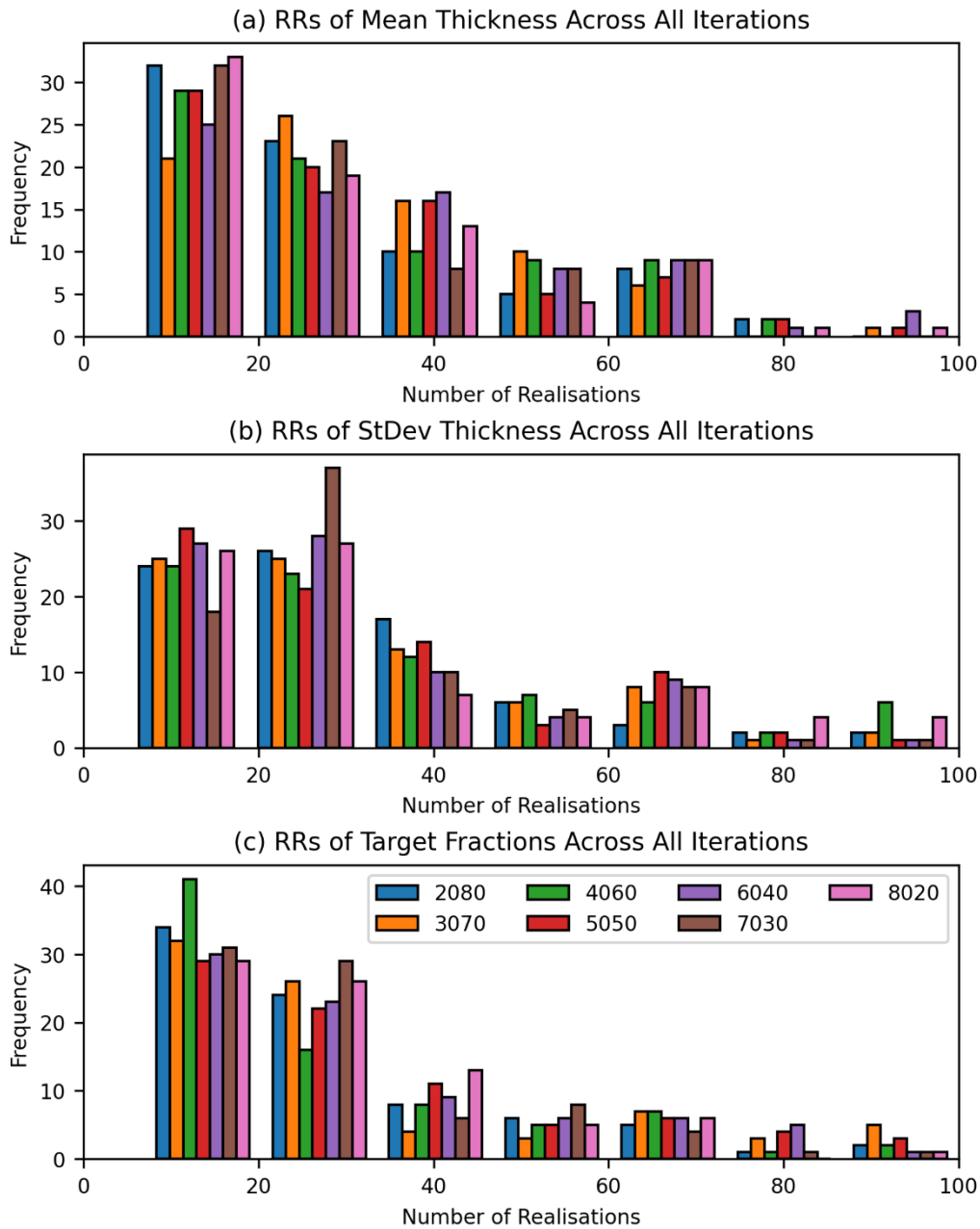


Figure 4.15: Distribution of the RR values for the (a) mean geobody thickness, (b) standard deviation of geobody thickness, and (c) output target fraction, for the SIS algorithm.

The RR values for the OBM algorithm (Figure 4.16) shows two distinct peaks in values, occurring at the 15 and 65 bins, with the 25 peak being almost identical to the 15 peak. The first of these peaks (15 realisations) is generally much larger at a frequency of approximately 70, in comparison to the second discrete peak (65 realisations), which generally has a frequency of 20, which is a significant decrease from the frequency of the largest peak. Furthermore, immediately after the 15 realisations bin, there is a constant decrease in frequency across the 25 (frequency of 70), 40

(frequency of 40) and 55 (frequency of 10) bins. Inclusive of the 15 realisations bin, this equates to approximately 75% of the entire dataset for the OBM algorithm having a RR value of less than 65 realisations, with the approximate average being found within the 30 realisations bin.

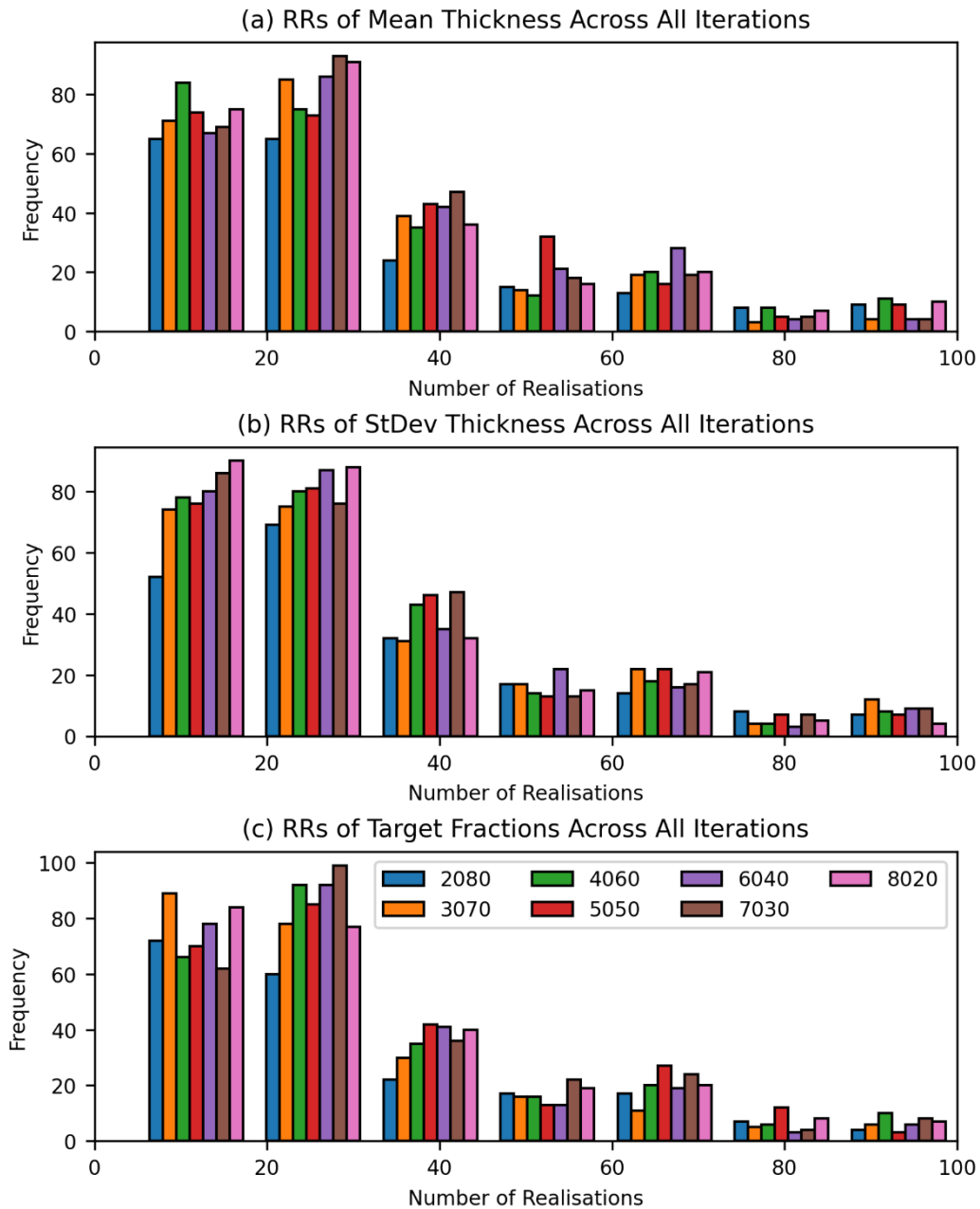


Figure 4.16: Distribution of the RR values for the (a) mean geobody thickness, (b) standard deviation of geobody thickness, and (c) output target fraction, for the OBM algorithm.

The RR values for the MPS algorithm (Figure 4.17) shows two distinct peaks in values, occurring at the 15 and 65 bins, with the 25 peak almost mimicking the 15 peak. The first of these peaks (15 realisations) is generally much larger at a frequency of approximately 80, in comparison to the second discrete peak (65 realisations), which generally has a frequency of 20, which is a significant decrease from the frequency of the largest peak. Furthermore, immediately after the 15 realisations bin, there is a constant decrease in frequency across the 25 (frequency of 80), 40 (frequency of 40) and 55 (frequency of 20) bins. Inclusive of the 15 realisations bin, this equates to approximately 86% of the entire dataset for the MPS algorithm having a RR value of less than 65 realisations, with the approximate average being found within the 30 realisations bin.

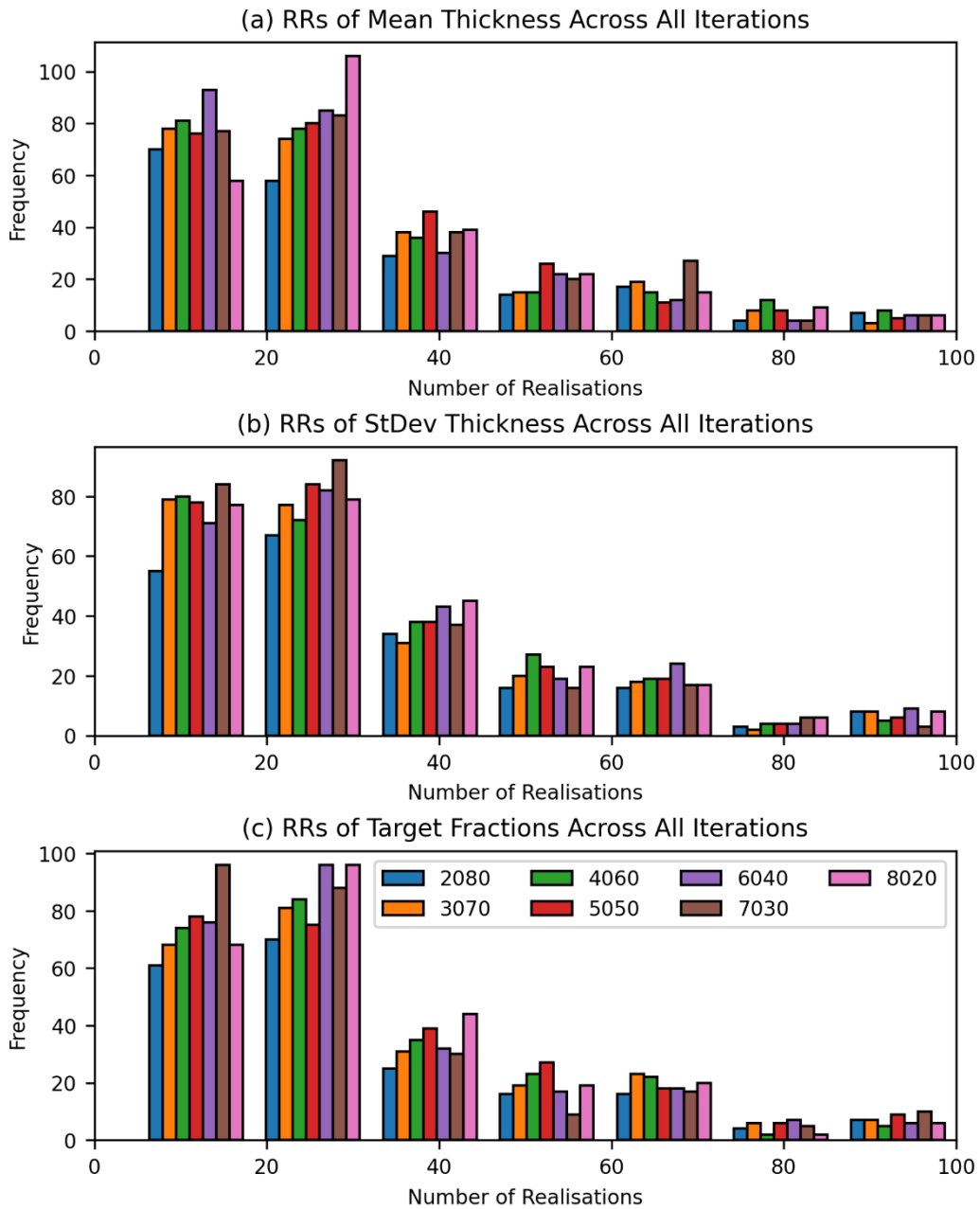


Figure 4.17: Distribution of the RR values for the (a) mean geobody thickness, (b) standard deviation of geobody thickness, and (c) output target fraction, for the MPS algorithm.

The CDF graph of the average RR values (Figure 4.18) corresponds to the histogram plots (Figure 4.15, Figure 4.16 and Figure 4.17). The effect of the modelling algorithm is relatively negligible (as seen within the CDF), with the majority of the different modelling algorithms along with what is being plotted (mean geobody thickness, standard deviation of geobody thickness and outputted target fraction) all showing the same general trends, along with roughly the same distribution of values. Across all the plotted lines, 20 realisations (Goovaerts, 1999) only encompasses about 40%

of all results, and as such is about as likely as unlikely to create a representative sample of values. Furthermore, the median value occurs at approximately 26 realisations, whilst the 60<sup>th</sup> percentile occurs at 30, and the final 20 percent of results fall above 45 realisations. Notably, just 5% of all values occur at values over and inclusive of 75 realisations.

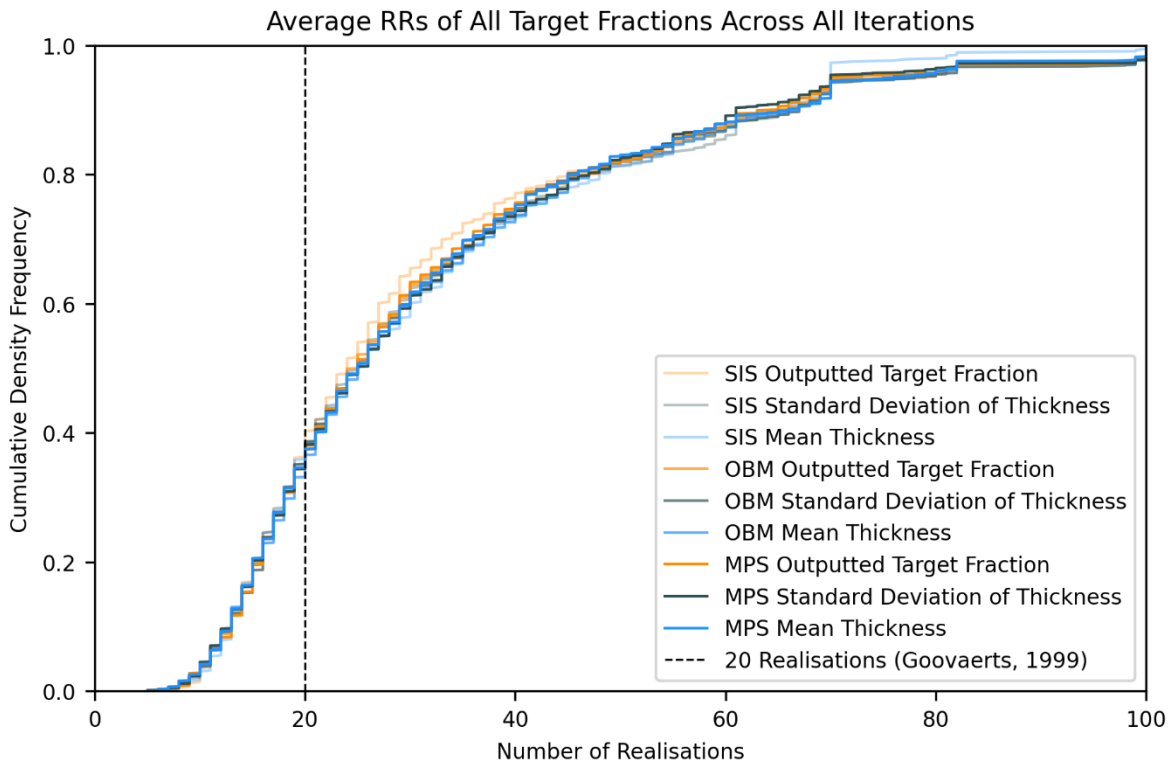


Figure 4.18: Cumulative distribution function (CDF) of the RR values for the mean geobody thickness, standard deviation of geobody thickness, and outputted target fraction, for each the SIS, OBM and MPS modelling algorithms, with the previously used 20 realisations marked on the graph.

Generally, the SIS (Figure 4.19a), OBM (Figure 4.19b) and MPS (Figure 4.19c) CDFs show almost identical trending, with the first 20 being almost identical to each other. Whilst the OBM (Figure 4.19b and Figure 4.19c) show very little difference as the cumulative distribution function increases (due to the OBM's acting as training images for the MPS models), there is some slight deviation of the SIS (Figure 4.19a) mean geobody thickness between approximately 25 and 55 realisations. The resultant discrepancy is a lack of grouping of the mean geobody thickness,

standard deviation of geobody thickness, and outputted target fraction, and is seen in both the PERG and RR values. This is likely due to the reduced number of models (560 compared to 1,792 for both the OBM and MPS algorithms).

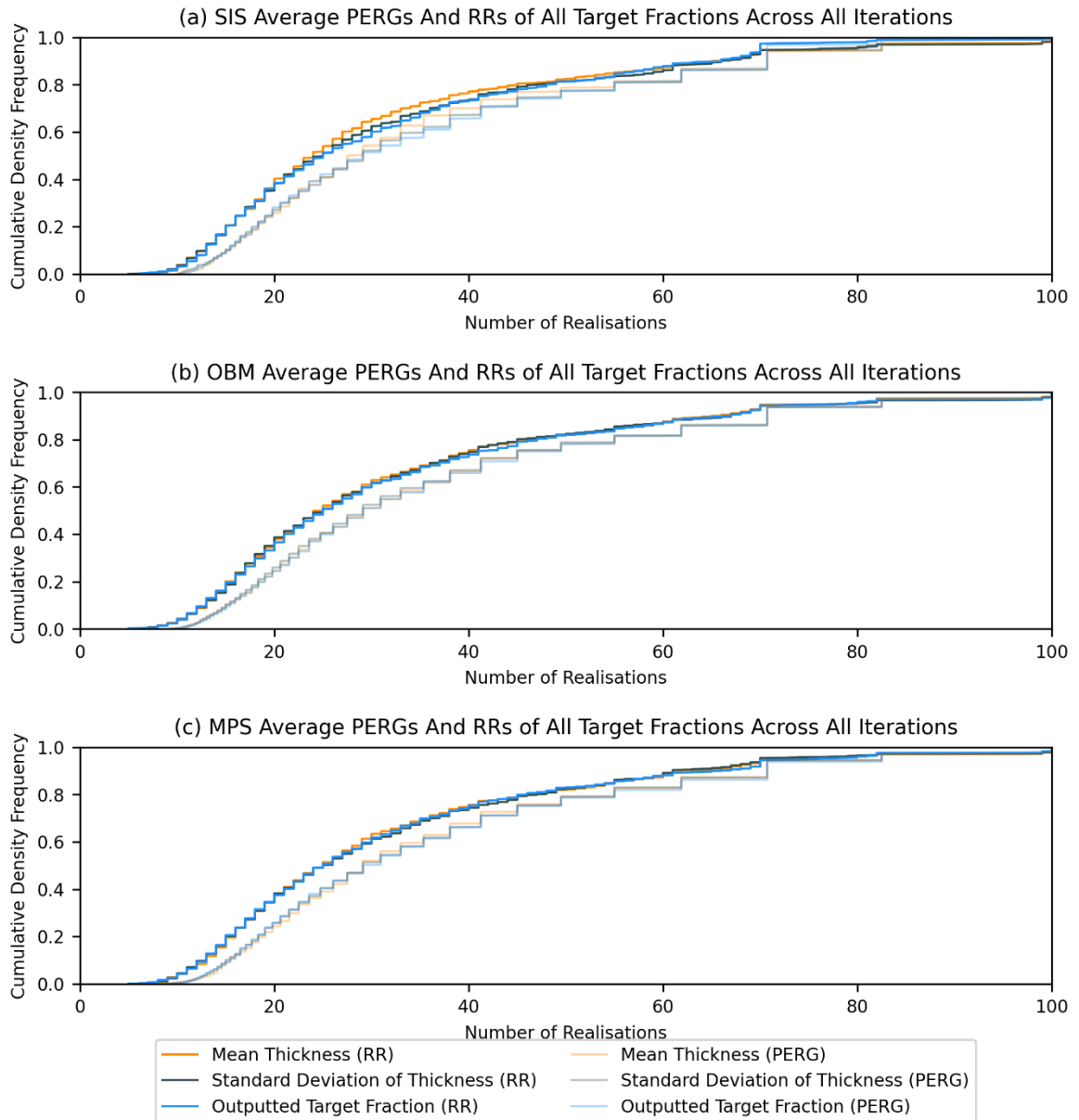


Figure 4.19: Comparison of cumulative distribution function (CDF) of the RR values for the mean geobody thickness, standard deviation of geobody thickness, and outputted target fraction, for each the (a) SIS, (b) OBM and (c) MPS modelling algorithms.

## 4.2 Percentage Similarity

The average percentage similarities for each the SIS, OBM and MPS algorithms (Figures 4.20a, Figure 4.20b and Figure 4.20c respectively), show a strong variation between the similarity from the RR value, and the similarity of the first 20 realisations (Goovaerts, 1999). For the SIS algorithm, there is, on average a 4.5% variation between the two, which is relatively consistent across each the mean geobody thickness (4.5%), standard deviation of geobody thickness (5%) and outputted target fraction values (4.5%). For the OBM algorithm, this variation rises to approximately 5%, which is also relatively consistent across each the mean geobody thickness (4.7%), standard deviation of geobody thickness (5.3%) and output target fraction (5%). Finally, the MPS algorithm, there is, on average a 5% increase on the variation between the RR value and the first 20 realisations. This is also consistent across each the mean geobody thickness (5%), standard deviation of geobody thickness (5%) and outputted target fraction (5%). Overall, on average there is an approximate 6% increase on the total representation of a much larger dataset (100), whilst also not including duplication of model property values for each of the modelling algorithms used, and as such suggests that this increase in models needing to be run is substantiated.

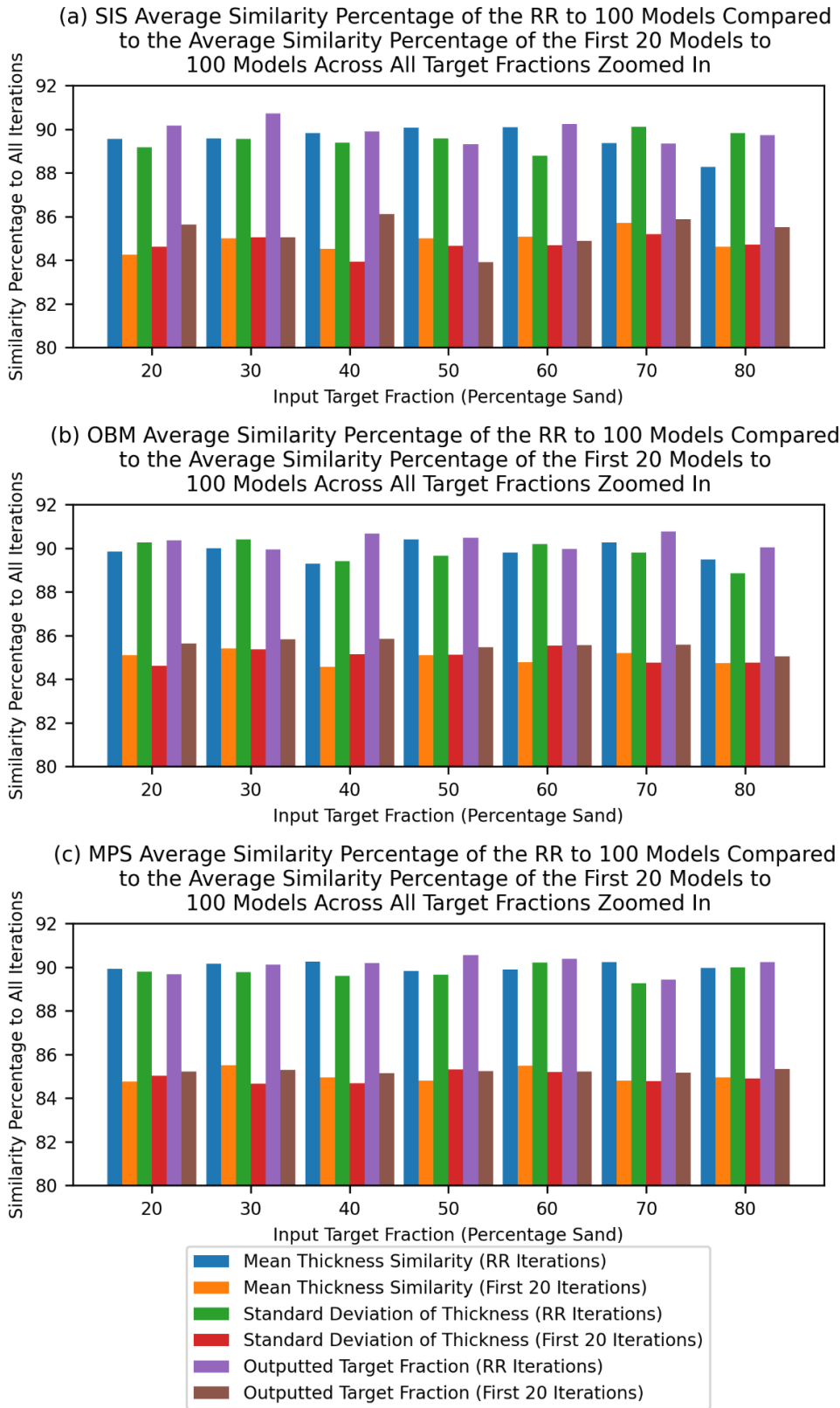


Figure 4.20: Comparison of the total similarity (intersectional percentages) of the first 20 realisations compared to the RR value across all input target fractions, for each the (a) SIS, (b) OBM, and (c) MPS modelling algorithm.

### 4.3 Summary

Overall, whilst all three modelling algorithms give very similar values for each the GOO, PERG and RR values for the mean geobody thickness, standard deviation of geobody thickness and output target fraction, there is still deviation between the results obtained for the SIS algorithm in comparison to the OBM and MPS algorithm. Since the SIS algorithm has fewer total runs (due to only having 3 variables to alter with every input target fraction, as seen in Table 3.1), the results appear refined, and more sporadic, with some large variations forming (Figure 4.6b). By contrast, realisations using the OBM and MPS algorithms, have 4 variables (wavelength, amplitude, width, and vertical height), which leads to far more realisations (which leads to a more refined values, and smoother graphs (and subsequent trends). Whilst this could be the result of averaging fewer realisations, it could also be due to the inherent uncertain nature of the SIS modelling algorithm, with the realisations tending to be more varied than both the OBM and MPS algorithms. The OBM and MPS algorithms both had very similar results across all graphs, which is probably due to one of the OBM realisations acting as a training image to inform the MPS algorithm about the model parameters. In turn, this causes the resultant values for the MPS algorithm to be similar to the OBM values. Interestingly, the standard deviations for both the PERG and RR values are very large (20), for what is a relatively small (and confined) dataset of 100 values. This would suggest that the resultant averaged values are not entirely representative. However, they do provide a good indication of the number of realisations required for a statistically significant three-dimensional reservoir model suite (32 realisations), the number of realisations for the standard deviation of values to plateau (13 realisations), and the number of realisations for the property values of the realisations to start to repeat (38 realisations). This synthetic study highlights the statistical insignificance of using just 20 realisations, with the average recommended number of realisations being 50% larger than this. These average values do not provide a 'one answer fits all' solution to the question of 'How many models do I need to generate?', but it does provide a framework, and provides significant evidence as to why developing just 20 realisations generates a statistically insignificant suite of three-dimensional stochastic reservoir models.

## 5 Application: Tuscher Canyon

Synthetic models give a general benchmark as to how a large suite of realisations is likely to respond to the methodology developed within this study. However, when a specific model is generated through values obtained from outcrops such as Jamuna River and Tuscher Canyon (Mitten, 2020), the resultant PERG, GOO and RR values tend to deviate from the averaged values that synthetic realisations indicate (Figure 4.4, Figure 4.5, and Figure 4.6).

The two study locations (Cretaceous Lower Castlegate Sandstone of Tuscher Canyon, Utah, and the Jamuna River, northern India) used to create the depositional conditioned fluvial reservoir models were selected due to their similarity (Mitten *et al.*, 2020), with both representing sand-dominated, low- to intermediate-sinuosity fluvial environments (Miall, 1993; 1994; Ashworth *et al.*, 2000; McLaurin and Steel, 2007). Both of these fluvial systems show variable discharge rates (Ashworth *et al.*, 2000), and approximately at the same global latitude, and similar, warm, humid climate throughout deposition (Kauffman and Caldwell, 1993; Hampson *et al.*, 2005).

In this chapter, the methodology described in Chapter 3 is applied to the depositional conditioned model of the Tuscher Canyon section, with measurements for the generated reservoir models coming from Mitten *et al.* (2020). The model combines outcrop photogrammetric models (Tuscher Canyon, Utah), and satellite imagery (Jamuna River, northern India) to determine the parameters for fluvial reservoir models to be generated. The values used to create the variograms (Figure 5.1) required to generate reservoir models using the SIS algorithm for the Tuscher Canyon model (vertical height, major direction and minor direction as described in Section 3.1). The values used to stochastically generate the various geobodies for the OBM and MPS algorithms for the Tuscher Canyon model (length, width, depth, amplitude and wavelength as described in Section 3.1) can be found within Table 5.1 when generating models using the OBM algorithm. These OBM models are then used as training images to inform the generation of models developed using the MPS algorithm. Four geobodies are used to create these models: channel element, thalweg bedform, lateral accretion element and downstream accretion element.

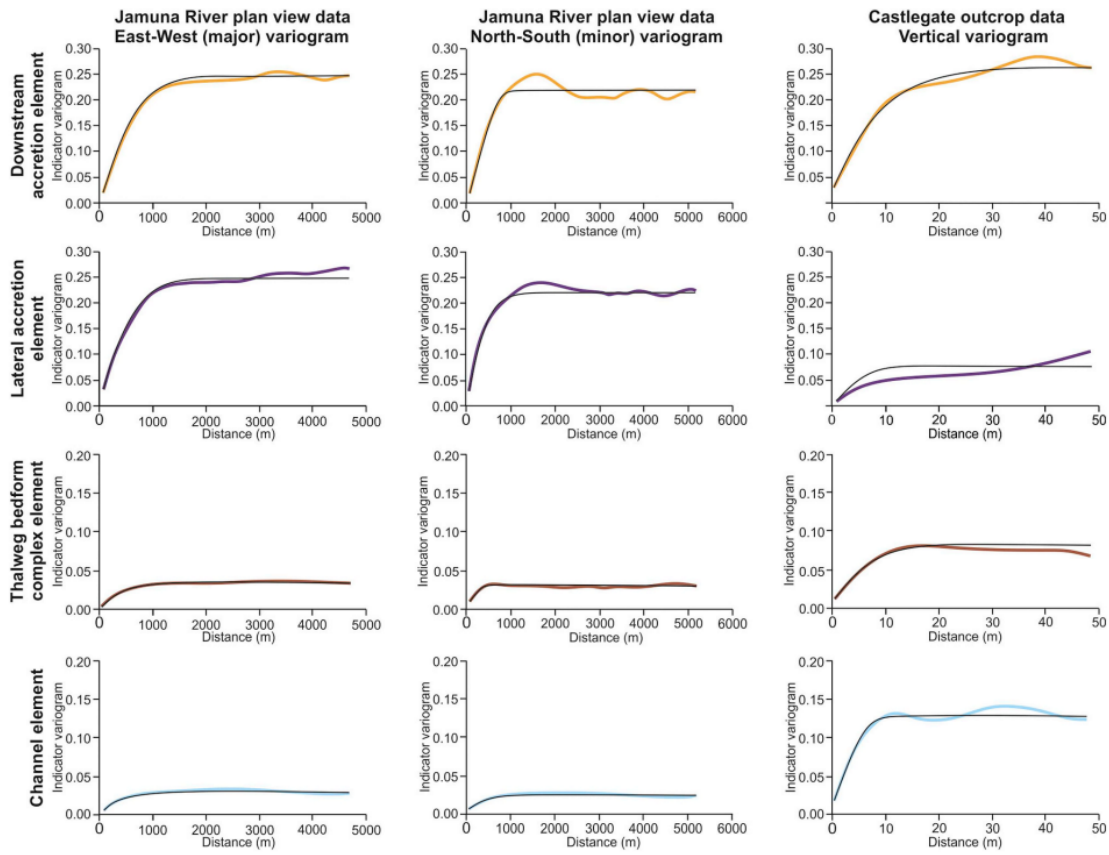


Figure 5.1: variogram input data for the downstream accretion, lateral accretion, thalweg bedform and channel element geobodies for the Tuscher Canyon SIS reservoir model (using data from the modern analogue of Jamuna River for the major and minor direction values) (from Mitten et al., 2020).

Architectural Element	Distribution	Dimensions	Proportion	Geometry	
Channel Fill (CH)	Subordinate CH elements cross cut DA	Length	N/A	26%	Plan: Ribbon
		Width	Min: 90 m		Cross-section: Lensoidal
			Max: 400 m		
		Depth	Min: 1 m		
			Max: 8 m		
		Amplitude	Min: 50 m		

			95		
			Max: 575 m		
		Wavelength	Min: 370 m		
			Max: 3400 m		
Thalweg		Length	Min: 50 m	8%	Plan: Irregular
Barform	TB must be				asymmetric
Complex	confined		Max: 400 m		lens
(TB)	within CH	Width	Min: 50 m		Cross-section:
			Max: 300 m		Lensoidal
		Depth	Min: 1 m		
			Max: 3 m		
					Plan:
Lateral	LA must be	Length	Min: 150 m	14%	Lensoidal
Accretion	located at		Max: 800 m		Cross-section:
(LA)	the CH/ DA	Width	Min: 75 m		Tabular
	boundary		Max: 800 m		
		Depth	Min: 1 m		
			Max: 5 m		
Downstream	DA must be	Length	Min: 400 m	52%	Plan: Irregular
Accretion	contained		Max: 2000 m		Kite
(DA)	within CH on	Width	Min: 200 m		Cross-section:
	a large scale		Max: 2000 m		Lensoidal
		Depth	Min: 4 m		
			Max: 12 m		

*Table 5.1: input values for the downstream accretion, lateral accretion, thalweg bedform and channel element geobodies for the Tuscher Canyon OBM model (also acting as the training image conditioning data for the MPS algorithm), using data from Tuscher Canyon, with supplementary data about channel dimensions provided from the Jamuna River modern analogue (after Mitten et al., 2020)*

## 5.1 Geological Background

The Tuscher Canyon and Jamuna River outcrops are not the same (Section 5), but the similarities between the two (Mitten et al., 2020) enable the satellite imagery from Jamuna River to be used to inform any missing values to help to create a fluvial reservoir model from the outcrop found at Tuscher Canyon.

### 5.1.1 Lower Castlegate Sandstone, Tuscher Canyon, Utah

The Upper Cretaceous Lower Castlegate Sandstone (Figure 2, Mitten et al., 2020) is part of the Mesaverde Group (Fouch et al., 1983; Miall, 1993; Olsen et al., 1995; Miall and Arush, 2001; McLaurin and Steel, 2007), which represents an eastward prograding clastic wedge into the Western Interior Basin during the Late Cretaceous (Miall, 1993). The Castlegate Sandstone is composed of three lithostratigraphical units (Chan and Pfaff, 1991; Olsen et al., 1995; McLaurin and Steel, 2007): the Lower Castlegate Sandstone, Middle Castlegate Sandstone and the Bluecastle Tongue. The Lower Castlegate Sandstone is a sandy, low-sinuosity, bedload-dominated fluvial system (Olsen et al., 1995; McLaurin and Steel, 2007). The Middle Castlegate Sandstone is representative of an isolated channel fluvial system with high preservation of overbank material (McLaurin and Steel, 2007). Finally, the Bluecastle Tongue is genetically similar to the Lower Castlegate Sandstone (Olsen et al., 1995). A thinner succession of the Lower Castlegate Sandstone crops out at Tuscher Canyon, close to Green River, where six architectural elements are present (Miall, 1993) (with the four most important for this study being the channel element, downstream accretion element, lateral accretion element and the thalweg bedform).

### 5.1.2 Jamuna River, northern India

Jamuna River (situated between Bangladesh and Bhutan in northern India) is a bar complex fluvial system (Figure 3, Mitten et al., 2020), and acts as a modern analogue to the Lower Castlegate Sandstone. It represents a sandy, low sinuosity, bedload dominated fluvial system and has been extensively studied as a modern analogue (Coleman, 1969; Bristow, 1993; Bristow, 1999;

Ashworth et al., 2000; Best et al., 2003). The river transports material down from the Himalayas down to the Bay of Bengal and feeds the Brahmaputra-Ganges river-deltaic system (Best et al., 2007). The bar form used within this study is a predominantly downstream accreting system with secondary channels reworking the top of the barform, preventing stabilization through soil formation and growth of vegetation (Bristow, 1993; Ashworth et al., 2000; Best et al., 2003).

## 5.2 Results

Concordant with the methodology and workflow outlined in Chapter 3, the discrete variables obtained from 100 realisations generated for the example Tuscher Canyon SIS, OBM and MPS models were analysed for their PERG, GOO and RR values for each the mean geobody thickness, standard deviation of geobody thickness and outputted target fraction. These values were then compared against the result from the synthetic model suites (Chapter 4), in an attempt to determine the accuracy and applicability of the developed methodology to a real-world scenario.

### 5.2.1 Mean geobody thickness

The Tuscher Canyon mean geobody thickness values for the SIS (Figure 5.2a), OBM (Figure 5.2b) and MPS (Figure 5.2c) algorithms are generally representative (albeit relatively loosely in places) when compared to the average PERG, GOO and RR values obtained from analysing numerous suites of reservoir models (Chapter 3). For the SIS algorithm (Figure 5.2a), the GOO values appear to be distributed approximately where expected and given by the average GOO values. This is also the same for the PERG and RR values, and whilst higher than the average values obtained from running an extensive suite of SIS reservoir models, they fall within the range of values that were retrieved. This is also the case for the OBM algorithm (Figure 5.2b), where the GOO values are distributed much closer to the average value. This also carries through to the PERG and RR values, which show much more consistent results than the SIS algorithm. Notably, the lowest input target fraction (the thalweg bedform) has a GOO, PERG and RR value of 1, which is due to the mean geobody thickness being consistent at 1.5m across all realisations. The MPS algorithm (Figure 5.2c) has no visible GOO values due to the nature of the model being created, whereby each of

the realisations is modelled based on the training image. From this, the various geobodies (channel element, downstream accretion, lateral accretion, and the thalweg bedform) are modelled based upon the mean geobody thickness values. As such, this means that the mean geobody thickness is largely the same for each of the geobodies (excluding the channel element, which is modelled separately), and consequently leads to each of these elements having GOO, PERG and RR values of 1. The channel element has a GOO value of 21, a PERG of 27, and an RR of 21. Whilst considerably different to the expected values from the suite of reservoir models, this is to be expected as each separate version of the 100 realisations generated has different output values, and whilst these do not reflect the average, they would sit within the range of GOO, PERG and RR values retrieved from the suite of models.

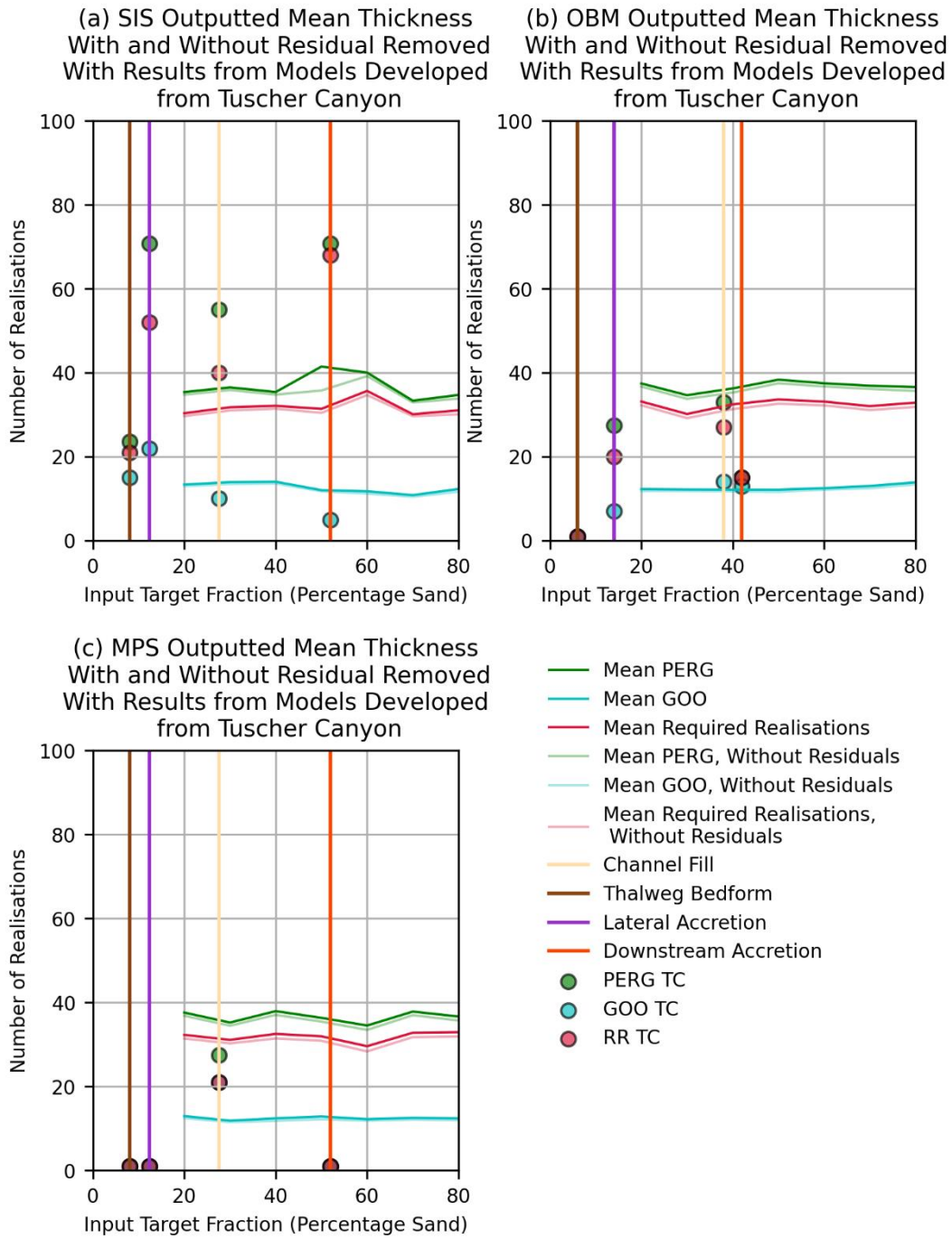


Figure 5.2: Comparison of the PERG, GOO and RR values for the mean geobody thickness values (bold lines), with the outlier values (residuals) removed (faint lines) for all values modelled in the developed suite of reservoir models, across the (a) SIS, (b) OBM, and (c) MPS modelling algorithms, with values shown for all input target fractions. The plots have then been overlaid with the actual PERG, GOO and RR values from the Tuscher Canyon model at each of the input target fractions for the specific architectural element (downstream accretion, lateral accretion, channel element, and thalweg bedform).

### 5.2.2 Standard Deviation of Geobody Thickness – StDev Thickness

When the Tuscher Canyon standard deviation of geobody thickness values for the SIS (Figure 5.3a), OBM (Figure 5.3b) and MPS (Figure 5.3c) algorithms are compared to those of the average PERG, GOO and RR values obtained from running an extensive suite of synthetic reservoir models (Chapter 3), there is a closer representation of the average PERG, GOO and RR values representing a similar value across the four target fractions when compared to the values for the mean geobody thickness. For the SIS algorithm (Figure 5.3a), the GOO values appear to be distributed approximately where expected and given by the average GOO values. This is also the same for the PERG and RR values, and whilst the channel and lateral accretion elements are significantly higher than the values obtained from the mean geobody thickness, and the average values obtained from running an extensive suite of synthetic SIS reservoir models, they do fall within the range of values that were retrieved. This is also the case for the OBM algorithm (Figure 5.3b), where the GOO values are distributed much closer to the average value. This also carries through to the PERG and RR values, which show much more consistent results than the SIS algorithm. Notably, the lowest input target fraction (the thalweg bedform) has a GOO, PERG and RR value of 1, which is due to the mean geobody thickness being consistent at 1.5m across all realisations. Notably, the MPS algorithm (Figure 5.3c) actually has values when compared to the mean geobody thickness. The various geobodies have a wide range of values for each the PERG, GOO and RR, but appears to show a closer distribution than the SIS and OBM algorithm values. Whilst considerably different to the expected values from the suite of reservoir models, this can be expected as each separate version of the 100 realisations generated has different output values, and whilst these do not reflect the average, they would sit within the range of GOO, PERG and RR values retrieved from the suite of models.

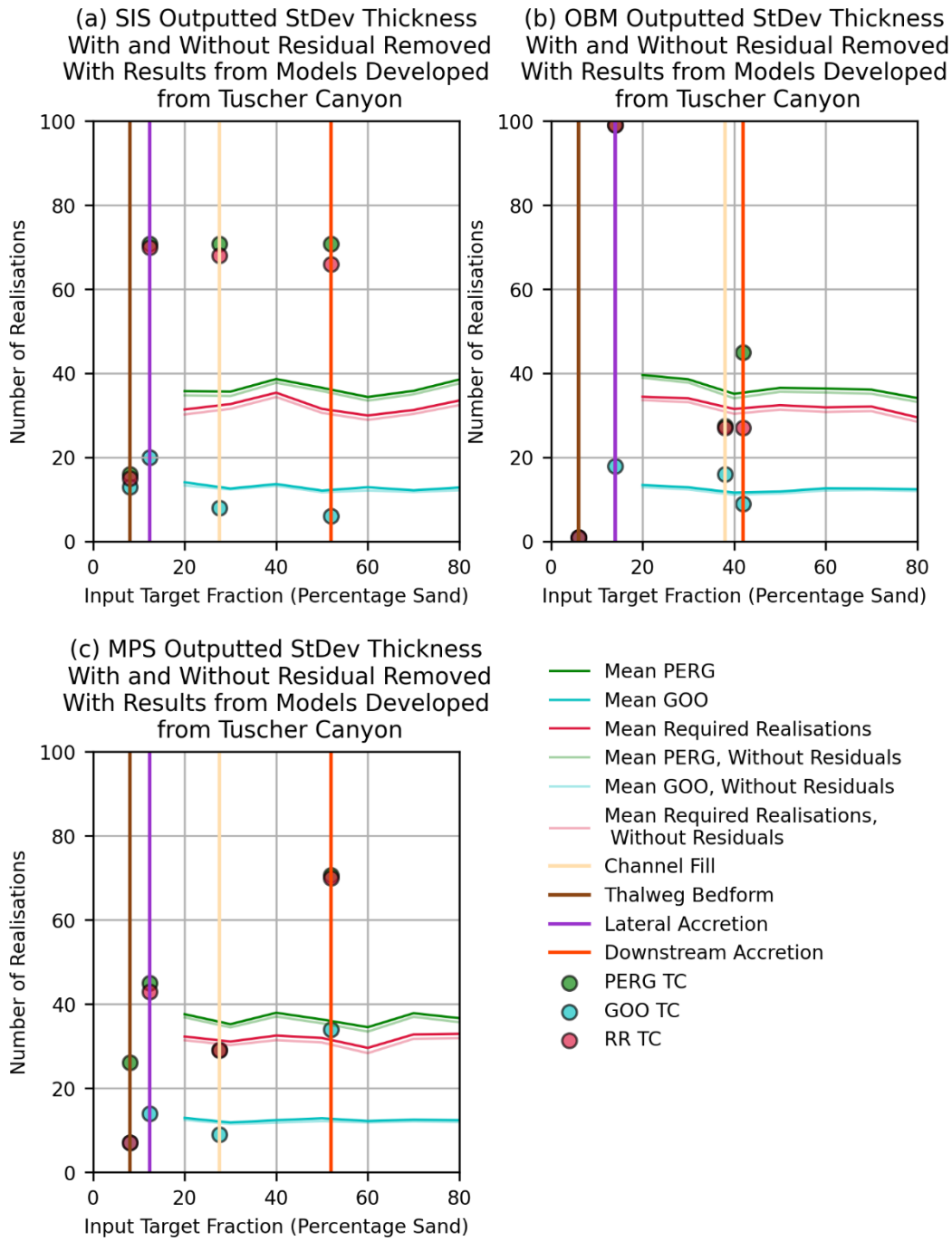


Figure 5.3: Comparison of the PERG, GOO and RR values for the standard deviation of geobody thickness values (bold lines), with the outlier values (residuals) removed (faint lines) for all values modelled in the developed suite of reservoir models, across the (a) SIS, (b) OBM, and (c) MPS modelling algorithms, with values shown for all input target fractions. The plots have then been overlaid with the actual PERG, GOO and RR values from the Tuscher Canyon model at each of the input target fractions for the specific architectural element (downstream accretion, lateral accretion, channel element, and thalweg bedform).

### 5.2.3 Target Fraction

When the Tuscher Canyon output target fraction values for the SIS (Figure 5.4a), OBM (Figure 5.4b) and MPS (Figure 5.4c) algorithms are compared to those of the average PERG, GOO and RR values obtained from running a vast suite of reservoir models (Chapter 3), there appears to be a better representation of the average PERG, GOO and RR values representing similar values compared to the values for the mean geobody thickness and standard deviation of geobody thickness. For the SIS algorithm (Figure 5.4a), the GOO values are distributed very close to where expected and given by the average GOO values, and shows the closest distribution when compared to the mean geobody thickness and standard deviation of geobody thickness. This is also the same for the PERG and RR values, with all geobodies showing far lower values than the values obtained from the mean geobody thickness. This means that these PERG, GOO and RR values are much closer to the average values obtained from running an extensive suite of synthetic SIS reservoir models. This is also the case for the OBM algorithm (Figure 5.4b), where the GOO values are distributed much closer to the average value. This also carries through to the PERG and RR values, which show much more consistent results than the SIS algorithm, and also lower PERG and RR values than the standard deviation of geobody thickness values. Notably, the lowest input target fraction (the thalweg bedform) has a GOO, PERG and RR value of 1 due to an underrepresentation of the architectural element within the generated realisations. The MPS algorithm (Figure 5.4c) has far more consistent values when compared to the mean geobody thickness. The various geobodies have a narrower range of values for each the PERG, GOO and RR, and seemingly a closer distribution than the SIS and OBM algorithm values. These values more closely represent the expected values from the suite of reservoir models than the previous output values and modelling algorithms.

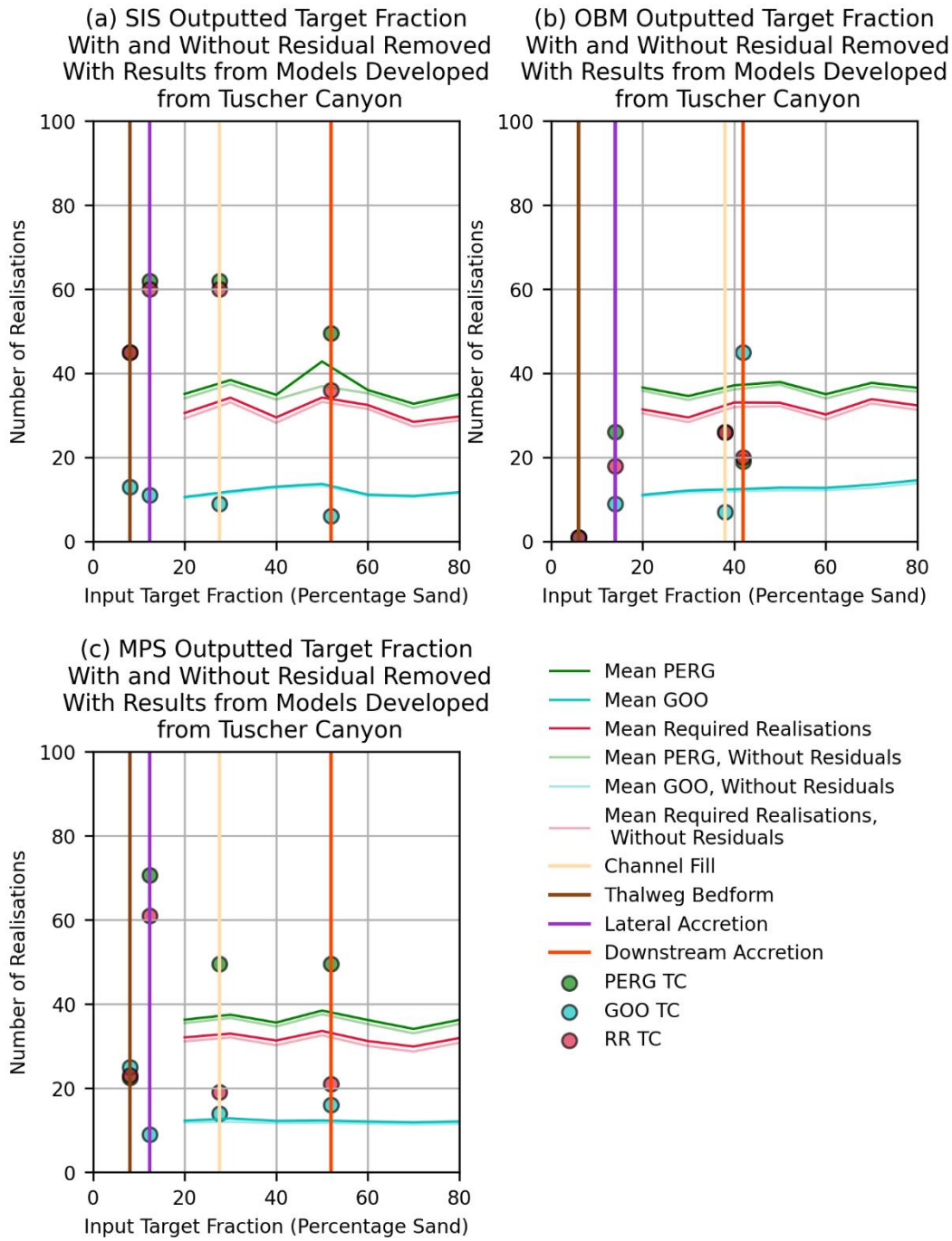


Figure 5.4: Comparison of the PERG, GOO and RR values for the outputted target fraction values (bold lines), with the outlier values (residuals) removed (faint lines) for all values modelled in the developed suite of reservoir models, across the (a) SIS, (b) OBM, and (c) MPS modelling algorithms, with values shown for all input target fractions. The plots have then been overlaid with the actual PERG, GOO and RR values from the Tuscher Canyon model at each of the input target fractions for the specific architectural element (downstream accretion, lateral accretion, channel element, and thalweg bedform).

### 5.3 Tuscher Canyon Similarity

When the data from the similarity plots (Chapter 4.2) using the RR (recommended number of realisations) are averaged and compared to the similarity of the first 20 realisations (Goovaerts, 1999), for the SIS (Figure 5.5a), OBM (Figure 5.5b) and MPS (Figure 5.5c) algorithms, there is also significant improvement in the representation of a much larger dataset (100 realisations in this case), as has also been seen with the average RR values for each of the modelling algorithms.

Across all geobodies modelled for the Tuscher Canyon section, and across all modelling algorithms, when the recommended number of realisations is used, there is an approximate 90-97% similarity percentage to 100 realisations, which suggests that a much larger dataset is being modelled extremely well, and effectively able to model the skew, kurtosis, and other features of 100 realisations, for all the modelling algorithms. In comparison, the similarity of the first 20 realisations to that of 100 realisations is approximately only 72-88%, meaning that the recommended number of realisations is approximately 18% more accurate. This also aligns with the Law of Large numbers (Bernoulli, 1713), since a larger sample size more accurately represents the whole population. The SIS algorithm (Figure 5.5a) shows the lowest average RR similarity values, with most values being approximately 94-96%, and as such is approximately a 10% improvement on using 20 realisations. The OBM algorithm (Figure 5.5b) has results between 88-98% which is approximately a 5% increase on using just 20 realisations. This is also the case for the MPS algorithm (Figure 5.5c), with a 4% increase on using 20 realisations, with the average RR similarity being approximately 90-91%. Whilst these results are not representative of the average similarity values discussed in Section 4.2, they are a good indicator as to how effective the methodology is for consistently returning a value for the number of realisations required for a statistically significant three-dimensional reservoir model suite to be developed, as is seen from the disparity between the similarity values for the RR number and 20 realisations.

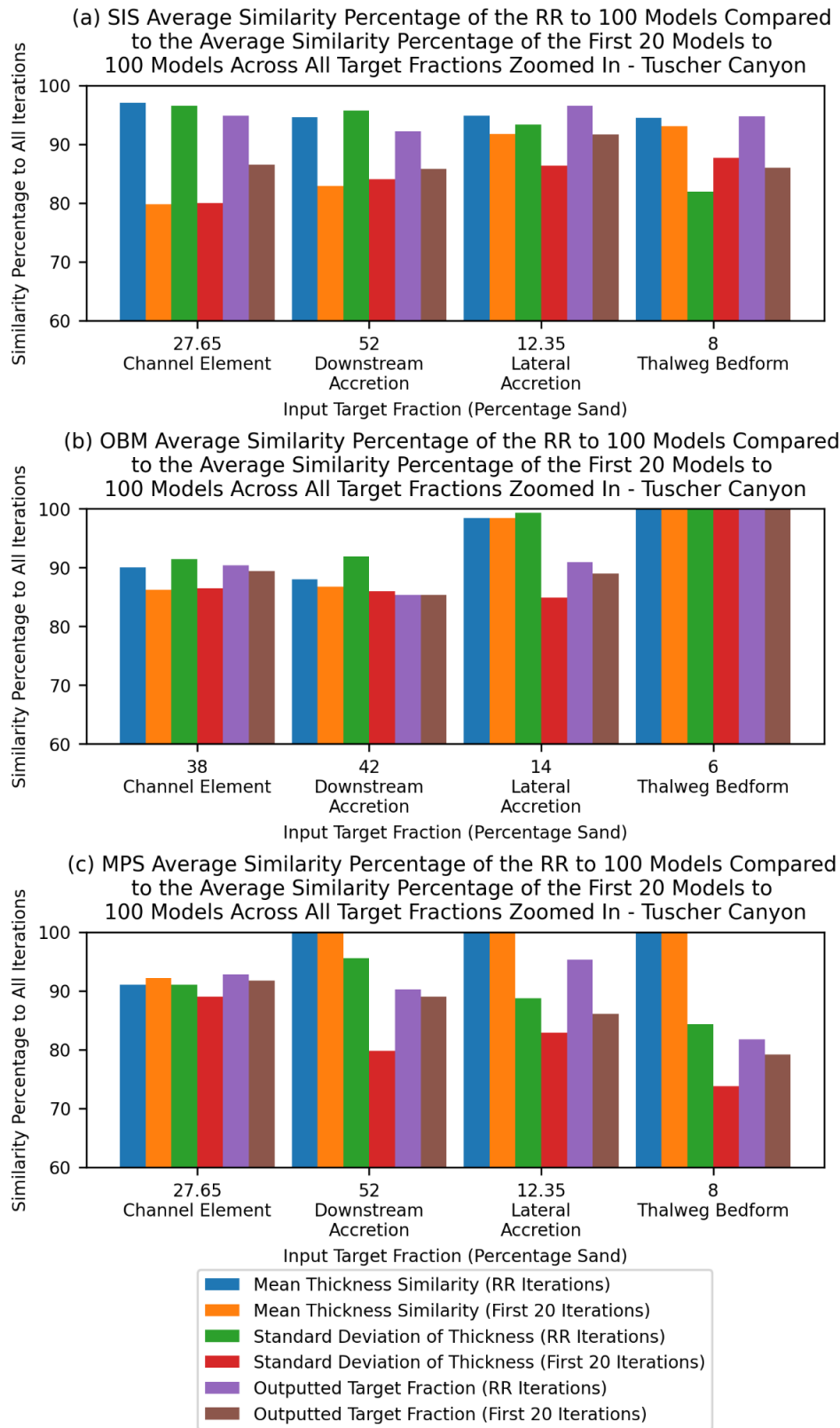


Figure 5.5: Comparison of the total similarity (intersectional percentages) of the first 20 realisations compared to the RR value across the input target fractions of the downstream accretion, lateral accretion, channel element and thalweg bedform geobodies, for the mean geobody thickness, standard deviation of

*geobody thickness and outputted target fraction, for each the (a) SIS, (b) OBM, and (c) MPS modelling algorithm.*

Comparison of the model suites generated with 20 (Goovaerts, 1999), 32 (average RR value obtained from the generated suite of fluvial reservoir models), RR (the specific recommended number of realisations for the model suite, restricted from 100 realisations), and 100 (all of the realisations generated for the model suite) realisations for the Tuscher Canyon reservoir models (Figure 5.6) clearly show increasing similarity percentage values with an increasing numbers of realisations. Ultimately, this was best represented by the specific RR for each of the geobodies within the model. In this case, the 100 realisation bins act as a control, to show the 'best case' similarity values.

Generally, the SIS algorithm produces a distribution most comparable to 100 realisations when the lower input target fraction geobodies are considered (thalweg bedform and the lateral accretion elements), whereas the larger input target fraction geobodies (channel element and downstream accretion element) are generally less comparable to 100 realisations for each the 20, 32 and individual RR (best case scenario between the GOO and PERG values) bins. It should be noted that the disparity between the four geobodies became negligible if the number of realisations being displayed was large enough, and seemingly, if too high (RR bin for the thalweg bedform in Figure 5.6b), the distributions would be over-modelled and consequently lead to overfitting and a lower similarity percentage. Generally, the same trend is present for the OBM algorithm (Figure 5.6d and Figure 5.6e), with the thalweg bedform consistently being represented as 100% similarity due to the highly constrained nature of the input vertical thickness, leading to the discrete statistics of the thalweg bedforms being the same for all realisations. The MPS algorithm however does not show these same results, with the mean geobody thickness similarity percentages being modelled at 100% for all geobodies (excluding channel element) across all realisation values, with only the channel element changing. Due to the nature of the MPS algorithm, there is a high degree of influence on the modelled mean geobody thickness values,

and consequently, all geobodies (excluding channel element) have a 100% similarity with the distributions as compared to all 100 realisations developed. Notably, the same general upward trend is present for both the standard deviation of geobody thickness and outputted target fraction, with the highest percentage similarity being present at the RR value.

Average Similarity Percentage for 20 (Goovaerts, 1999),  
32 (Theoretical required number of realisations),  
RR (Actual required number of realisations for the Tuscher Canyon models),  
and all 100 realisations developed

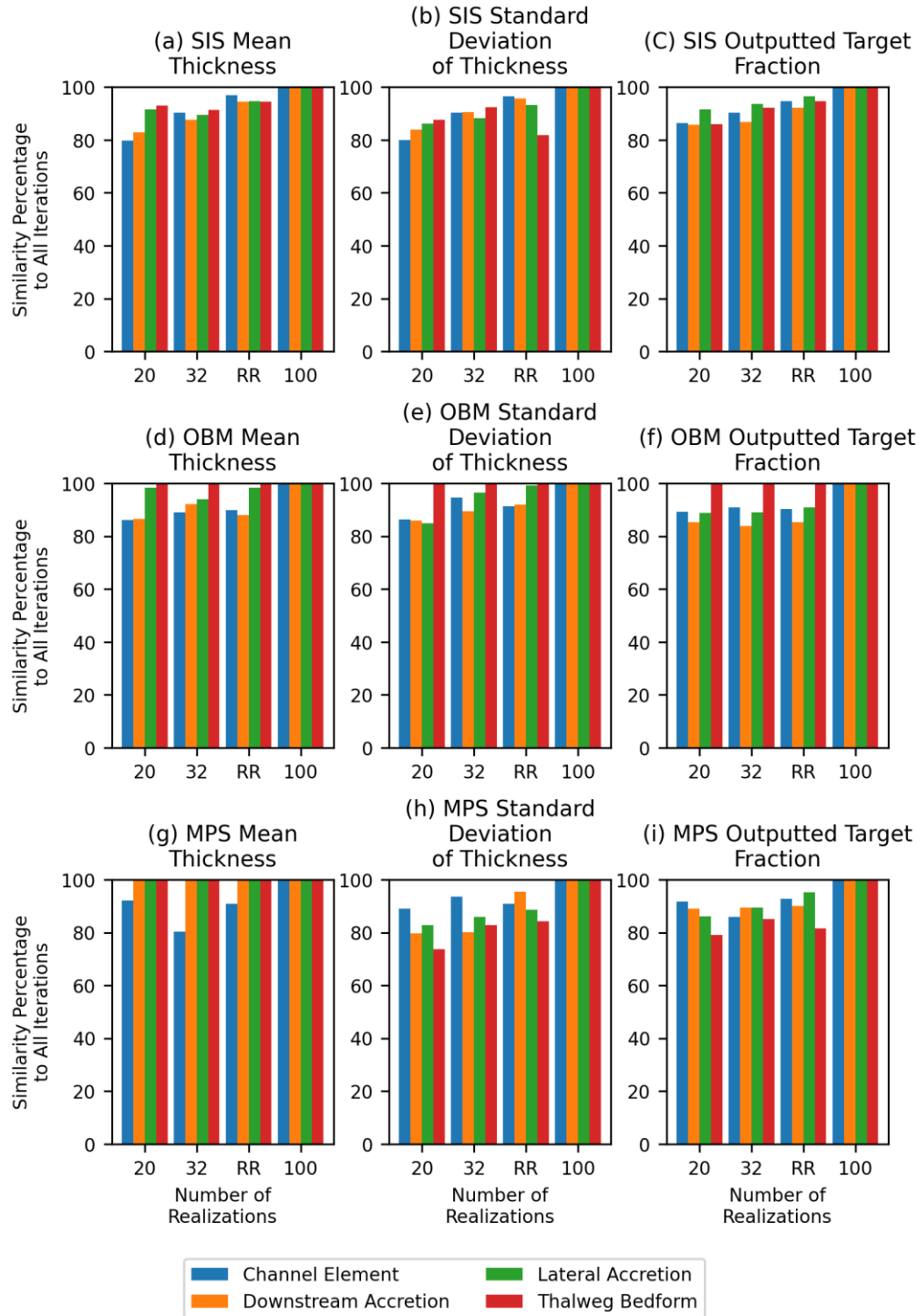


Figure 5.6: Comparison of the total similarity (intersectional percentages) of the first 20, 32 (RR for the suite of generated models), specific RR value for the Tuscher Canyon models, against 100 realisations. This is shown for the (a, d and g) mean geobody thickness, (b, e and h) standard deviation of geobody thickness,

*and (c, f and i) outputted target fraction, for each the (a, b and c) SIS, (d, e and f) OBM, and (g, h and i) MPS modelling algorithms.*

In this instance, since the RR value is variable for each architectural element, and for each the mean geobody thickness, standard deviation of geobody thickness and output target fraction, one overall best-case value is difficult to suggest without compromising somewhere. For the applied use of these models, two of the three factors analysed are less important (mean geobody thickness and output target fraction) due to these factors being controlled to some extent through the input parameters to generate the models (vertical thickness and input target fraction respectively). The most important discrete variable is the standard deviation of geobody thickness due to it not being directly controlled by an input, whilst also allowing for more variation of the other discrete variables to be included. This is important since realisations with the same geobody thickness could produce completely different models, which is important for developing a restricted suite of reservoir models with the largest amount of variation between each of the realisations.

An important factor for risk analysis of a reservoir model is that a representative sample is taken, which is why the standard deviation of geobody thickness is important to consider, as it enables multiple realisations with the same mean geobody thickness to be considered, whilst also enabling more extensive model variation to be accounted for. The other main factor for fluvial reservoir risk analysis is static connectivity, in this case, of the channel elements. Consequently, it would be suggested that the recommended number of realisations used is the value determined for the RR value for the standard deviation of geobody thickness for the channel element. When this is used for the Tuscher Canyon example (Figure 5.7), there is still significant improvement on the similarity percentage for both 20 (Goovaerts, 1999) and 32 realisations (average RR from the suite of developed models) being used. For the SIS algorithm, this value is 68 (Table 5.2), for the OBM this is 27 (Table 5.3), and for the MPS, this is 29 (Table 5.4).

Architectural Element	Mean Geobody Thickness RR	Standard deviation of geobody thickness RR	Output Target Fraction RR
Channel Element	40	<b>68</b>	60
Lateral Accretion	52	70	60
Downstream Accretion	52	70	60
Thalweg Bedform	21	15	45

Table 5.2: Recommended number of realisations required for a statistically significant three-dimensional reservoir model suite to be developed for each the mean geobody thickness, standard deviation of geobody thickness and output target fraction for each of the studied geobodies for the Tuscher Canyon model using the SIS modelling algorithm. This shows significant variation across the different geobodies, with 68 realisations being shown to be the value for the channel elements standard deviation of geobody thickness value.

Architectural Element	Mean Geobody Thickness RR	Standard deviation of geobody thickness RR	Output Target Fraction RR
Channel Element	27	<b>27</b>	26
Lateral Accretion	15	27	20
Downstream Accretion	20	99	18
Thalweg Bedform	1	1	1

Table 5.3: Recommended number of realisations required for a statistically significant three-dimensional reservoir model suite to be developed for each the mean geobody thickness, standard deviation of geobody thickness and output target fraction for each of the studied geobodies for the Tuscher Canyon model using the OBM modelling algorithm. This shows significant variation across the different geobodies, with 27 realisations being shown to be the value for the channel elements standard deviation of geobody thickness value.

Architectural Element	Mean Geobody Thickness RR	Standard deviation of geobody thickness RR	Output Target Fraction RR
Channel Element	21	<b>29</b>	19
Lateral Accretion	1	70	21
Downstream Accretion	1	43	61
Thalweg Bedform	1	7	23

Table 5.4: Recommended number of realisations required for a statistically significant three-dimensional reservoir model suite to be developed for each the mean geobody thickness, standard deviation of geobody thickness and output target fraction for each of the studied geobodies for the Tuscher Canyon model using the MPS modelling algorithm. This shows significant variation across the different geobodies, with 29

*realisations being shown to be the value for the channel elements standard deviation of geobody thickness value.*

Whilst the similarity results for these newly used RR values (Figure 5.8) are comparable to the previously suggested best case RR values (Figure 5.7), there does appear to be more consistency of the representation of all geobodies. This is in comparison to the previously used best case RR value, where larger variations could be seen across geobodies. This increased consistency also leads to better, more representative results, which should lead to a better, more statistically significant three-dimensional reservoir model suite.

Average Similarity Percentage for 20 (Goovaerts, 1999),  
 32 (Theoretical required number of realisations),  
 RR (Actual required number of realisations for the Tuscher Canyon models),  
 and all 100 realisations developed

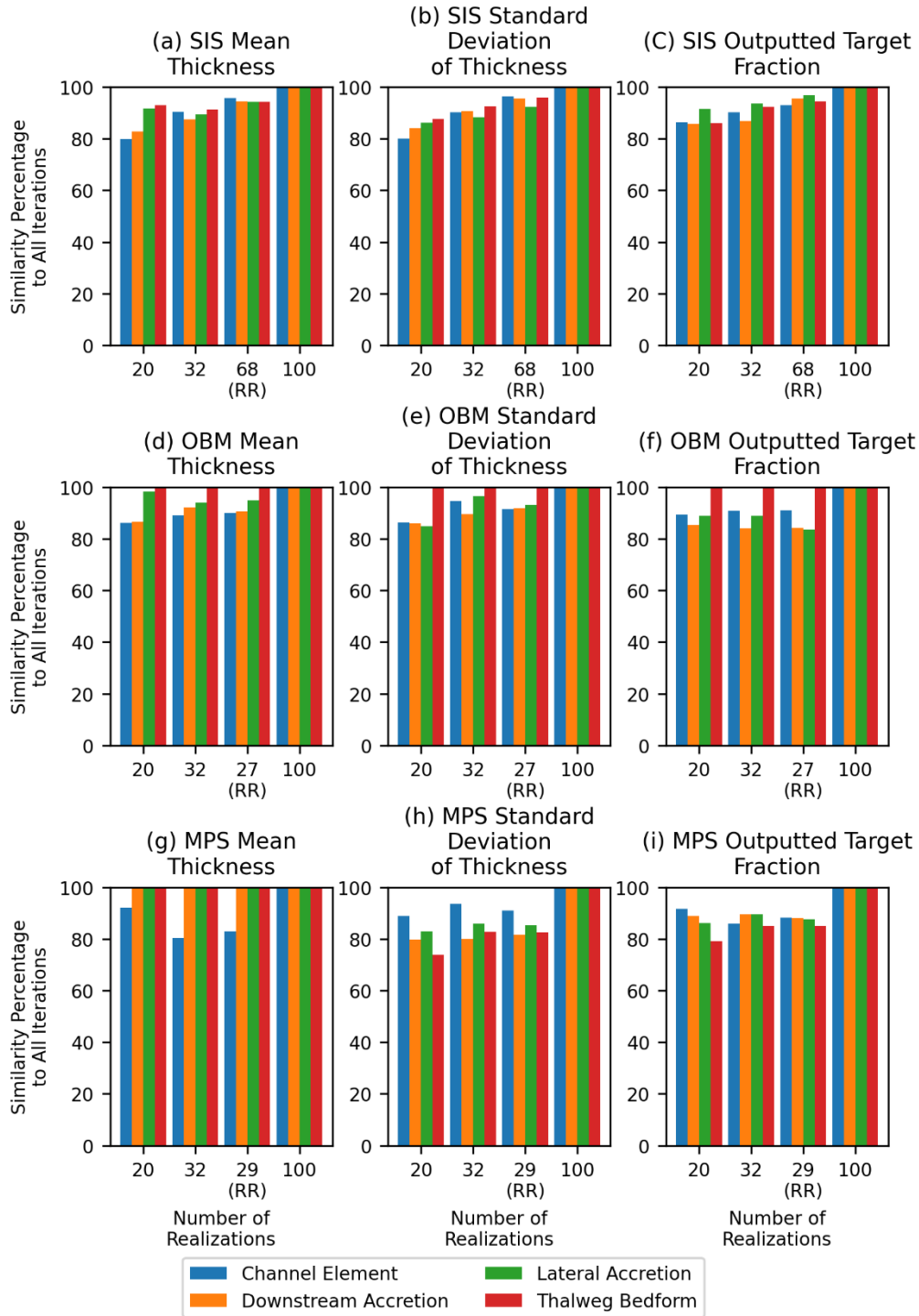


Figure 5.7: Comparison of the total similarity (intersectional percentages) of the first 20, 32 (RR for the standard deviation of geobody thickness of the channel element for the suite of generated models), specific RR value for the Tuscher Canyon models, against 100 realisations. This is shown for the (a, d and g) mean

*geobody thickness, (b, e and h) standard deviation of geobody thickness, and (c, f and i) outputted target fraction, for each the (a, b and c) SIS, (d, e and f) OBM, and (g, h and i) MPS modelling algorithms.*

## 5.4 Summary

Overall, when 100 realisations of the Tuscher Canyon model are developed using the SIS, OBM and MPS modelling algorithms, there is a significant difference to the results gained from the synthetic suite of models generated and analysed (Chapter 4). This variation is probably caused by a single set of input parameters used to generate the single suite of reservoir models rather than an average of an extensive set of synthetic reservoir model suites being developed with a range of input parameters, which probably would have viewed this set of 100 realisations as a residual case that would have been averaged out. Whilst not a perfect representation of the suite of models, the Tuscher Canyon example does show good general trending for each of the PERG, GOO and RR values with SIS algorithm being the most representative, and the MPS algorithm showing the most variation. This example highlights just how much variation is possible for a model set (a specific set of parameters) to have. Consequently, this would suggest that instead of developing a model suite of 32 realisations, a larger suite of reservoir models should be developed, with the excess models<sup>11</sup> being removed.

Depending on the use of this suite of reservoir models, it would be recommended that 100 realisations are developed initially, with the workflow then followed to reduce this model suite prior to fluid-flow, or other computationally heavy tasks being modelled. If the reservoir models are larger, or higher resolution, then this number could be reduced to 50 (50% larger than the average RR for the synthetic model suites), and the methodology being followed. If there is no repetition (PERG) of the standard deviation of geobody thickness for the channel element, then more realisations should be added onto the previous 50, and the methodology followed again. This should be repeated until a PERG value can be found to be used as an upper bound, for the recommended number of realisations to then be determined. Development of a larger initial suite of realisations is preferred since there would be a larger sample of variation of the standard

---

<sup>11</sup> Realisations larger than the recommended number of realisations for the standard deviation of geobody thickness for the channel element for the suite of reservoir models (e.g., if this number was 32, then all realisations after this would be removed from the model suite).

deviation of geobody thickness values. This would lead to a better, more representative comparison between the initial suite of reservoir models and the prospective RR value, leading to a much more accurate recommended number of realisations being suggested. This in turn will lead to a more representative suite of three-dimensional stochastic reservoir models being developed, and used for the determination of economic viability of hydrocarbon recovery, or carbon storage reservoirs.

## 6 Discussion

This discussion will focus on the applicability to other sedimentological environments, uncertainties within the methodology and possible mitigation, the number of realisations required to develop a statistically significant three-dimensional reservoir model suite for the generated suite of fluvial reservoir models, and then will focus on the application of the methodology developed on a model representing Tuscher Canyon, and finally will look at the limitations of this study.

### 6.1 Application to other environments

Whilst this methodology has only been applied to fluvial systems within this study, it is likely that it has wider scale applicability to any clastic sedimentary environment where multiple facies are interacting and modelled using a non-deterministic algorithm. This is due to the methodology focussing on the characteristics and properties of the reservoir rather than individual geobodies or specific facies. The main challenges of applying this methodology to other environments will arise from the ability to create both viable and realistic reservoir models. Without a good quality set of inputs (reservoir models), any uncertainty analysis would be unproductive as whilst it will undoubtedly create a better set of reservoir models, they would not be representative of the reservoir.

### 6.2 Methodology uncertainties and potential mitigation

The main uncertainty with the proposed methodology will be introduced when selecting the initial sample of reservoir models to be analysed. The uncertainty arises from an unrepresentative selection of facies models being created within the reservoir modelling stage. Whilst this cannot be completely mitigated it would be recommended for the reservoir models to be visually checked over before they are analysed to ensure they are representative of the reservoir being modelled. It is also suggested that a larger initial sample of reservoir models is more likely to represent the total population (Law of Large Numbers). It is suggested that an initial sample size of at least 30 is used so that the distribution of values for the sample is approximately normal

(according to the Central Limit Theorem), consequently reducing the impact of bias appearing within the sample population.

### 6.3 Number of Realisations

The number of realisations used typically to develop three-dimensional fluvial reservoir models is inherently flawed. Whilst it is commonplace for between 10 and 20 realisations to be developed for a three-dimensional fluvial reservoir model for any modelling algorithm (Haldorsen and Damsleth, 1990; Seifert and Jensen, 1999; Caers, Srinivasan and Journel, 2000; Liu et al., 2004; Tureyen and Caers, 2005; Falivene et al., 2006; Nordahl and Ringrose, 2008; Daly and Caers, 2010; Mitten et al., 2020; Benetatos and Giglio, 2021; Montero et al., 2021), these values were originally intended for use for two-dimensional permeability models using the SIS algorithm (among others) (Goovaerts, 1999), rather than three-dimensional fluvial reservoir models across all modelling algorithms. Alternatively, 10 realisations are used commonly to reduce the effect of ergodic fluctuation within the fluvial reservoir models (Falivene et al., 2006). The extensive suite of synthetic fluvial reservoir models developed using the SIS, OBM and MPS modelling algorithms serves to confirm that even 20 realisations isn't sufficient enough to develop a statistically significant three-dimensional reservoir model suite.

#### 6.3.1 Test Suite of Models

The relatively large standard deviations of the test suites of reservoir models (Figure 6.1b, Figure 6.1d and Figure 6.1f) even whilst there is a consistent average of 32 for the SIS (Figure 6.1a, Figure 6.1c and Figure 6.1f), OBM (Figure 6.1a, Figure 6.1c and Figure 6.1f) and MPS (Figure 6.1a, Figure 6.1c and Figure 6.1f) algorithms, there is still a high degree of uncertainty. The standard deviation of 20 for the values in the dataset (Figure 6.1b, Figure 6.1d and Figure 6.1e) is incredibly large for what is a relatively small set of data for each input target fraction (80 values for each input target fraction for the SIS algorithm, and 256 for each input target fraction for the OBM and MPS algorithms). This standard deviation highlights the variation of the returned values for each of the

modelling algorithms and suggests that regardless of how large that the suite of fluvial reservoir models is, there is still an incredible amount of uncertainty associated with modelling algorithms.

Two possible answers exist for this problem, the first of these is the generation of 32 realisations regardless of the input parameters. This solution provides enough realisations for the standard deviation of the discrete variables returned from the models to plateau off and is similar to the solution proposed for a two-dimensional reservoir model of 20 realisations (Goovaerts, 1999). However, this does not address the problem of oversampling that could arise when using a specific number of realisations. For example, since 32 is the average number of required realisations for a statistically significant three-dimensional reservoir model suite to be developed (Figure 6.1), that would mean that there are ~50% of models that have a value of less than 32, which would imply that 50% of the time there would be duplication in the properties of the realisations generated. In turn this would lead to oversampling of these property values, and consequently lead to either too much, or too little, de-risking. This could then lead to a project deemed to be too risky, or not profitable enough.

The other case would be that the project is deemed to be extremely profitable, and the actual reservoir is disappointing (false-positive). Irrespective of this, both are possibilities when a non-specific solution is used. The second solution involves far less risk and uses a bespoke number for each model developed. In this case, 100 realisations are developed, and then the discrete variables obtained from this are then analysed using the methodology described in Chapter 3. This would then return a bespoke value (RR) for that specific dataset. The user would then remove all of the excess realisations (if the RR was 28, then the realisations of 29 to 100 inclusive would be disregarded), and the remaining realisations would be analysed. This process can be automated using a software application such as StReAMS (Davies and Mitten, 2023), where a result would be returned in seconds. Whilst this second solution does not reduce the time expended on creating the realisations, it does lead to the de-risking of using fluvial reservoir models for industrial use, and ultimately producing a better and more consistent three-

dimensional stochastic fluvial reservoir modelling process.

Mean Thickness PERG, GOO and RR Values  
Across All Algorithms

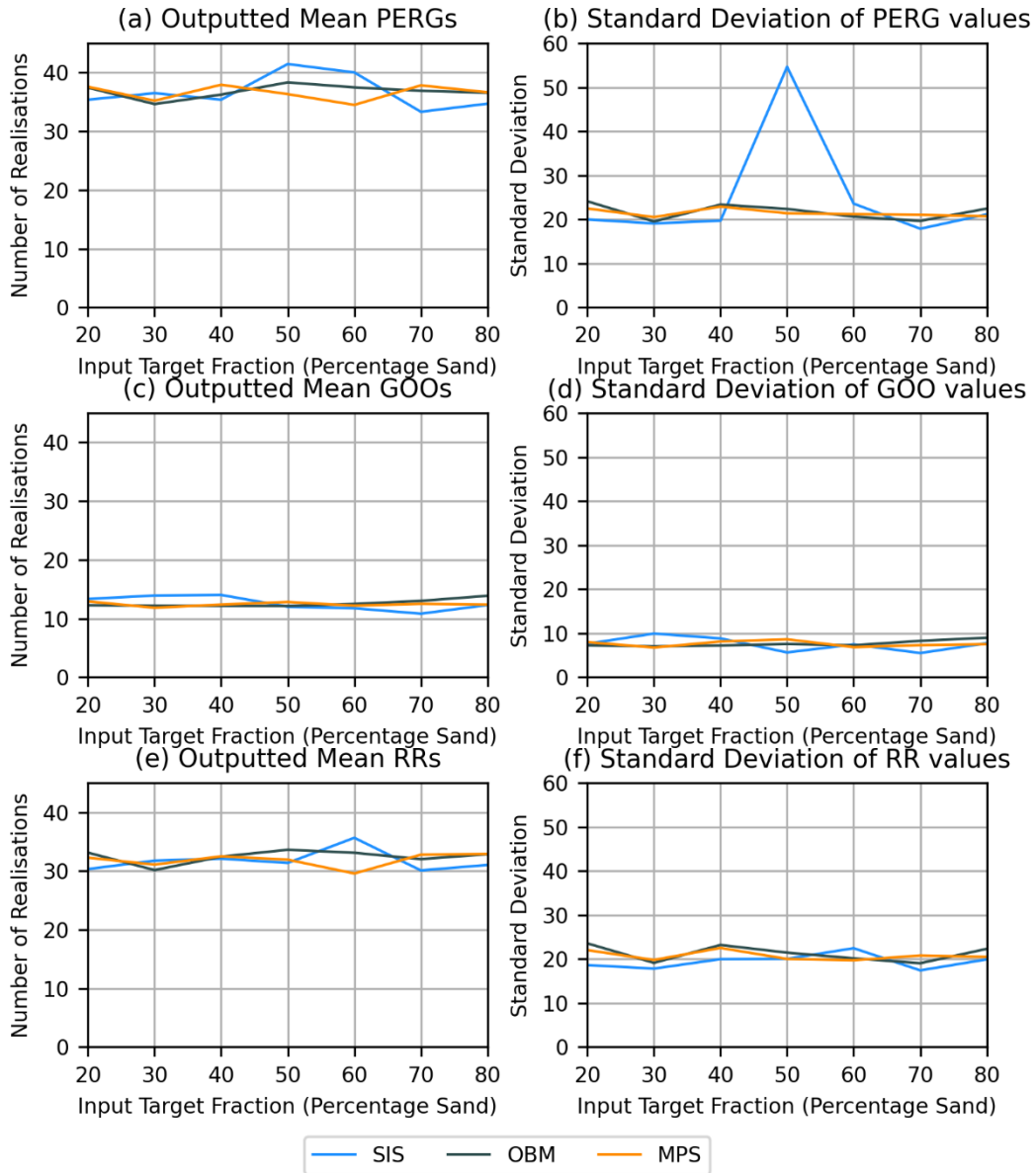


Figure 6.1: Comparison of the (a) PERG, (c) GOO and (e) RR values for the mean geobody thickness values, for each of the SIS, OBM, and MPS modelling algorithms, with values shown for all input target fractions. The standard deviations of these average results (detailing how spread out the values are) is given for the (b) PERG, (d) GOO, and (f) RR values.

6.3.2 Tuscher Canyon Model

Whilst the test suite of models recommends an average of 32 realisations to be used to generate a statistically significant three-dimensional reservoir model suite, further analysis (Chapter 4)

demonstrates discrepancy as to the distribution of the datasets used to arrive at this number. Consequently, a straightforward approach of using just 32 realisations is unlikely to create a statistically significant three-dimensional reservoir model suite. When the usage of fluvial reservoir models is considered, it becomes clear that some factors are more appropriate and important than others. The most important of these, when considering static connectivity, would be the channel element connectivity. Whilst connectivity data haven't been used within this study, it can be approximated by using the standard deviation of geobody thickness. This method allows repetition of the mean geobody thickness, whilst also representing the spread of data for the entire dataset. When the RR value is used for the channel elements standard deviation of geobody thickness (Figure 6.2), there is a significant increase in the overall similarity percentage (Chapter 5.3) when compared to 100 models in comparison to both the 20 realisations (Goovaerts, 1999) (approximately a 7.5% increase), and the 32 realisations given by the test suite of models (approximately a 2.5% increase). This dynamic approach to statistical significance of fluvial reservoir modelling incorporates flexibility with statistical certainty, and overall combines efficiency with statistical accuracy, leading to more reliable results, and consequently, de-risking of three-dimensional fluvial reservoir modelling.

It would be recommended that 100 realisations are developed initially, with the workflow then followed to reduce this model suite prior to fluid-flow, or other computationally heavy tasks being modelled. If the reservoir models are more computationally intensive, or less accuracy is required then this number could be reduced to 50 (50% larger than the average RR for the synthetic model suites), and the methodology being followed. If no repetition (PERG) of the standard deviation of geobody thickness for the channel element is detected, then more realisations should be added onto the previous 50, and the methodology followed again. This should be repeated until a PERG value can be found to be used as an upper bound, for the recommended number of realisations to then be determined. Development of a larger initial suite of realisations is preferred since there

would be a larger, and more representative sample of reservoir models<sup>12</sup> to use when determining the RR value during comparison of distributions. This in turn will lead to a more representative and statistically significant suite of three-dimensional stochastic reservoir models being developed.

---

<sup>12</sup> Law of large numbers (Bernoulli, 1713) states that a larger sample will be more representative of an entire population

Average Similarity Percentage for 20 (Goovaerts, 1999),  
 32 (Theoretical required number of realisations),  
 RR (Required number of realisations for the standard deviation of  
 thickness for the channel element from the Tüscher Canyon models),  
 and all 100 realisations developed

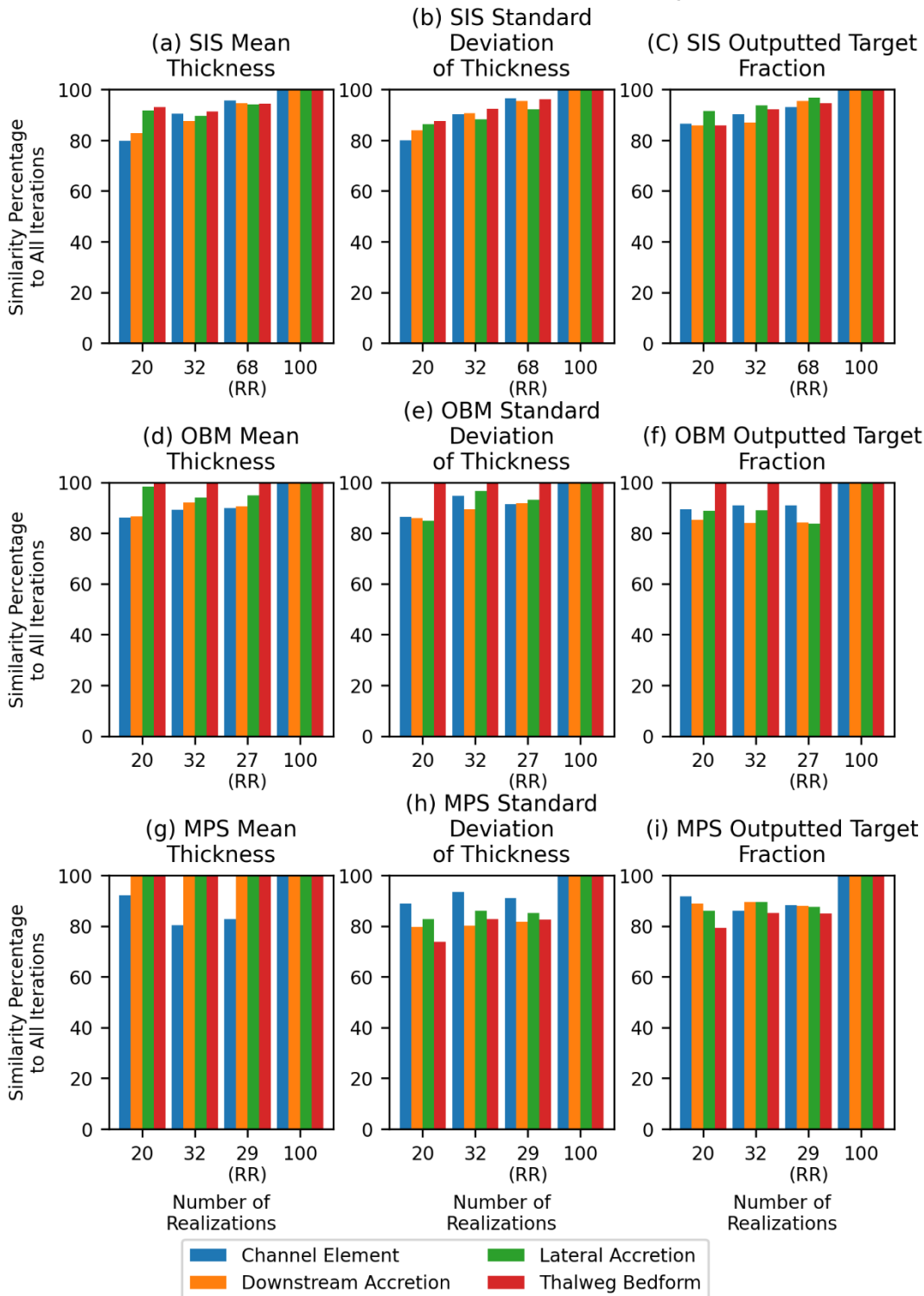


Figure 6.2: Comparison of the total similarity (intersectional percentages) of the first 20, 32 (RR for the standard deviation of geobody thickness of the channel element for the suite of generated models), specific

*RR value for the Tuscher Canyon models, against 100 realisations. This is shown for the (a, d and g) mean geobody thickness, (b, e and h) standard deviation of geobody thickness, and (c, f and i) outputted target fraction, for each the (a, b and c) SIS, (d, e and f) OBM, and (g, h and i) MPS modelling algorithms.*

## 6.4 Limitations

Whilst steps have been taken in the work presented here to ensure that the models are as representative as possible, the reproducibility of the individual model suites will vary (even when the same input parameters are used), due to the inherent stochastic nature of the modelling algorithms. To reduce the effect of this on the entire dataset, a large suite of models was carried out (4,144 models across three different modelling algorithms), thereby reducing the total impact of non-standard cases, and overall increasing the reliability of the study. It should also be noted that for this reason, no two datasets will have the same GOO, PERG or RR values, and as such presents the need for more a tailored approach to determine these values, such as StReAMS (Davies and Mitten, 2023), which was developed to bulk analyze Petrel outputs to determine these values. Other limitations of this study are that the suite of models developed were completely synthetic, as such, models with hard data inputs (such as well logs) have not been considered, nor have the number of input parameters, or the relative effect of the different input parameters.

Due to the nature of reservoir exploration, real world scenarios are more likely to be probabilistic rather than stochastic. Since probabilistic reservoir models have a strong stochastic element to them, this study should still be applicable. The methodology suggested within Section 5.3 would be ideal for the determination of the number of realisation required for a statistically significant suite of probabilistic three-dimensional reservoir models. This would involve creating a model suite of 100 realisations, and determining the GOO and the PERG values for the channel element standard deviation of thickness. After this, all realisations between the GOO and the PERG would be iteratively used to search for the realisation number with the highest intersection percentage. Once found, the original suite of reservoir models would be restricted to the first X amount of

realisations to create a statistically significant suite of realisations. This model suite can then be used to determine the economic viability of the reservoir for either hydrocarbon recovery, or carbon storage.

Overall, the novel methodology proposed within this study is a useful workflow for the determination of the number of realisations required for the suite of three-dimensional fluvial reservoir models to be deemed as statistically significant. This is a significant advancement from the previously used two-dimensional work in this field (Goovaerts, 1999), and its application to real-world models such as Tuscher Canyon verifies its validity. The usage of the StReAMS (Davies and Mitten, 2023) software package is ideal for determining the PERG, GOO and RR values for either a singular model, or a set of models that have been developed. The methodology proposed within this study is ideal for both saving time when analyzing the generated fluvial reservoir models, and leads to the de-risking of generated reservoir models (through the use of periodograms to eliminate repetition of model properties, and the use of the Goovaerts plot to ensure that the range of values used represents a wide enough range of results), leading to increased accuracy of the models, and better, more informed decisions based on these models. When using the workflow, the RR value for the standard deviation of geobody thickness of the channel element should be used to produce the most accurate, and representative fluvial reservoir models to be generated and used.

## 7 Conclusion

Presented within this research is sufficient evidence to demonstrate a new methodology for the determination of a minimum number of realisations required for a statistically significant three-dimensional fluvial reservoir model suite to be developed, and subsequent application to a previously studied geological model through the completion of the aims and objectives proposed in Chapter 1.1.

### 7.1 Research aims and objectives

A suite of reservoir models (4,144 total) of a range of input parameters was developed in Chapter 3, enabling the three modelling algorithms used (SIS, OBM and MPS) to be analysed and compared. This search area is then analysed to return the number of realisations required for the best representation (intersectional percentage) of 100 realisations.

Compilation and analysis of the synthetic suites of reservoir models, the recommended number of realisations required for a statistically significant three-dimensional fluvial reservoir model suite is, on average, 32. This is the same for the SIS, OBM and MPS algorithms (Chapter 4), regardless of which discrete variable (mean geobody thickness, standard deviation of geobody thickness and outputted target fraction) from the synthetic suite of reservoir models is used. Application of this to previously studied examples (such as Tuscher Canyon, Utah), leads to a discrepancy in the RR value across the discrete variables, which also extends into the different geobodies being modelled. When more than two geobodies are modelled, the RR value for the standard deviation of geobody thickness of the largest connecting body (for fluvial reservoir models, channel element should be used). Application of this methodology to the Tuscher Canyon model proves its validity, and provides the basis for a statistically significant three-dimensional reservoir model suite to be generated for any three-dimensional fluvial reservoir model.

## 7.2 Further Work

Significant advancement has been made from the initial work of Goovaerts (1999), but there are still so many unknowns about three-dimensional fluvial reservoir modelling that still need to be quantified and determined. For example, how does model size, a larger initial suite of realisations, analysis of the static connectivity, and the nugget effect (for the SIS algorithm) alter the GOO, PERG and RR values?

### 7.2.1 Probabilistic Reservoir Models

Since probabilistic models are heavily influenced by stochastic processes, it is likely that this work would also be applicable to them. This could be tested by creating various suites of probabilistic models, with varying degrees of determinism in order to suggest how applicable this methodology would be. This would provide sufficient evidence for this methodology to be used for industrial application.

### 7.2.2 Model Size

It is possible that the alteration of the dimensions of the reservoir model would lead to alterations in the discrete statistics that would be used to analyze the generated models. This would probably lead to higher values for larger reservoirs due to the increased volume being represented (and consequently more chance for variation), and probably the opposite for smaller scaled models. It is also important to consider how a change in the ratio of the X, Y or Z axis would affect the results. It is possible this too would lead to an increase in model variation, and consequently larger PERG, GOO and RR values.

### 7.2.3 Static Connectivity

Whilst only the direct discrete statistics generated from the realisations have been used within this study, there is also the opportunity for individual connected geobodies to be evaluated. This would produce better insight into the variation of static connectivity of the models, and help to better characterise the effect of the various input parameters on reservoir performance. Finally, it is also important to consider the effect of using the discrete statistics for the static connectivity

values. The reduced (and focused) sampling is likely to lead to far higher GOO, PERG and RR values, and would likely be unrepresentative of the entire model – but it is still worth exploring to see if this is the case.

#### 7.2.4 Nugget Effect

When developing models using the SIS modelling algorithm, along with the vertical thickness, and major and minor directions, the nugget value can also be changed. This nugget value is the y-intercept on the semi-variograms used to develop the models, and act as the input parameters for the model. The nugget value is the overall uncertainty in the variogram, the higher the value, the more uncertainty (Camana and Deutsch, 2019). A higher nugget effect would typically lead to a smoother estimated variogram used for developing the models (Camana and Deutsch, 2019). For this study, the nugget was kept at 0.0001 due to time constraints, but further work could show large variation for the PERG, GOO and RR values.

#### 7.2.5 Input Parameters

The number of input parameters, nor the relative effect of the different input parameters were considered during this study. The uncertain nature of stochastic reservoir modelling means that either of these would have a noticeable effect on the reservoir models. Preliminary primary component analysis (PCA) showed that there was no discernible connection between the recommended number of realisations for any of the input parameters, but more in-depth analysis could prove to be useful for overall understanding of three-dimensional stochastic reservoir modelling.

## 8 References

- Alabert, F.G. and Massonnat, G.J. (1990) 'Heterogeneity in a Complex Turbiditic Reservoir: Stochastic Modelling of Facies and Petrophysical Variability', in *All Days. SPE Annual Technical Conference and Exhibition*, New Orleans, Louisiana: SPE, p. SPE-20604-MS. Available at: <https://doi.org/10.2118/20604-MS>.
- Allard, D. and HERESIM Group (1993) 'On the Connectivity of Two Random Set Models: The Truncated Gaussian and the Boolean', in A. Soares (ed.) *Geostatistics Tróia '92*. Dordrecht: Springer Netherlands (Quantitative Geology and Geostatistics), pp. 467–478. Available at: [https://doi.org/10.1007/978-94-011-1739-5\\_37](https://doi.org/10.1007/978-94-011-1739-5_37).
- Allen, J.R.L. (1978) 'Studies in fluvial sedimentation: an exploratory quantitative model for the architecture of avulsion-controlled alluvial suites', *Sedimentary Geology*, 21(2), pp. 129–147. Available at: [https://doi.org/10.1016/0037-0738\(78\)90002-7](https://doi.org/10.1016/0037-0738(78)90002-7).
- Andersson, J. and Hudson, J.A. (2004) 'T-H-M-C Modelling of Rock Mass Behaviour - 1: The Purposes, The Procedures and The Products', in *Elsevier Geo-Engineering Book Series*. Elsevier, pp. 433–438. Available at: [https://doi.org/10.1016/S1571-9960\(04\)80079-X](https://doi.org/10.1016/S1571-9960(04)80079-X).
- Ashworth, P.J. *et al.* (2000) 'Morphological evolution and dynamics of a large, sand braid-bar, Jamuna River, Bangladesh: Evolution of a large sand braid-bar', *Sedimentology*, 47(3), pp. 533–555. Available at: <https://doi.org/10.1046/j.1365-3091.2000.00305.x>.
- Bernoulli, J. (1713) *Ars Conjectandi*.
- Best, J.L. *et al.* (2003) 'Three-Dimensional Sedimentary Architecture of a Large, Mid-Channel Sand Braid Bar, Jamuna River, Bangladesh', *Journal of Sedimentary Research*, 73(4), pp. 516–530. Available at: <https://doi.org/10.1306/010603730516>.
- Best, J.L. *et al.* (2007) 'The Brahmaputra-Jamuna River, Bangladesh', in *Large Rivers*. John Wiley & Sons, Ltd, pp. 395–433. Available at: <https://doi.org/10.1002/9780470723722.ch19>.
- Blanchard, A.E., Stanley, C. and Bhowmik, D. (2021) 'Using GANs with adaptive training data to search for new molecules', *Journal of Cheminformatics*, 13(1), p. 14. Available at: <https://doi.org/10.1186/s13321-021-00494-3>.
- Bristow, C.S. (1993) 'Sedimentary structures exposed in bar tops in the Brahmaputra River, Bangladesh', *Geological Society, London, Special Publications*, 75(1), pp. 277–289. Available at: <https://doi.org/10.1144/GSL.SP.1993.075.01.17>.
- Bristow, C.S. (1999) 'Gradual Avulsion, River Metamorphosis and Reworking by Underfit Streams: a Modern Example from the Brahmaputra River in Bangladesh and a Possible Ancient Example in the Spanish Pyrenees', in N.D. Smith and J. Rogers (eds) *Fluvial Sedimentology VI*. John Wiley & Sons, Ltd, pp. 221–230. Available at: <https://doi.org/10.1002/9781444304213.ch17>.
- Caers, J. (2000) 'Direct sequential indicator simulation'.
- Caers, J. (2001) 'Geostatistical reservoir modelling using statistical pattern recognition', *Journal of Petroleum Science and Engineering*, 29(3–4), pp. 177–188. Available at: [https://doi.org/10.1016/S0920-4105\(01\)00088-2](https://doi.org/10.1016/S0920-4105(01)00088-2).
- Caers, J. and Zhang, T. (2004) 'Multiple-point Geostatistics: A Quantitative Vehicle for Integrating Geologic Analogs into Multiple Reservoir Models', *AAPG Memoir*, 80, pp. 383–394.

- Caers, J.K., Srinivasan, S. and Journel, A.G. (2000) 'Geostatistical Quantification of Geological Information for a Fluvial-Type North Sea Reservoir', *SPE Reservoir Evaluation & Engineering*, 3(05), pp. 457–467. Available at: <https://doi.org/10.2118/66310-PA>.
- Camana, F.A. and Deutsch, C.V. (2019) *The Nugget Effect, Geostatistics Lessons*. Available at: <http://geostatisticslessons.com/lessons/nuggeteffect>.
- Cannon, S. (2018) *Reservoir modelling: a practical guide*. First edition. Hoboken, NJ: Wiley.
- Cao, R., Zee Ma, Y. and Gomez, E. (2014) 'Geostatistical applications in petroleum reservoir modelling', *South African Institute of Mining and Mineralogy*, 114.
- Carle, S.F. and Fogg, G.E. (2020) 'Integration of Soft Data Into Geostatistical Simulation of Categorical Variables', *Frontiers in Earth Science*, 8, p. 565707. Available at: <https://doi.org/10.3389/feart.2020.565707>.
- Chan, M.A. and Pfaff, B.J. (1991) 'Fluvial Sedimentology of the Upper Cretaceous Castlegate Sandstone, Book Cliffs, Utah', pp. 95–110.
- Clemetsen, R. *et al.* (1990) 'A Computer Program for Evaluation of Fluvial Reservoirs', in A.T. Buller *et al.* (eds) *North Sea Oil and Gas Reservoirs—II*. Dordrecht: Springer Netherlands, pp. 373–385. Available at: [https://doi.org/10.1007/978-94-009-0791-1\\_32](https://doi.org/10.1007/978-94-009-0791-1_32).
- Coleman, J.M. (1969) 'Brahmaputra river: Channel processes and sedimentation', *Sedimentary Geology*, 3(2), pp. 129–239. Available at: [https://doi.org/10.1016/0037-0738\(69\)90010-4](https://doi.org/10.1016/0037-0738(69)90010-4).
- Colombi, C.E., Limarino, C.O. and Alcober, O.A. (2017) 'Allogenic controls on the fluvial architecture and fossil preservation of the Upper Triassic Ischigualasto Formation, NW Argentina', *Sedimentary Geology*, 362, pp. 1–16. Available at: <https://doi.org/10.1016/j.sedgeo.2017.10.003>.
- Corlett, H. *et al.* (2021) 'A geocellular modelling workflow for partially dolomitized remobilized carbonates: An example from the Hammam Faraun Fault block, Gulf of Suez, Egypt', *Marine and Petroleum Geology*, 126, p. 104831. Available at: <https://doi.org/10.1016/j.marpetgeo.2020.104831>.
- Daly, C. and Caers, J. (2010) 'Multi-point geostatistics – an introductory overview', *First Break*, 28(9). Available at: <https://doi.org/10.3997/1365-2397.2010020>.
- Davies, C. and Mitten, A.J. (2022) 'StReAMS (Statistical Reservoir and Model Significance)'. Available at: <https://github.com/chesterdavies/StReAMS>.
- Deutsch, C.V. (2006) 'A sequential indicator simulation program for categorical variables with point and block data: BlockSIS', *Computers & Geosciences*, 32(10), pp. 1669–1681. Available at: <https://doi.org/10.1016/j.cageo.2006.03.005>.
- Deutsch, C.V. and Cockerham, P.W. (1994) 'Practical considerations in the application of simulated annealing to stochastic simulation', *Mathematical Geology*, 26(1), pp. 67–82. Available at: <https://doi.org/10.1007/BF02065876>.
- Deutsch, C.V. and Journel, A.G. (1992) 'Principles of Stochastic Simulation', in *GSLIB: Geostatistical Software Library and user's guide*. New York: Oxford University Press.
- Deutsch, C.V. and Tran, T.T. (2002) 'FLUVSIM: a program for object-based stochastic modeling of fluvial depositional systems', *Computers & Geosciences*, 28(4), pp. 525–535. Available at: [https://doi.org/10.1016/S0098-3004\(01\)00075-9](https://doi.org/10.1016/S0098-3004(01)00075-9).

- Deutsch, C.V. and Wang, L. (1996) 'Hierarchical object-based stochastic modeling of fluvial reservoirs', *Mathematical Geology*, 28(7), pp. 857–880. Available at: <https://doi.org/10.1007/BF02066005>.
- Doyen, P.M., Psaila, D.E. and Strandenes, S. (1994) 'Bayesian Sequential Indicator Simulation of Channel Sands From 3-D Seismic Data in The Oseberg Field, Norwegian North Sea', in *SPE Annual Technical Conference and Exhibition. SPE Annual Technical Conference and Exhibition*, New Orleans, Louisiana: Society of Petroleum Engineers. Available at: <https://doi.org/10.2118/28382-MS>.
- Dubrule, O. (1993) 'Introducing More Geology in Stochastic Reservoir Modelling', in A. Soares (ed.) *Geostatistics Tróia '92*. Dordrecht: Springer Netherlands (Quantitative Geology and Geostatistics), pp. 351–369. Available at: [https://doi.org/10.1007/978-94-011-1739-5\\_29](https://doi.org/10.1007/978-94-011-1739-5_29).
- Emery, X. (2004) 'Properties and limitations of sequential indicator simulation', *Stochastic Environmental Research and Risk Assessment*, 18(6), pp. 414–424. Available at: <https://doi.org/10.1007/s00477-004-0213-5>.
- Enge, H.D. et al. (2007) 'From outcrop to reservoir simulation model: Workflow and procedures', *Geosphere*, 3(6), p. 469. Available at: <https://doi.org/10.1130/GES00099.1>.
- Eskandari, K. and Srinivasan, S. (2010) 'Reservoir Modelling of Complex Geological Systems--A Multiple-Point Perspective', *Journal of Canadian Petroleum Technology*, 49(08), pp. 59–69. Available at: <https://doi.org/10.2118/139917-PA>.
- Falivene, O. et al. (2006) 'Best practice stochastic facies modeling from a channel-fill turbidite sandstone analog (the Quarry outcrop, Eocene Ainsa basin, northeast Spain)', *AAPG Bulletin*, 90(7), pp. 1003–1029. Available at: <https://doi.org/10.1306/02070605112>.
- Ferguson, M. (2019) 'Permeability Modeling', in Ma, Y. Z., *Quantitative Geosciences: Data Analytics, Geostatistics, Reservoir Characterization and Modeling*. Cham: Springer International Publishing, pp. 495–515. Available at: [https://doi.org/10.1007/978-3-030-17860-4\\_20](https://doi.org/10.1007/978-3-030-17860-4_20).
- Feyen, L. and Caers, J. (2006) 'Quantifying geological uncertainty for flow and transport modeling in multi-modal heterogeneous formations', *Advances in Water Resources*, 29(6), pp. 912–929. Available at: <https://doi.org/10.1016/j.advwatres.2005.08.002>.
- Fisher, Q. et al. (2017) 'Laboratory characterization of the porosity and permeability of gas shales using the crushed shale method: Insights from experiments and numerical modelling', *Marine and Petroleum Geology*, 86, pp. 95–110. Available at: <https://doi.org/10.1016/j.marpetgeo.2017.05.027>.
- Fouch, T.D. et al. (1983) 'Patterns and Timing of Synorogenic Sedimentation in Upper Cretaceous Rocks of Central and Northeast Utah', pp. 305–336.
- Gill, S.-J. (2009) *The Nugget Effect*. Rhodes University.
- Gómez-Hernández, J.J. and Cassiraga, E.F. (1994) 'Theory and Practice of Sequential Simulation', in M. Armstrong and P.A. Dowd (eds) *Geostatistical Simulations*. Dordrecht: Springer Netherlands (Quantitative Geology and Geostatistics), pp. 111–124. Available at: [https://doi.org/10.1007/978-94-015-8267-4\\_10](https://doi.org/10.1007/978-94-015-8267-4_10).
- Gómez-Hernández, J.J. and Journel, A.G. (1989) 'Conditional Simulation of the Wilmington Sand-Shale Sequence, Los Angeles Basin', *Hydraulic Engineering*, pp. 801–806.

- Gómez-Hernández, J.J. and Srivastava, R.M. (2021) 'One Step at a Time: The Origins of Sequential Simulation and Beyond', *Mathematical Geosciences*, 53(2), pp. 193–209. Available at: <https://doi.org/10.1007/s11004-021-09926-0>.
- Goodfellow, I.J. *et al.* (2014) 'Generative Adversarial Networks'. Available at: <https://doi.org/10.48550/ARXIV.1406.2661>.
- Goovaerts, P. (1999) 'Impact of the simulation algorithm, magnitude of ergodic fluctuations and number of realizations on the spaces of uncertainty of flow properties', *Stochastic Environmental Research and Risk Assessment (SERRA)*, 13(3), pp. 161–182. Available at: <https://doi.org/10.1007/s004770050037>.
- Gringarten, E. and Deutsch, C.V. (2003) *Methodology for Improved Variogram Interpretation and Modeling for Petroleum Reservoir Characterization*. Austin, Texas: Landmark Graphics Corporation.
- Gu, J., Shen, Y. and Zhou, B. (2019) 'Image Processing Using Multi-Code GAN Prior'. Available at: <https://doi.org/10.48550/ARXIV.1912.07116>.
- Guardiano, F.B. and Srivastava, R.M. (1993) 'Multivariate Geostatistics: Beyond Bivariate Moments', in A. Soares (ed.) *Geostatistics Tróia '92*. Dordrecht: Springer Netherlands (Quantitative Geology and Geostatistics), pp. 133–144. Available at: [https://doi.org/10.1007/978-94-011-1739-5\\_12](https://doi.org/10.1007/978-94-011-1739-5_12).
- Gundesø, R. and Egeland, O. (1990) 'SESIMIRA—A New Geological Tool for 3D Modelling of Heterogeneous Reservoirs', in A.T. Buller *et al.* (eds) *North Sea Oil and Gas Reservoirs—II*. Dordrecht: Springer Netherlands, pp. 363–371. Available at: [https://doi.org/10.1007/978-94-009-0791-1\\_31](https://doi.org/10.1007/978-94-009-0791-1_31).
- Haldorsen, H.H. and Chang, D.M. (1986) 'NOTES ON STOCHASTIC SHALES; FROM OUTCROP TO SIMULATION MODEL', in *Reservoir Characterization*. Elsevier, pp. 445–485. Available at: <https://doi.org/10.1016/B978-0-12-434065-7.50020-4>.
- Haldorsen, H.H. and Damsleth, E. (1990) 'Stochastic Modeling (includes associated papers 21255 and 21299)', *Journal of Petroleum Technology*, 42(04), pp. 404–412. Available at: <https://doi.org/10.2118/20321-PA>.
- Haldorsen, H.H. and MacDonald, C.J. (1987) 'Stochastic Modeling of Underground Reservoir Facies (SMURF)', in *All Days. SPE Annual Technical Conference and Exhibition*, Dallas, Texas: SPE, p. SPE-16751-MS. Available at: <https://doi.org/10.2118/16751-MS>.
- Henriquez, A., Tyler, K.J. and Hurst, A. (1990) 'Characterization of Fluvial Sedimentology for Reservoir Simulation Modeling', *SPE Formation Evaluation*, 5(03), pp. 211–216. Available at: <https://doi.org/10.2118/18323-PA>.
- Holden, L. *et al.* (1998) 'Modeling of Fluvial Reservoirs with Object Models', *Mathematical Geology*, 30(5), pp. 473–496. Available at: <https://doi.org/10.1023/A:1021769526425>.
- Hosseini, S.A. *et al.* (2013) 'Static and dynamic reservoir modeling for geological CO<sub>2</sub> sequestration at Cranfield, Mississippi, U.S.A.', *International Journal of Greenhouse Gas Control*, 18, pp. 449–462. Available at: <https://doi.org/10.1016/j.ijggc.2012.11.009>.
- Hovadik, J.M. and Larue, D.K. (2010) 'Stratigraphic and structural connectivity', *Geological Society, London, Special Publications*, 347(1), pp. 219–242. Available at: <https://doi.org/10.1144/SP347.13>.

- Hu, L.Y. *et al.* (2014) 'Multiple-Point Simulation with an Existing Reservoir Model as Training Image', *Mathematical Geosciences*, 46(2), pp. 227–240. Available at: <https://doi.org/10.1007/s11004-013-9488-8>.
- Jacks, H.H., Smith, O.J.E. and Mattax, C.C. (1973) 'The Modeling of a Three-Dimensional Reservoir with a Two-Dimensional Reservoir Simulator-The Use of Dynamic Pseudo Functions', *Society of Petroleum Engineers Journal*, 13(03), pp. 175–185. Available at: <https://doi.org/10.2118/4071-PA>.
- Jacobi, D. *et al.* (2008) 'Integrated Petrophysical Evaluation of Shale Gas Reservoirs', in *All Days. CIPC/SPE Gas Technology Symposium 2008 Joint Conference*, Calgary, Alberta, Canada: SPE, p. SPE-114925-MS. Available at: <https://doi.org/10.2118/114925-MS>.
- Jika, H.T. *et al.* (2020) 'Application of sequential indicator simulation, sequential Gaussian simulation and flow zone indicator in reservoir-E modelling; Hatch Field Niger Delta Basin, Nigeria', *Arabian Journal of Geosciences*, 13(11), p. 410. Available at: <https://doi.org/10.1007/s12517-020-05332-8>.
- Journel, A.G. and Alabert, F.G. (1990) 'New Method for Reservoir Mapping', *Journal of Petroleum Technology*, 42(02), pp. 212–218. Available at: <https://doi.org/10.2118/18324-PA>.
- Juang, K.-W., Chen, Y.-S. and Lee, D.-Y. (2004) 'Using sequential indicator simulation to assess the uncertainty of delineating heavy-metal contaminated soils', *Environmental Pollution*, 127(2), pp. 229–238. Available at: <https://doi.org/10.1016/j.envpol.2003.07.001>.
- Kazemina, S. *et al.* (2020) 'GANs for medical image analysis', *Artificial Intelligence in Medicine*, 109, p. 101938. Available at: <https://doi.org/10.1016/j.artmed.2020.101938>.
- de Kemp, E.A. (2021) 'Spatial agents for geological surface modelling', *Geoscientific Model Development*, 14(11), pp. 6661–6680. Available at: <https://doi.org/10.5194/gmd-14-6661-2021>.
- King, P.R. (1990) 'The Connectivity and Conductivity of Overlapping Sand Bodies', in A.T. Buller *et al.* (eds) *North Sea Oil and Gas Reservoirs—II*. Dordrecht: Springer Netherlands, pp. 353–362. Available at: [https://doi.org/10.1007/978-94-009-0791-1\\_30](https://doi.org/10.1007/978-94-009-0791-1_30).
- Larue, D.K. and Hovadik, J. (2006) 'Connectivity of channelized reservoirs: a modelling approach', *Petroleum Geoscience*, 12(4), pp. 291–308. Available at: <https://doi.org/10.1144/1354-079306-699>.
- Le Coz, M., Genthon, P. and Adler, P.M. (2011) 'Multiple-Point Statistics for Modeling Facies Heterogeneities in a Porous Medium: The Komadugu-Yobe Alluvium, Lake Chad Basin', *Mathematical Geosciences*, 43(7), pp. 861–878. Available at: <https://doi.org/10.1007/s11004-011-9353-6>.
- Li, M. and Zhao, Y. (2014) 'Applicable Scope, Advantages, and Disadvantages of Major Software Packages', in *Geophysical Exploration Technology*. Elsevier, pp. 305–335. Available at: <https://doi.org/10.1016/B978-0-12-410436-5.00010-1>.
- Lia, O., Tjelmeland, H. and Kjellesvik, L.E. (1996) 'Modelling of facies architecture by marked point models', in *The Fifth International Geostatistical Congress*, Wollongong, Australia.
- Lomb, N.R. (1976) 'Least-squares frequency analysis of unequally spaced data', *Astrophysics and Space Science*, 39(2), pp. 447–462. Available at: <https://doi.org/10.1007/BF00648343>.
- MacDonald, A.C. *et al.* (1992) 'Stochastic flow unit modelling of a North Sea coastal-deltaic reservoir', *First Break*, 10(4). Available at: <https://doi.org/10.3997/1365-2397.1992008>.

- Maharaja, A. (2008) 'TiGenerator: Object-based training image generator', *Computers & Geosciences*, 34(12), pp. 1753–1761. Available at: <https://doi.org/10.1016/j.cageo.2007.08.012>.
- Mallet, J.-L. (2002) *Geomodelling*. Oxford ; New York: Oxford University Press (Applied geostatistics series).
- Manzocchi, T. *et al.* (2007) 'Static and dynamic connectivity in bed-scale models of faulted and unfaulted turbidites', *Geological Society, London, Special Publications*, 292(1), pp. 309–336. Available at: <https://doi.org/10.1144/SP292.18>.
- Martinius, A.W. *et al.* (2017) 'Reservoir characterization and multiscale heterogeneity modeling of inclined heterolithic strata for bitumen-production forecasting, McMurray Formation, Corner, Alberta, Canada', *Marine and Petroleum Geology*, 82, pp. 336–361. Available at: <https://doi.org/10.1016/j.marpetgeo.2017.02.003>.
- McLaurin, B.T. and Steel, R.J. (2007) 'Architecture and origin of an amalgamated fluvial sheet sand, lower Castlegate Formation, Book Cliffs, Utah', *Sedimentary Geology*, 197(3–4), pp. 291–311. Available at: <https://doi.org/10.1016/j.sedgeo.2006.10.005>.
- Metropolis, N. and Ulam, S. (1949) 'The Monte Carlo Method', *Journal of the American Statistical Association*, 44(247), pp. 335–341. Available at: <https://doi.org/10.1080/01621459.1949.10483310>.
- Miall, A.D. (1993) 'The architecture of fluvial-deltaic sequences in the Upper Mesaverde Group (Upper Cretaceous), Book Cliffs, Utah', *Geological Society, London, Special Publications*, 75(1), pp. 305–332. Available at: <https://doi.org/10.1144/GSL.SP.1993.075.01.19>.
- Miall, A.D. (1994) 'Reconstructing Fluvial Macroform Architecture from Two-Dimensional Outcrops: Examples from the Castlegate Sandstone, Book Cliffs, Utah', *SEPM Journal of Sedimentary Research*, Vol. 64B. Available at: <https://doi.org/10.1306/D4267F78-2B26-11D7-8648000102C1865D>.
- Miall, A.D. and Arush, M. (2001) 'The Castlegate Sandstone of the Book Cliffs, Utah: Sequence Stratigraphy, Paleogeography, and Tectonic Controls', *Journal of Sedimentary Research*, 71(4), pp. 537–548. Available at: <https://doi.org/10.1306/103000710537>.
- Mitten, A.J. *et al.* (2020) 'Depositional conditioning of three dimensional training images: Improving the reproduction and representation of architectural elements in sand-dominated fluvial reservoir models', *Marine and Petroleum Geology*, 113, p. 104156. Available at: <https://doi.org/10.1016/j.marpetgeo.2019.104156>.
- Montero, J.M. *et al.* (2021) 'A workflow for modelling fluvial meander-belt successions: Combining forward stratigraphic modelling and multi-point geostatistics', *Journal of Petroleum Science and Engineering*, 201, p. 108411. Available at: <https://doi.org/10.1016/j.petrol.2021.108411>.
- Nilsen, H.M., Lie, K.-A. and Andersen, O. (2016) 'Robust simulation of sharp-interface models for fast estimation of CO2 trapping capacity in large-scale aquifer systems', *Computational Geosciences*, 20(1), pp. 93–113. Available at: <https://doi.org/10.1007/s10596-015-9549-9>.
- Nordahl, K. and Ringrose, P.S. (2008) 'Identifying the Representative Elementary Volume for Permeability in Heterolithic Deposits Using Numerical Rock Models', *Mathematical Geosciences*, 40(7), pp. 753–771. Available at: <https://doi.org/10.1007/s11004-008-9182-4>.

- Nyberg, B. *et al.* (2019) *Characterizing user-defined objects from outcrop and modern system interpretations for stochastic object-based reservoir modelling*. preprint. Physical Sciences and Mathematics. Available at: <https://doi.org/10.31223/OSF.IO/7KUZR>.
- Okabe, H. and Blunt, M.J. (2004) 'Prediction of permeability for porous media reconstructed using multiple-point statistics', *Physical Review E*, 70(6), p. 066135. Available at: <https://doi.org/10.1103/PhysRevE.70.066135>.
- Olsen, T. *et al.* (1995) 'Sequential architecture in a fluvial succession; sequence stratigraphy in the Upper Cretaceous Mesaverde Group, Prince Canyon, Utah', *Journal of Sedimentary Research*, 65(2b), pp. 265–280. Available at: <https://doi.org/10.1306/D426822A-2B26-11D7-8648000102C1865D>.
- Ortiz, J.M. and Deutsch, C.V. (2004) 'Indicator Simulation Accounting for Multiple-Point Statistics', *Mathematical Geology*, 36(5), pp. 545–565. Available at: <https://doi.org/10.1023/B:MATG.0000037736.00489.b5>.
- Ortiz, J.M. and Emery, X. (2005) 'Integrating Multiple-point Statistics into Sequential Simulation Algorithms', in O. Leuangthong and C.V. Deutsch (eds) *Geostatistics Banff 2004*. Dordrecht: Springer Netherlands (Quantitative Geology and Geostatistics), pp. 969–978. Available at: [https://doi.org/10.1007/978-1-4020-3610-1\\_101](https://doi.org/10.1007/978-1-4020-3610-1_101).
- Pickel, A. *et al.* (2015) 'Building a training image with Digital Outcrop Models', *Journal of Hydrology*, 531, pp. 53–61. Available at: <https://doi.org/10.1016/j.jhydrol.2015.08.049>.
- Postma, G. (2014) 'Generic autogenic behaviour in fluvial systems: lessons from experimental studies', in A.W. Martinius *et al.* (eds) *From Depositional Systems to Sedimentary Successions on the Norwegian Continental Margin*. Chichester, UK: John Wiley & Sons, Ltd, pp. 1–18. Available at: <https://doi.org/10.1002/9781118920435.ch1>.
- Pranter, M.J. *et al.* (2007) 'Analysis and modeling of intermediate-scale reservoir heterogeneity based on a fluvial point-bar outcrop analog, Williams Fork Formation, Piceance Basin, Colorado', *AAPG Bulletin*, 91(7), pp. 1025–1051. Available at: <https://doi.org/10.1306/02010706102>.
- Pranter, M.J., Reza, Z.A. and Budd, D.A. (2006) 'Reservoir-scale characterization and multiphase fluid-flow modelling of lateral petrophysical heterogeneity within dolomite facies of the Madison Formation, Sheep Canyon and Lysite Mountain, Wyoming, USA', *Petroleum Geoscience*, 12(1), pp. 29–40. Available at: <https://doi.org/10.1144/1354-079305-660>.
- Pranter, M.J., Vargas, M.F. and Davis, T.L. (2008) 'Characterization and 3D reservoir modelling of fluvial sandstones of the Williams Fork Formation, Rulison Field, Piceance Basin, Colorado, USA', *Journal of Geophysics and Engineering*, 5(2), pp. 158–172. Available at: <https://doi.org/10.1088/1742-2132/5/2/003>.
- Pyrcz, M. and Deutsch, C.V. (2014) *Geostatistical reservoir modeling*. Second edition. Oxford: New York, New York : Oxford University Press.
- Qadri, S.M.T., Islam, Md.A. and Shalaby, M.R. (2019) 'Three-Dimensional Petrophysical Modelling and Volumetric Analysis to Model the Reservoir Potential of the Kupe Field, Taranaki Basin, New Zealand', *Natural Resources Research*, 28(2), pp. 369–392. Available at: <https://doi.org/10.1007/s11053-018-9394-3>.
- Renard, P., Alcolea, A. and Ginsbourger, D. (2013) 'Stochastic versus Deterministic Approaches', in J. Wainwright and M. Mulligan (eds) *Environmental Modelling*. Chichester, UK: John Wiley & Sons, Ltd, pp. 133–149. Available at: <https://doi.org/10.1002/9781118351475.ch8>.

- Renard, P. and Allard, D. (2013) 'Connectivity metrics for subsurface flow and transport', *Advances in Water Resources*, 51, pp. 168–196. Available at: <https://doi.org/10.1016/j.advwatres.2011.12.001>.
- Rezaee, H. *et al.* (2013) 'Multiple-point geostatistical simulation using the bunch-pasting direct sampling method', *Computers & Geosciences*, 54, pp. 293–308. Available at: <https://doi.org/10.1016/j.cageo.2013.01.020>.
- Ringrose, P. and Bentley, M. (2015) *Reservoir model design: a practitioner's guide*. New York: Springer.
- Sacchi, Q. *et al.* (2016) 'Increasing the predictive power of geostatistical reservoir models by integration of geological constraints from stratigraphic forward modeling', *Marine and Petroleum Geology*, 69, pp. 112–126. Available at: <https://doi.org/10.1016/j.marpetgeo.2015.10.018>.
- Scargle, J.D. (1982) 'Studies in astronomical time series analysis. II - Statistical aspects of spectral analysis of unevenly spaced data', *The Astrophysical Journal*, 263, p. 835. Available at: <https://doi.org/10.1086/160554>.
- Schlumberger Limited (2022) *Schlumberger Energy Glossary*, *Schlumberger Energy Glossary*. Available at: <https://glossary.slb.com/en/> (Accessed: 27 September 2022).
- Seifert, D. and Jensen, J.L. (1999) 'Using Sequential Indicator Simulation as a Tool in Reservoir Description: Issues and Uncertainties', *Mathematical Geology*, 31(5), pp. 527–550. Available at: <https://doi.org/10.1023/A:1007563907124>.
- Seifert, D. and Jensen, J.L. (2000) 'Object and Pixel-Based Reservoir Modeling of a Braided Fluvial Reservoir', *Mathematical Geology*, 32(5), pp. 581–603. Available at: <https://doi.org/10.1023/A:1007562221431>.
- Shepherd, M. (2009) '3-D Geocellular Modeling', in *Oil Field Production Geology*. American Association of Petroleum Geologists, pp. 175–188. Available at: <https://doi.org/10.1306/13161205M913372>.
- Skorstad, A., Hauge, R. and Holden, L. (1999) 'Well Conditioning in a Fluvial Reservoir Model', *Mathematical Geology*, 31(7), pp. 857–872. Available at: <https://doi.org/10.1023/A:1007576801266>.
- Soares, A. (2001) 'Direct Sequential Simulation and Cosimulation', *Mathematical Geology*, 33(8), pp. 911–926. Available at: <https://doi.org/10.1023/A:1012246006212>.
- Soleimani, M., Jodeiri Shokri, B. and Rafiei, M. (2017) 'Integrated Petrophysical Modeling for a Strongly Heterogeneous and Fractured Reservoir, Sarvak Formation, SW Iran', *Natural Resources Research*, 26(1), pp. 75–88. Available at: <https://doi.org/10.1007/s11053-016-9300-9>.
- Strebelle, S. (2000) *Sequential Simulation Drawing Structures From Training Images*. PhD Thesis. Stanford University.
- Strebelle, S. (2002) 'Conditional Simulation of Complex Geological Structures Using Multiple-Point Statistics', *Mathematical Geology*, 34(1), pp. 1–21. Available at: <https://doi.org/10.1023/A:1014009426274>.
- Strebelle, S. (2012) 'Multiple-Point Geostatistics: from Theory to Practice', in *Ninth International Geostatistics Congress*, Oslo, Norway.

- Strebelle, S. and Cavelius, C. (2014) 'Solving Speed and Memory Issues in Multiple-Point Statistics Simulation Program SNESIM', *Mathematical Geosciences*, 46(2), pp. 171–186. Available at: <https://doi.org/10.1007/s11004-013-9489-7>.
- Strebelle, S. and Levy, M. (2008) 'Using multiple-point statistics to build geologically realistic reservoir models: the MPS/FDM workflow', *Geological Society, London, Special Publications*, 309(1), pp. 67–74. Available at: <https://doi.org/10.1144/SP309.5>.
- Strebelle, S. and Zhang, T. (2005) 'Non-Stationary Multiple-point Geostatistical Models', in O. Leuangthong and C.V. Deutsch (eds) *Geostatistics Banff 2004*. Dordrecht: Springer Netherlands (Quantitative Geology and Geostatistics), pp. 235–244. Available at: [https://doi.org/10.1007/978-1-4020-3610-1\\_24](https://doi.org/10.1007/978-1-4020-3610-1_24).
- Strebelle, S.B. and Journel, A.G. (2001) 'Reservoir Modeling Using Multiple-Point Statistics', in *All Days. SPE Annual Technical Conference and Exhibition*, New Orleans, Louisiana: SPE, p. SPE-71324-MS. Available at: <https://doi.org/10.2118/71324-MS>.
- Sun, C., Demyanov, V. and Arnold, D. (2023a) 'A conditional GAN-based approach to build 3D facies models sequentially upwards', *Computers & Geosciences*, 181, p. 105460. Available at: <https://doi.org/10.1016/j.cageo.2023.105460>.
- Sun, C., Demyanov, V. and Arnold, D. (2023b) 'Geological realism in Fluvial facies modelling with GAN under variable depositional conditions', *Computational Geosciences*, 27(2), pp. 203–221. Available at: <https://doi.org/10.1007/s10596-023-10190-w>.
- Tahmasebi, P. (2018) 'Multiple Point Statistics: A Review', in B.S. Daya Sagar, Q. Cheng, and F. Agterberg (eds) *Handbook of Mathematical Geosciences*. Cham: Springer International Publishing, pp. 613–643. Available at: [https://doi.org/10.1007/978-3-319-78999-6\\_30](https://doi.org/10.1007/978-3-319-78999-6_30).
- Tyler, N. and Finley, R.J. (1991) 'Architectural Controls on the Recovery of Hydrocarbons From Sandstone Reservoirs', in A.D. Miall and N. Tyler (eds) *The Three-Dimensional Facies Architecture of Terrigenous Clastic Sediments and its Implications for Hydrocarbon Discovery and Recovery*. SEPM Society for Sedimentary Geology, p. 0. Available at: <https://doi.org/10.2110/csp.91.03.0001>.
- VanderPlas, J.T. (2018) 'Understanding the Lomb–Scargle Periodogram', *The Astrophysical Journal Supplement Series*, 236(1), p. 16. Available at: <https://doi.org/10.3847/1538-4365/aab766>.
- Vevle, M.L., Skorstad, A. and Vonnet, J. (2018) 'Recent developments in object modelling opens new era for characterization of fluvial reservoirs', *First Break*, 36(6), pp. 85–89. Available at: <https://doi.org/10.3997/1365-2397.n0103>.
- Vidal-Royo, O. *et al.* (2015) 'Introduction to special section: Balancing, restoration, and palinspastic reconstruction', *Interpretation*, 3(4), p. SAAi-SAAiii. Available at: <https://doi.org/10.1190/INT2015-0916-SPSEINTRO.1>.
- Villamizar, C.A. *et al.* (2015) 'Object-based modelling of avulsion-generated sandbody distributions and connectivity in a fluvial reservoir analogue of low to moderate net-to-gross ratio', *Petroleum Geoscience*, 21(4), pp. 249–270. Available at: <https://doi.org/10.1144/petgeo2015-004>.
- Vo Thanh, H. *et al.* (2019) 'Integrated workflow in 3D geological model construction for evaluation of CO<sub>2</sub> storage capacity of a fractured basement reservoir in Cuu Long Basin, Vietnam', *International Journal of Greenhouse Gas Control*, 90, p. 102826. Available at: <https://doi.org/10.1016/j.ijggc.2019.102826>.

- Weber, K.J. and van Geuns, L.C. (2005) 'PETROLEUM GEOLOGY | Production', in *Encyclopedia of Geology*. Elsevier, pp. 308–330. Available at: <https://doi.org/10.1016/B0-12-369396-9/00249-5>.
- Yeste, L.M. *et al.* (2021) 'Integrating outcrop and subsurface data to improve the predictability of geobodies distribution using a 3D training image: A case study of a Triassic Channel – Crevasse-splay complex', *Marine and Petroleum Geology*, 129, p. 105081. Available at: <https://doi.org/10.1016/j.marpetgeo.2021.105081>.
- Yoshida, S. (2000) 'Sequence and facies architecture of the upper Blackhawk Formation and the Lower Castlegate Sandstone (Upper Cretaceous), Book Cliffs, Utah, USA', *Sedimentary Geology*, 136(3–4), pp. 239–276. Available at: [https://doi.org/10.1016/S0037-0738\(00\)00104-4](https://doi.org/10.1016/S0037-0738(00)00104-4).
- Zhang, T., Switzer, P. and Journel, A. (2006) 'Filter-Based Classification of Training Image Patterns for Spatial Simulation', *Mathematical Geology*, 38(1), pp. 63–80. Available at: <https://doi.org/10.1007/s11004-005-9004-x>.
- Zhao, J. *et al.* (2019) '3D-Aided Dual-Agent GANs for Unconstrained Face Recognition', *IEEE Transactions on Pattern Analysis and Machine Intelligence*, 41(10), pp. 2380–2394. Available at: <https://doi.org/10.1109/TPAMI.2018.2858819>.
- Zhou, F. *et al.* (2018) 'Comparison of sequential indicator simulation, object modelling and multiple-point statistics in reproducing channel geometries and continuity in 2D with two different spaced conditional datasets', *Journal of Petroleum Science and Engineering*, 166, pp. 718–730. Available at: <https://doi.org/10.1016/j.petrol.2018.03.043>.